VOLUME 85 NO. HY10
OCTOBER 1959
PART 1

JOURNAL of the

Hydraulics Division

PROCEEDINGS OF THE

AMERICAN SOCIETY OF CIVIL ENGINEERS

BASIC REQUIREMENTS FOR MANUSCRIPTS

This Journal represents an effort by the Society to deliver information to th reader with the greatest possible speed. To this end the material herein ha none of the usual editing required in more formal publications.

Original papers and discussions of current papers should be submitted to th Manager of Technical Publications, ASCE. Authors should indicate the technica division to which the paper should be referred. The final date on which a dis cussion should reach the Society is given as a footnote with each paper. Thos who are planning to submit material will expedite the review and publicatio procedures by complying with the following basic requirements:

1. Titles should have a length not exceeding 50 characters and spaces.

2. A 50-word summary should accompany the paper.

3. The manuscript (a ribbon copy and two copies) should be double-space on one side of 8½-in. by 11-in. paper. Papers that were originally prepared fo oral presentation must be rewritten into the third person before being submitted

4. The author's full name, Society membership grade, and footnote referenc stating present employment should appear on the first page of the paper.

5. Mathematics are reproduced directly from the copy that is submitted Because of this, it is necessary that capital letters be drawn, in black ink, ⅛-in high (with all other symbols and characters in the proportions dictated b standard drafting practice) and that no line of mathematics be longer than 6½-in Ribbon copies of typed equations may be used but they will be proportionatel smaller on the printed version.

6. Tables should be typed (ribbon copies) on one side of 8½-in. by 11-in paper with a 6½-in. by 10½-in. invisible frame. Small tables should be groupe within this frame. Specific reference and explanation should be made in the tex for each table.

7. Illustrations should be drawn in black ink on one side of 8½-in. by 11-in paper within an invisible frame that measures 6½-in. by 10½-in.; the caption should also be included within the frame. Because illustrations will be reduce to 69% of the original size, the capital letters should be ⅛-in. high. Photograph should be submitted as glossy prints in a size that is less than 6½-in. by 10½-in Explanations and descriptions should be made within the text for each illustration

8. Papers should average about 12,000 words in length and should be n longer than 18,000 words. As an approximation, each full page of typed text table, or illustration is the equivalent of 300 words.

Further information concerning the preparation of technical papers is con tained in the "Technical Publications Handbook" which can be obtained fro the Society.

This Journal is published monthly by the American Society of Civ Engineers. Publication office is at 2500 South State Street, Ann Arbor, Michiga Editorial and General Offices are at 33 West 39 Street, New York 18, New York $4.00 of a member's dues are applied as a subscription to this Journal. Second class postage paid at Ann Arbor, Michigan.

Subject and author indexes, with abstracts, are published at the end of eac year for the Proceedings of ASCE. The index for 1958 was published as Pro Paper 1891; indexes for previous years are also available.

Journal of the

HYDRAULICS DIVISION

Proceedings of the American Society of Civil Engineers

CONTENTS

October, 1959

Papers

Journal of the
HYDRAULICS DIVISION
Proceedings of the American Society of Civil Engineers

THE HYDRAULIC DESIGN OF SLOTTED SPILLWAY BUCKETS

G. L. Beichley,[1] M. ASCE and A. J. Peterka,[2] F. ASCE

SYNOPSIS

A slotted roller bucket for use as a submerged energy dissipator at the base of an overfall is developed from hydraulic model tests and is compared with a solid-type bucket. Charts are presented in dimensionless form so that a slotted bucket may be hydraulically designed for most combinations of discharge, height of fall, and tail water range. Tail water requirements are compared with those necessary for a hydraulic jump stilling basin, and the bucket is shown to be particularly suited to installations where the tail water is too deep for a hydraulic jump. Sample problems are used to illustrate the use of the recommended general design procedures. Steps required to design a bucket for any particular installation are given in the Summary of this paper.

INTRODUCTION

In 1933 with the aid of hydraulic models, the Bureau of Reclamation developed a submerged solid bucket of the type shown in Figure 1A for use at Grand Coulee Dam.* In 1945, a submerged slotted bucket of the type shown in Figure 1B was developed by the Bureau for use at Angostura Dam.** In 1953

Note: Discussion open until March 1, 1960. To extend the closing date one month, a written request must be filed with the Executive Secretary, ASCE. Paper 2200 is part of the copyrighted Journal of the Hydraulics Division, Proceedings of the American Society of Civil Engineers, Vol. 85, No. HY 10, October, 1959.

1,2. Hydr. Engrs., Bureau of Reclamation, Denver, Colo.

* Grand Coulee Dam is a major feature of the Columbia Basin Project, is located on the Columbia River in northeastern Washington, and is a concrete gravity-type dam having an overfall spillway 1,650 feet wide by 390 feet high from the bucket invert to crest elevation. The spillway is designed for 1 million second-feet.

** Angostura Dam is a principal structure of the Angostura Unit of the Missouri River Basin Project, is located on the Cheyenne River in southwestern South Dakota, and is an earthfull structure having a concrete overfall spillway 274 feet wide by 117.2 feet high from the bucket invert to crest elevation. The spillway is designed for 247,000 second-feet.

FIGURE 1

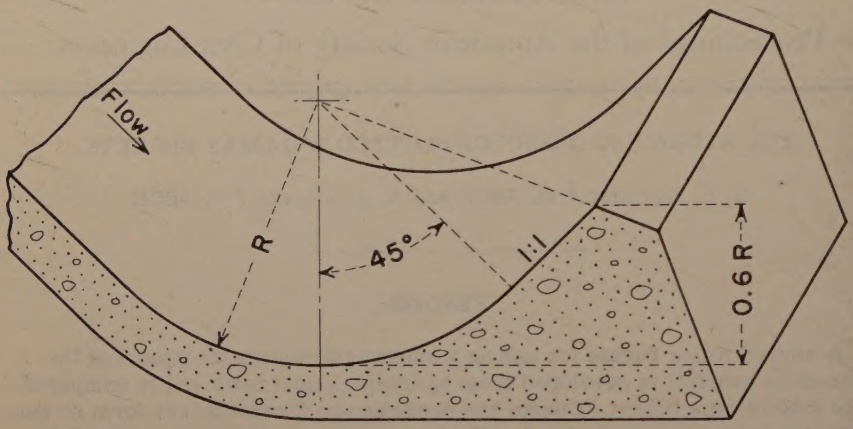

A. GRAND COULEE TYPE SOLID BUCKET

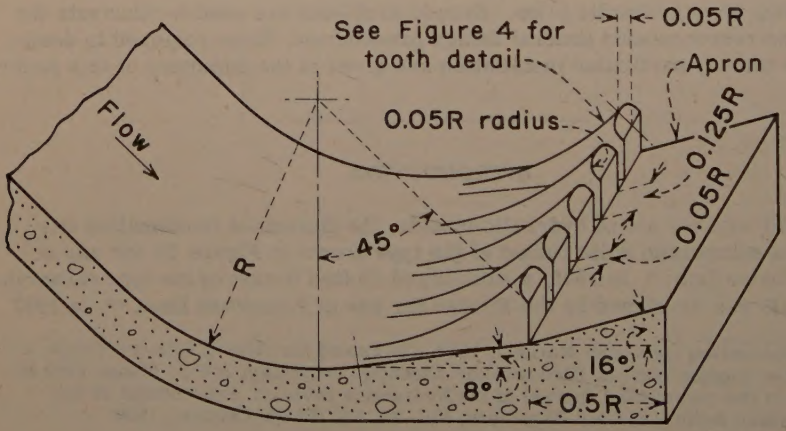

B. ANGOSTURA TYPE SLOTTED BUCKET

SUBMERGED BUCKETS

437

and 1954, extensive hydraulic model tests, covering a complete range of bucket sizes and tail water elevations, were conducted to verify the bucket dimensions and details obtained in 1945 and to establish general relations between bucket size, discharge capacity, height of fall, and the maximum and minimum tail water depth limits. The 1945 and 1953-54 studies are the subject of this paper.

Using the 1953-54 data, dimensionless curves were plotted which may be used in the hydraulic design of slotted buckets for most combinations of spillway height and discharge capacity without the need for individual hydraulic model tests. Strict adherence to the charts and rules presented will provide the designer with the smallest possible structure consistent with good performance and a moderate factor of safety. It is suggested, however, that confirming hydraulic model tests be performed whenever: (a) sustained operation near the limiting conditions is expected, (b) discharges per foot of width exceed 500 to 600 second-feet, (c) velocities entering the bucket are over 75 feet per second, (d) eddies appear to be possible at the ends of the spillway, and (e) waves in the downstream channel would be a problem.

Performance of Solid and Slotted Buckets

The solid and slotted buckets are shown operating in Figure 2.* The hydraulic action and the resulting performance of the two buckets are quite different. Both types require more tail water depth than a hydraulic jump basin. In the solid bucket, all of the flow is directed upward by the bucket lip to create a boil on the water surface and a violent ground roller on the riverbed. The severity of the high boil and the ground roller depends upon tail water depth. Low tail water produces the most violent boils and ground rollers. The upstream current in the ground roller moves bed material from downstream and deposits it at the bucket lip. Here, it is picked up, carried away, and dropped again. The constant motion of the loose material against the concrete lip and the fact that unsymmetrical spillway operation can cause eddies to sweep the piled-up material into the bucket make this bucket undesirable in some installations. Trapped material can cause abrasion damage in the bucket itself. With the slotted bucket, part of the flow passes through the slots, spreads laterally, and is lifted away from the channel bottom by the apron. Thus, the flow is dispersed and distributed over a greater area, providing less violent flow concentrations than occur with a solid bucket. Bed material is neither deposited nor carried away from the bucket lip. Debris that might get into the bucket is immediately washed out.

With the slotted bucket, sweepout occurs at a slightly higher tail water elevation than with the solid bucket, and if the tail water is extremely high, the flow may dive from the apron lip to scour the channel bed, as shown in Figure 3. With the solid bucket, diving does not occur. In general, however, the slotted bucket is an improvement over the solid type, particularly for lower ranges of tail water depths.

Slotted Bucket Development Tests

General

The slotted bucket was developed as a result of tests made to adapt the solid bucket for use at Angostura Dam. These tests, made on a 1:42 scale

*Figure 2 and other drawings showing flow currents have been traced from one or more photographs.

FIGURE 2

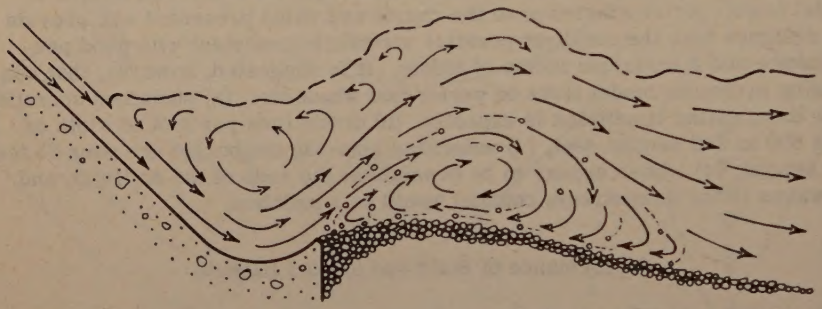

A. SOLID TYPE BUCKET

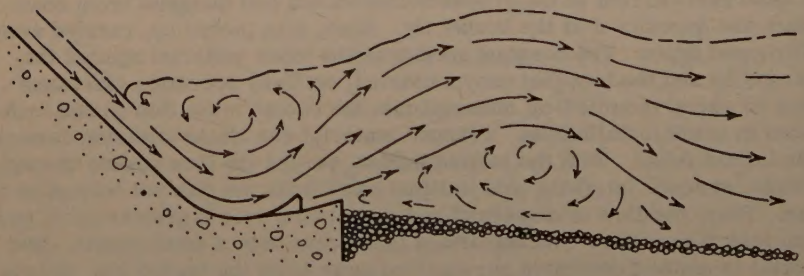

B. ANGOSTURA TYPE SLOTTED BUCKET

Bucket radius = 12", Discharge (q) = 3 c.f.s.,
Tailwater depth = 2.3'
Crest elevation to Bucket invert = 5.0'

PERFORMANCE OF SOLID AND SLOTTED BUCKETS

437

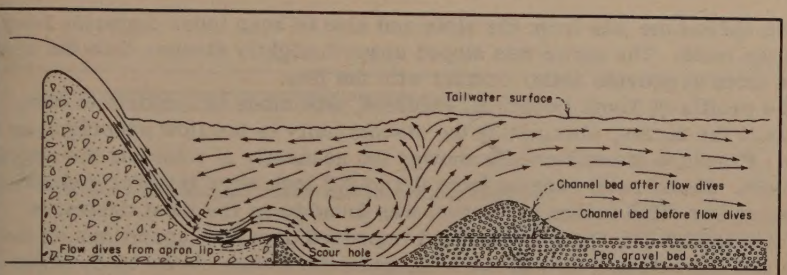

Note: The diving flow condition occurs with the slotted bucket only when the tailwater depth becomes too great.

DIVING FLOW CONDITION
SLOTTED BUCKET

437 FIGURE 3

sectional model, are summarized in the following paragraphs.

Development from Solid Bucket

Solid buckets were used to determine the minimum radius and required elevation of the bucket invert for the existing tail water conditions since the slotted bucket had not yet been anticipated. A 42-foot radius bucket was found to be the smallest bucket which would provide satisfactory performance for 1,010 second-feet per foot of width and a velocity of 75 feet per second. Best performance occurred when the bucket invert was 77 feet below tail water elevation. For all invert elevations tested, however, a ground roller, Figure 2A, moved bed material from downstream and deposited it against the bucket lip. The second stage in the development was to modify the bucket to prevent the piling of bed material along the lip. Tubes were placed in the bucket lip through which jets of water flowed to sweep away the deposited material. Results were satisfactory at low discharges, but for the higher flows loose material piled deeply over the tube exits.

Slots in the bucket lip were then used instead of larger tubes. The slots were found to not only keep the bucket lip free of loose material, but also provided exits for debris that might find its way into the bucket.

To maintain the effectiveness of the bucket action in dissipating energy, the slots were made just wide enough to prevent deposition at the bucket lip. The solid portions between the slots then became known as teeth. Three tooth designs, shown in Figure 4, were tested.

Tooth Shape, Spacing, and Pressures

With Tooth Design I, the energy dissipating action of the bucket and the elimination of piled material along the bucket lip were both satisfactory. However, small eddies, formed by the jets leaving the slots, lifted loose gravel to produce abrasive action on the downstream face of the teeth. Therefore, an upward sloping apron was installed downstream from the teeth

to help spread the jets from the slots and also to keep loose material away from the teeth. The apron was sloped upward slightly steeper than the slope of the slots to provide better contact with the jets.

The profile of Tooth Design II, Figure 4, was made to conform to the radius of the bucket, eliminating the discontinuity in the flow passing over the teeth. Pressure measurements showed the necessity of rounding the edges of the teeth. Model radii ranging from 0.1 to 0.3 inch were investigated. The larger radius (12.6 inches prototype) was found to be the most desirable.

Tooth Design III, Figure 4, showed improved pressure conditions on the sides and downstream face of the teeth when the radius on the tooth edges was increased to 15 inches. These tests showed that pressures on the teeth varied according to the tooth spacing. The most favorable pressures, Table 1, consistent with good bucket performance occurred with Tooth Design III, tooth width 0.125 R and spacing 0.05R at the downstream end.

Table 1

PRESSURES ON TOOTH DESIGN III
0.125 R Width, 0.05 R Spacing
1,000 cfs per foot—TW depth, 77 feet

Piezometer No.	Pressure ft of water	Piezometer No.	Pressure ft of water
1	+1 to +16	9	+58
2	+5 to +13	10	+42
3	-2 to +15	11	+68
4	-13 to +16	12	+49
5	-9 to +11	13	+11
6	+8 to +16	14	+13
7	+22	15	+21
8	+62	16	+34
		17	+39

For 1,000 second-feet per foot of width in a 42-foot radius bucket, Piezometers 1 through 6 fluctuated between the limits shown. Piezometers 3, 4, and 5 on the downstream face of the teeth were subatmospheric at times. According to the pressure data, significant cavitation should not occur for velocities up to about 75 feet per second; i.e., velocity computed from the difference between headwater and tail water elevations. Table 2 shows increased pressures for Piezometers 3, 4, and 5 with tooth spacing 0.035R.

For 0.035R spacing, the teeth should be safe against cavitation for velocities up to 75 feet per second. For small buckets, the spaces may be too small for convenient construction.

Apron Downstream from Teeth

The short apron downstream from the teeth serves to spread the jets from the slots and improve the stability of the flow leaving the bucket. A 16° upward sloping apron was found to be most satisfactory. With a 12° slope, the flow was unstable, intermittently diving from the end of the apron to scour the riverbed. With a 20° slope, the spreading action of the flow was counteracted to some degree by the directional effect of the steep apron.

FIGURE 4

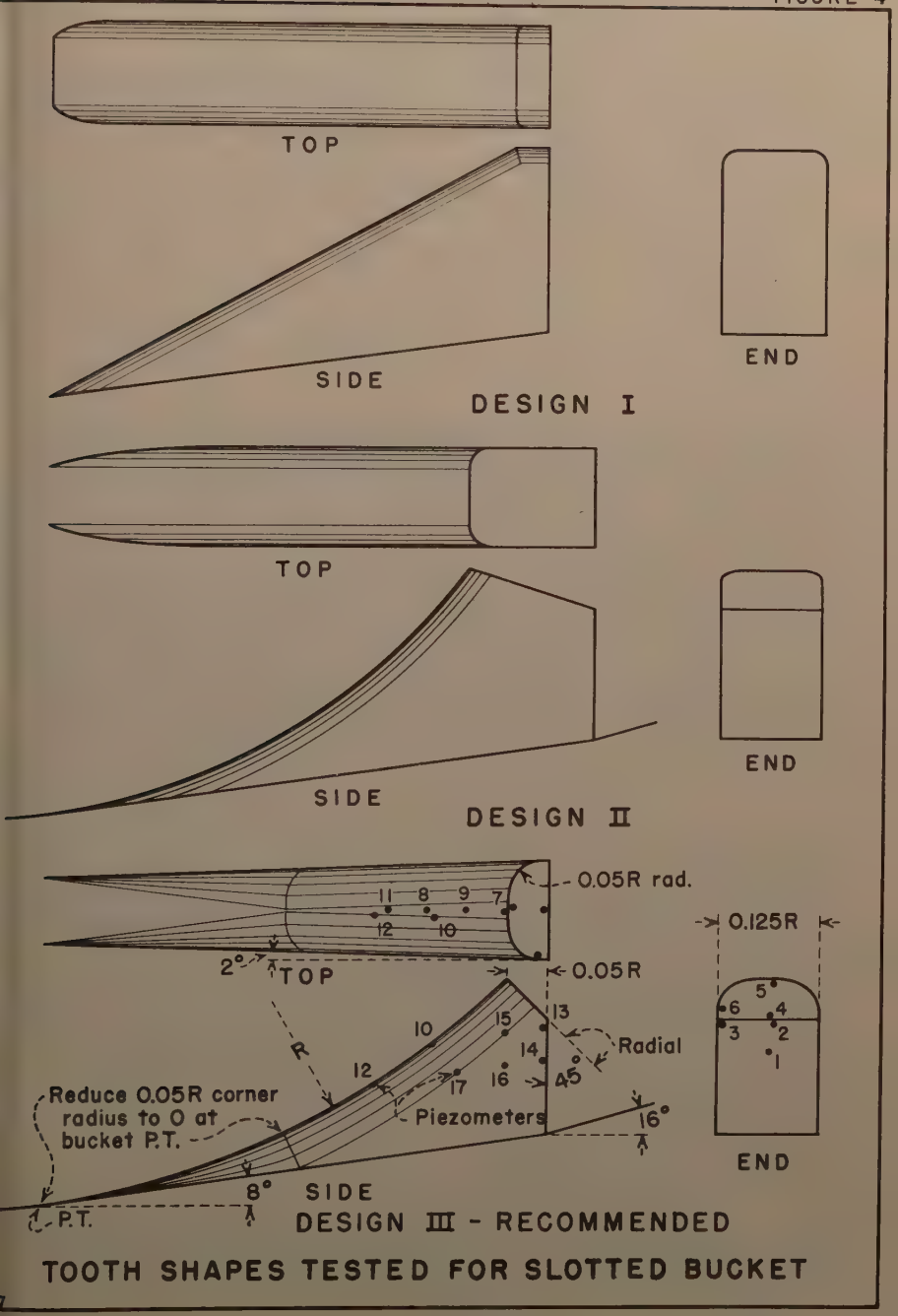

TOOTH SHAPES TESTED FOR SLOTTED BUCKET

Table 2

PRESSURES ON TOOTH DESIGN III
0.125 R Width, 0.035R Spacing
1,000 cfs per foot—TW depth, 77 feet

Piezometer No.	Pressure ft of water	Piezometer No.	Pressure ft of water
1	+36	9	+62
2	+27	10	+57
3	+30	11	+71
4	+26	12	+63
5	+14	13	+21
6	+27	14	+28
7	+39	15	+40
8	+64	16	+47
		17	+58

Two apron lengths, one 10 feet and one 20 feet, were tested to determine the minimum length required for satisfactory operation. The longer apron, 0.5R in length, was found necessary to accomplish the spreading of the jets and produce uniform flow leaving the apron.

Slotted Bucket Performance

The slotted bucket thus developed, shown in Figure 1B, operated well over the entire range of discharge and tail water conditions in the sectional model, scale 1:42. The bucket was also tested at a scale of 1:72 on a model of the entire spillway where end effects of the bucket could also be observed and evaluated. Performance was excellent in all respects and was better than for any of the solid buckets or other slotted buckets investigated.

Slotted Bucket Generalization Tests

Test Equipment

A testing flume and sectional model were constructed, as shown in Figure 5 and used in all subsequent tests. The discharge end of the flume was equipped with a motor-driven tailgate geared to raise or lower the tail water slowly so that continuous observations could be made.

Four interchangeable buckets having radii of 6, 9, 12, and 18 inches, constructed according to the dimensionless ratios shown in Figure 1B, were designed so that they could be installed with the bucket inverts located 5 feet below the spillway crest and about 6 inches above the floor of the flume. The downstream channel was a movable bed molded in 3/8-inch pea gravel.

Verification of the Slotted Bucket

General

The generalization tests began by first verifying and then attempting to improve the performance of the slotted bucket. The performance of the slotted bucket with the teeth removed was evaluated, and the performance of the slotted and solid buckets was compared.

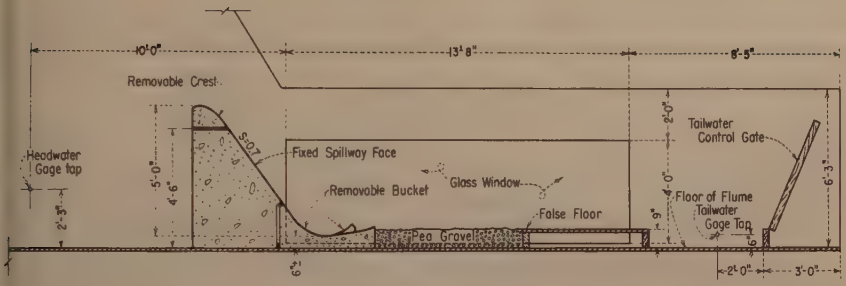

SECTION ON ℄ OF TEST FLUME

TEST FLUME AND SECTIONAL SPILLWAY

Fig. 5

To determine whether practical modifications could be made to improve performance, a 12-inch radius slotted bucket was used. The Angostura type shown in Figure 1 and Figure 6 was tested first to establish a performance standard with which to compare modified buckets. Since little bed erosion occurred with this bucket, improvements in bucket performance were directed toward reducing wave action in the downstream channel. Each modification was subjected to a standard test of 3 second-feet per foot of bucket width, with the tail water 2.3 feet above the bucket invert, Figure 2B. This was judged to be bucket capacity at a normal tail water. The movable bed was molded level, just below the bucket apron lip, at the start of each test.

Four modifications of the bucket teeth, the bucket with teeth removed, and a solid bucket were investigated. The modifications tested are shown in Figure 6. Tooth Modifications I, III and IV proved to be of no value. Tooth Modification II was an improvement, but was not considered to be of practical use for large buckets.

Tooth Modification II

The teeth were extended in height along the arc of the bucket radius to an angle of 90°, as shown in Figure 6. Performance was excellent for the standard test. A large portion of the flow was turned directly upward to the water surface where it rolled back into the bucket. The tail water depth in the bucket was about the same as the depth downstream. Only a slight boil would be detected over the teeth. The flow passing between the teeth provided uniform distribution of velocity from the channel bed to the water surface in the channel downstream. The downstream water surface was smooth, and the channel bed was not disturbed. The bucket also performed well for high and low tail water elevations. In fact, the range of tail water depths for which the bucket operated satisfactorily was greater than for any other slotted bucket tested. The teeth are suggested for possible use in small buckets; in large buckets, they may be too tall to be structurally stable.

Slotted bucket with teeth removed

Tests were made to indicate the value of the teeth and slots in dissipating energy. The bucket without teeth is shown in Figure 6. Operation was

FIGURE

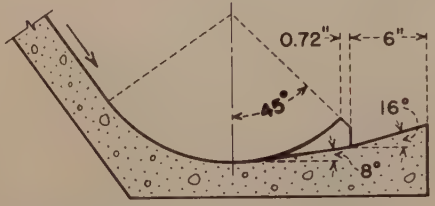

ANGOSTURA TYPE SLOTTED BUCKET

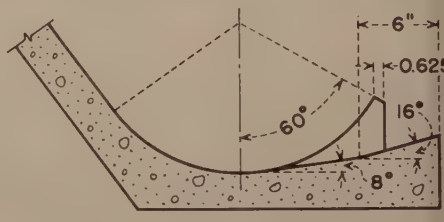

SLOTTED BUCKET MODIFICATION I

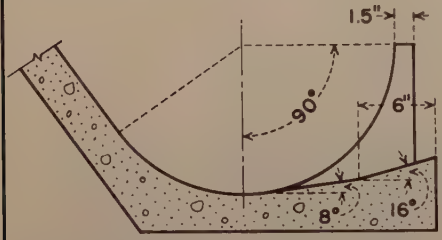

SLOTTED BUCKET MODIFICATION II

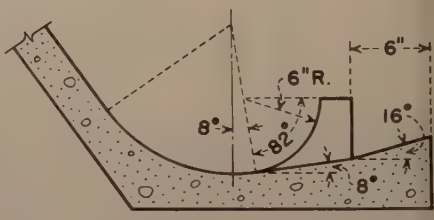

SLOTTED BUCKET MODIFICATION III

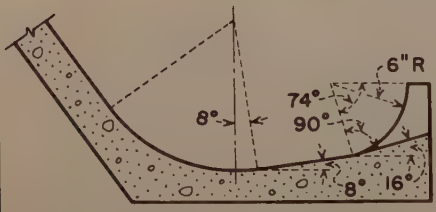

SLOTTED BUCKET MODIFICATION IV

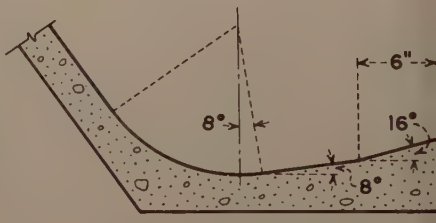

ANGOSTURA TYPE BUCKET WITHOUT TEETH

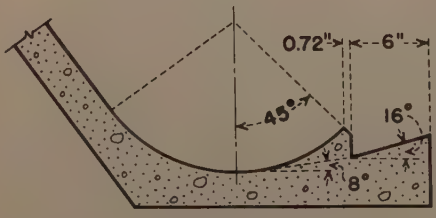

SOLID BUCKET

Dimensions applicable to all designs—
Bucket invert to downstream edge of structure = 15.21".
Approach chute slope = 7:10.
Bucket radius = 12".
Where shown,
tooth width = 1.5" and
space between teeth = 0.72".

SLOTTED BUCKET MODIFICATIONS TESTED

satisfactory for flows up to 2 second-feet per foot of width, about two-thirds maximum capacity of the bucket. For larger discharges, the flow leaving the bucket was unstable, and the water surface was rough. For a few seconds, the boil would be quite high, then suddenly would become quite low. However, erosion of the riverbed was negligible for all flows.

The tests indicated that the primary function of the teeth is to stabilize the flow and reduce water surface fluctuations in the channel downstream. The tests also suggested that should the teeth in a prototype slotted bucket deteriorate over a period of time, the rate of deterioration could be evaluated from the change in appearance of the surface flow.

Solid bucket

The solid bucket, Figure 6, was tested to compare its action with that of a slotted bucket. The performance was similar to that shown in Figure 2A and described previously. These tests confirmed the conclusion that a solid bucket may not be desirable when loose material can be carried into the bucket, when the high boil would create objectionable waves, or when a deep erosion hole located from 1 to 3 bucket radii downstream from the bucket lip would be objectionable.

Bucket Size and Tail Water Limits

General

The investigation to determine the minimum bucket size and tail water limits for a range of structure sizes, discharges, and overall height was accomplished by the testing of 6-, 9-, 12-, and 18-inch radius buckets over a range of discharges and tail water elevations with the bed molded in two different positions. For each test, the head and discharge were measured and recorded.

Lower and upper tail water limits

Testing began with the bed molded slightly below the apron lip at a distance of approximately 0.05 of the bucket radius, R. For each discharge, the tail water was lowered slowly until the flow swept out of the bucket, as shown in Figure 7A. The sweepout depth, considered to be too low for proper bucket performance, was a limiting tail water depth and was recorded and plotted in Figure 8. Tail water depth is the difference in elevation between the bucket invert and the tail water surface. The tail water depth just safely above the sweepout depth will henceforth in this paper be called the lower or minimum tail water limit.

At the sweepout depth, the flow left the bucket in the form of a jet, Figure 7A. The jet scoured the channel bed at the point of contact but did not cause excessive water surface roughness downstream. However, a more undesirable flow pattern occurred just before sweepout. An unstable condition developed in the bucket causing excessive erosion and water surface roughness. It is, therefore, undesirable to design a bucket for both submerged and flip action because of this transition region. The lower tail water limit was found to be from 0.05 to 0.15 foot above the sweepout depth. Only the sweepout depth was actually measured since it was a more definite point. A safe lower limit, T_{min}, was established at the conclusion of all model testing by adding 0.2 foot to the sweepout tail water depth.

For each discharge, the upper tail water limit was investigated. The tail water was raised slowly until the flow dived from the apron lip, as shown in

FIGURE

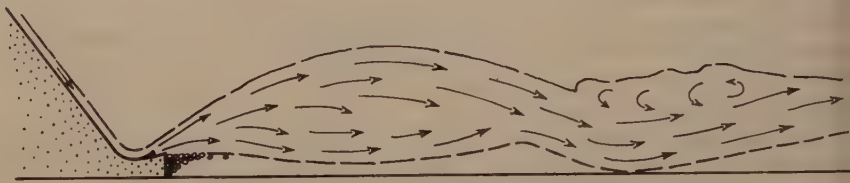

A. Tailwater below minimum. Flow sweeps out.

B. Tailwater below average but above minimum.
Within normal operating range.

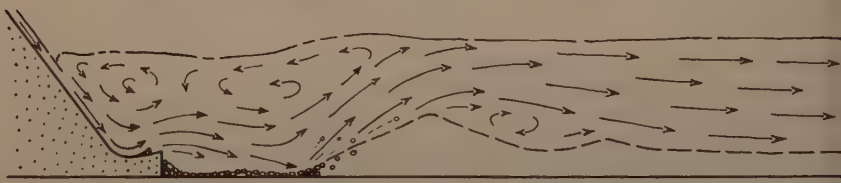

C. Tailwater above maximum. Flow diving from
apron scours channel

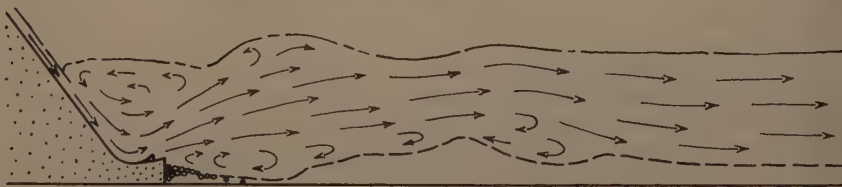

D. Tailwater same as in C. Diving jet is lifted by ground
roller. Scour hole backfills similar to B. Cycle repeats.

(Bed level 0.3-inch below apron lip at start of test)

6-INCH BUCKET – DISCHARGE (q) = 1.75 C.F.S.
(DESIGN CAPACITY)

437

Figures 3 and 7C. When diving occurred, a deep hole was scoured in the channel bed near the bucket. The tail water depth was also recorded and plotted in Figure 8. The tail water depth just safely below the depth required for diving will, henceforth, be called the upper or maximum tail water limit.

At the tail water depth required for diving to occur, Figure 7C, it was noted that after 3 or 4 minutes (model time) diving suddenly ceased, and the flow rose to the surface shown in Figure 7D. The changeover occurred only after the movable bed had become sufficiently scoured to allow a ground roller to form beneath the jet and lift the flow from the apron lip to the water surface. The ground roller then moved the deposited gravel upstream into the scoured hole until the riverbed was nearly level with the apron lip. At the same time, the strength of the ground roller was reduced until it was no longer capable of lifting the flow to the water surface and the flow dived again to start another cycle, which was repeated over and over. Very little bed material was moved downstream out of reach of the ground roller even after several cycles. Five or six minutes were required for one cycle as a general rule.

When the flow was diving, the water surface was very smooth; but when the flow was directed toward the surface, a boil formed, and a rough downstream water surface was in evidence. In the former case, part of the energy was dissipated on the channel bed; in the latter case, energy was dissipated on the surface.

In approaching the upper tail water limit, diving occurred in spurts not sufficiently long to move bed material. As the depth approached that required for sustained periods of diving, the momentary spurts occurred more often. The tail water depth required to cause sustained diving was used because it was a definite point. At the conclusion of all model testing, the upper tail water limit, T_{max}, was established by subtracting 0.5 foot from the tail water depth at which sustained diving occurred.

It was difficult to obtain consistent results for the tail water depth at which diving occurred because the upper tail water limit was affected by the shape and elevation of the channel bed with respect to the apron lip. Since it was difficult to maintain the bed shape during the starting of a run, the gravel was removed from the model in anticipation that the upper tail water limit could be determined from observations of the flow pattern. This arrangement proved unsuccessful since diving did not occur. However, this test, using the 6-inch bucket, showed that excellent performance occurred, Figure 9A, when the tail water depth above the bucket invert was less than the bucket radius. With deeper tail water, performance was not as good but was still satisfactory.

The channel bed represented by a wood floor at the elevation of the apron lip produced flow currents that followed along the floor for quite some distance before rising to the surface, Figure 9C. The flow followed along the floor for a greater distance with higher tail water. No other changes in flow pattern occurred at high tail water elevations, and again no upper limit could be found.

Testing was continued with the gravel bed molded level slightly below the apron lip. It was necessary to reshape the bed before each test to obtain consistent upper limit results; even then it was difficult. Testing showed that it was important that the channel bed be below the apron lip elevation to prevent the diving flow pattern from occurring at a much lower tail water elevation. Therefore, a sloping bed was included in the investigation.

For the 9- and 12-inch buckets, upper and lower tail water limits were also determined with the bed sloping 16° upward from the apron lip to

FIGURE

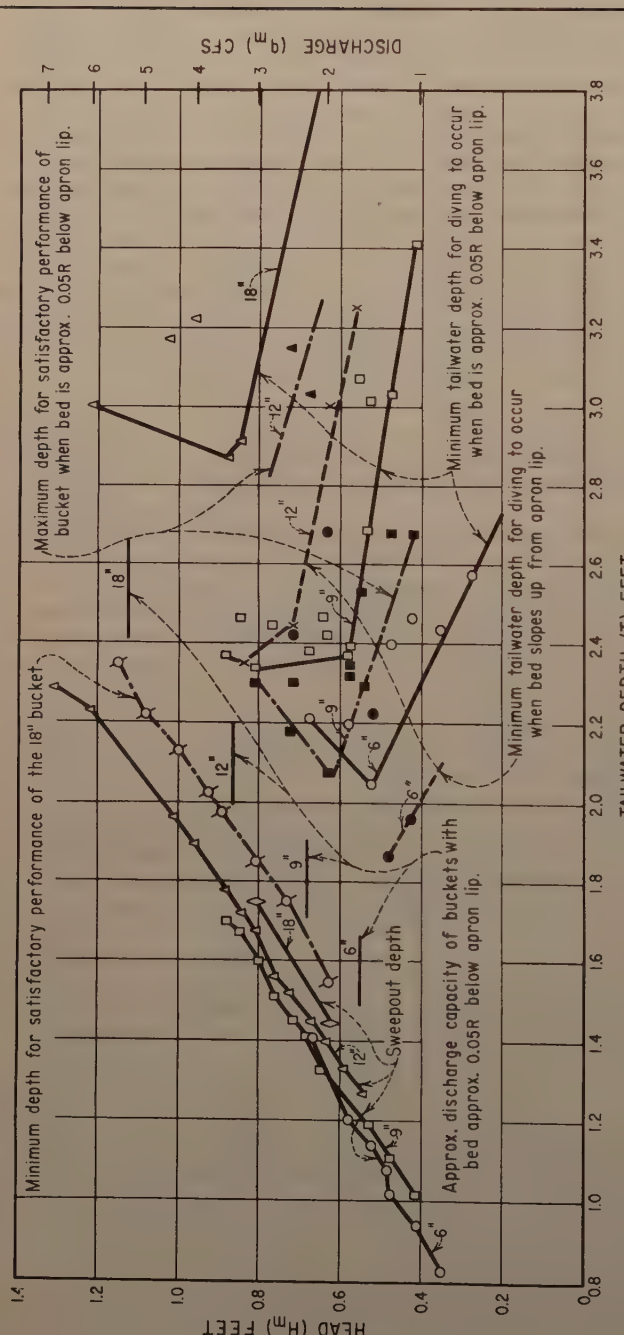

TAILWATER LIMITS AND BUCKET CAPACITIES

FIGURE 9

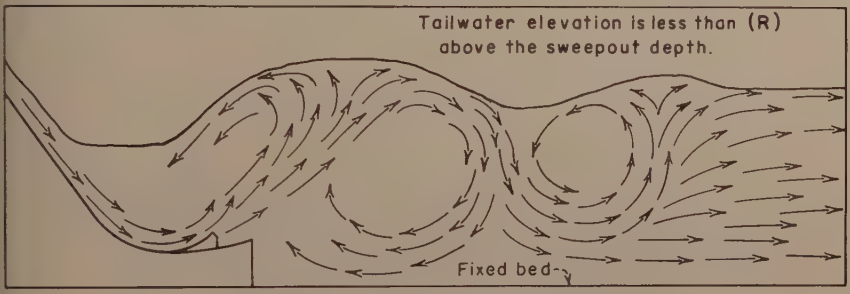

A. FIXED BED BELOW BUCKET INVERT.
DESIRABLE TAILWATER DEPTH

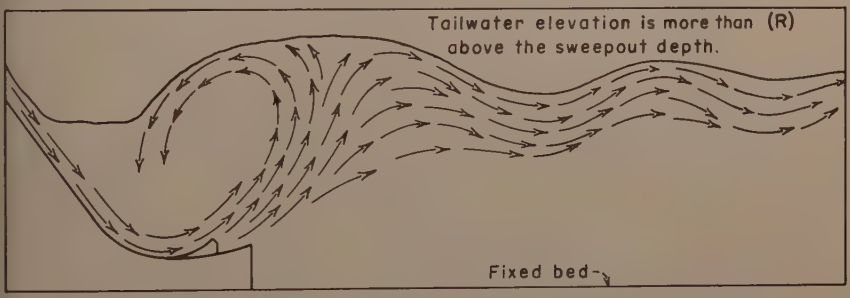

B. FIXED BED BELOW BUCKET INVERT.
LESS DESIRABLE TAILWATER DEPTH

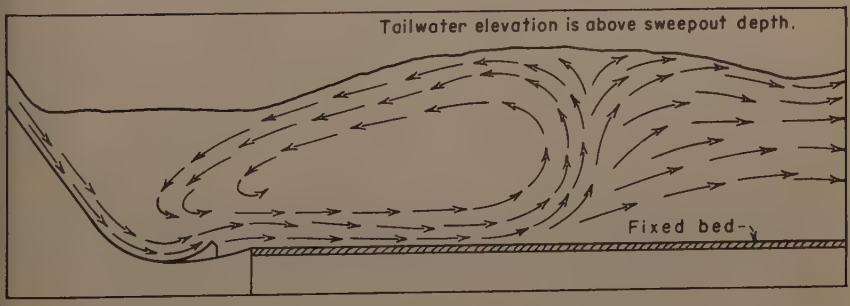

C. FIXED BED AT APRON LIP LEVEL

Note:
Bucket radius (R) is 6 inches.
Design discharge - 1.75 second feet per unit foot of width.

FLOW CURRENTS FOR VARIOUS
ARRANGEMENTS OF FIXED BEDS

437

approximately 6 inches above the lip. Tests showed that sweepout occurred at the same depth, but diving occurred at a much lower tail water depth. For the 9-inch bucket, diving occurred at about the same tail water depth as for the 6-inch bucket with bed level 0.05R below the lip. For the 12-inch bucket, it occurred at about the same tail water depth as for the 9-inch bucket with bed level 0.05R below the lip. Thus, the effect of the sloping bed was to reduce the operating range between minimum and maximum tail water depth limits by lowering the upper tail water limit.

Depths for sweepout and diving were difficult to determine precisely for the larger buckets. In fact, for the 18-inch bucket, the sustained diving condition could not be reached at any discharge, even when the tail water was raised to crest elevation. However, the tendency to dive was present, and momentary diving occurred, but in no case was it sustained.

Maximum capacity

As the discharge capacity of the bucket was approached, the difference between the upper and lower tail water limits became smaller. The maximum capacity of the bucket was judged from its general performance and by the range of useful tail water elevations between the upper and lower tail water limits, Figure 8.

When the bed sloped upward, the useful range of tail water was reduced, but since the general performance appeared to be changed very little, the capacity of the bucket was said to be the same for either bed condition. The maximum capacity of the 6-inch bucket was found to be 1.5 to 1.75 second-fee per foot of bucket width. The performance of the bucket for 1.75 second-feet and normal tail water elevation is shown in Figure 7B.

The maximum capacity of the 9-inch bucket was determined to be 2 to 2.5 second-feet per foot of width. Discharges of 1.5 to 3 second-feet with a normal tail water depth of 1.85 feet are shown in Figure 10.

Figure 11 shows the performance of the 12-inch bucket for unit flows ranging from 2.5 to 4 second-feet with normal tail water depth of 2.3 feet. The maximum capacity of the bucket was determined to be from 3.0 to 3.5 second-feet.

The performance of the 18-inch bucket is shown in Figure 12 for unit discharges ranging from 3 to 5.5 second-feet with normal tail water depths. The capacity of the bucket was determined to be 5 to 5.5 second-feet.

Water surface characteristics

Figure 13 shows water surface characteristics for the 9- and 12-inch buckets. To aid in defining water surface profiles, measurements were made for a range of flows with the tail water at about halfway between the upper and lower limits.

Larger and smaller buckets

Increasing difficulties in determining bucket capacity and tail water depth limits for near capacity flows made it inadvisable to test larger buckets on the 5-foot spillway. In addition, maximum tail water depths would have submerged the crest, and it was not intended at this time to investigate submerged crest spillways.

It was unnecessary to test smaller buckets because a bucket radius smalle than one-tenth the height of the spillway would seldom be used. Therefore, the available data were analyzed and, with some extrapolation, found to be sufficient.

FIGURE 10

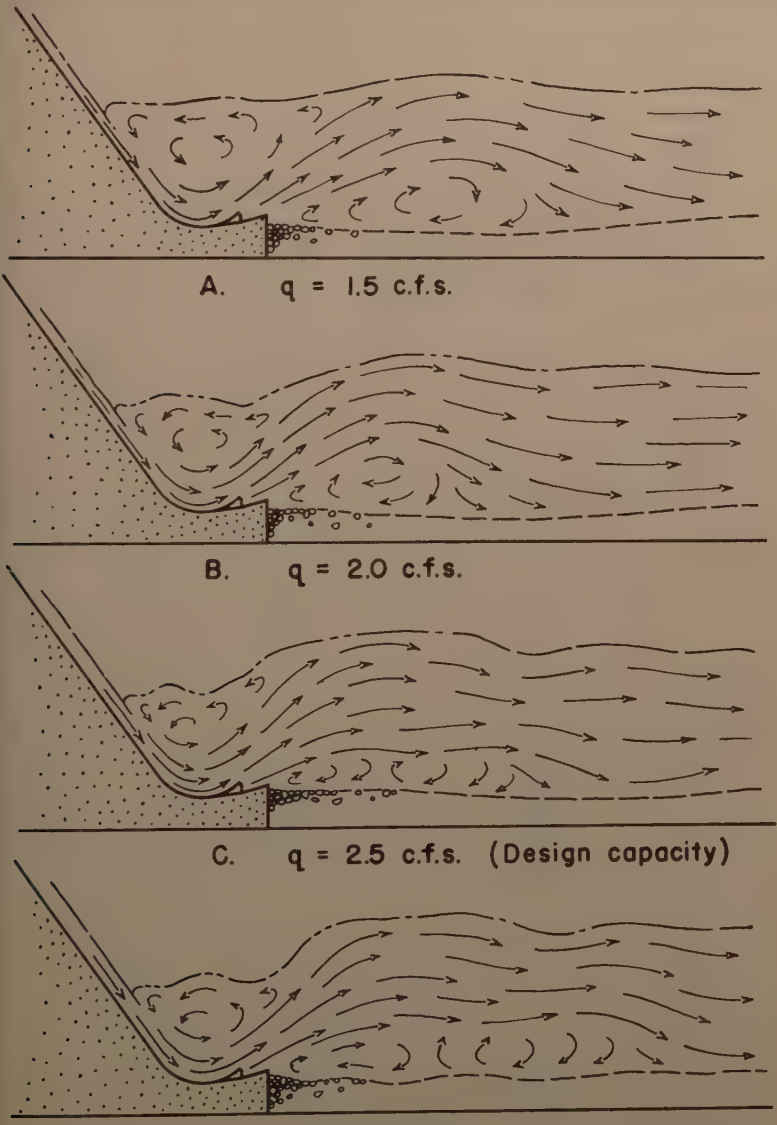

(Bed level 0.5-inch below apron lip at start of test.)

9-INCH BUCKET — TAILWATER DEPTH = 1.85 FEET

FIGURE 11

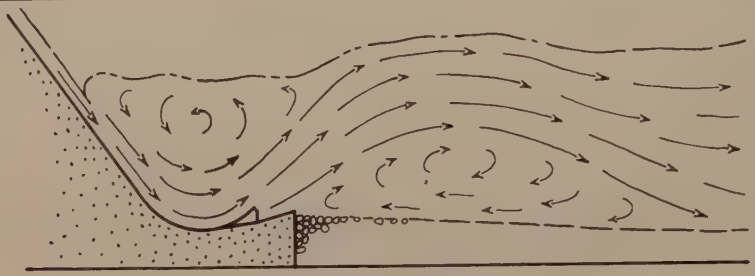

A. q = 2.5 c.f.s.

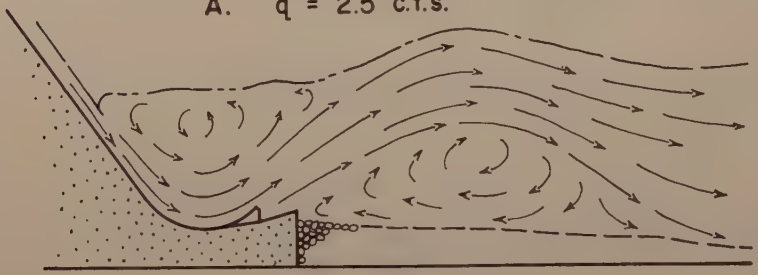

B. q = 3.0 c.f.s.

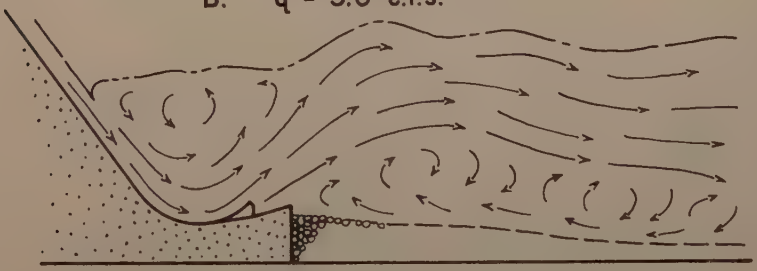

C. q = 3.5 c.f.s. (Design capacity)

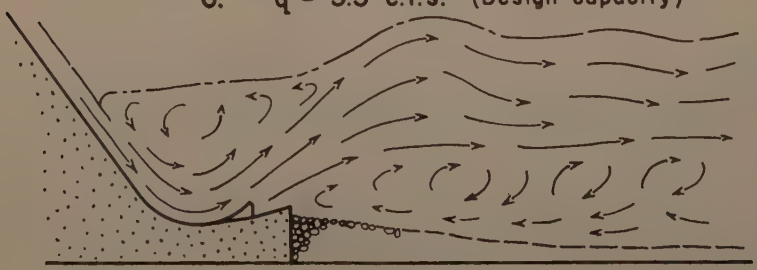

D. q = 4.0 c.f.s.

(Bed level 0.6-inch below apron lip at start of test.)

12-INCH BUCKET — TAILWATER DEPTH = 2.30 FEET

437

FIGURE 12

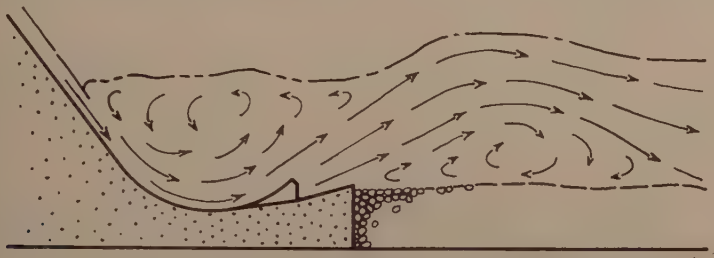

A. q = 3 c.f.s., Tailwater depth = 2.30 feet.

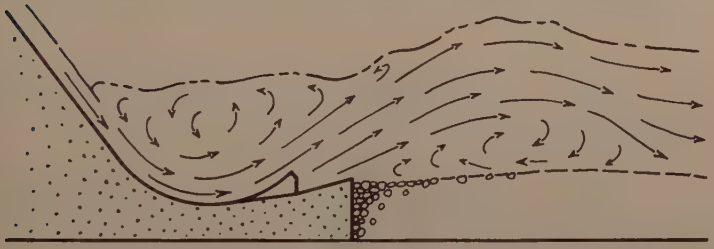

B. q = 3.5 c.f.s., Tailwater depth = 2.30 feet.

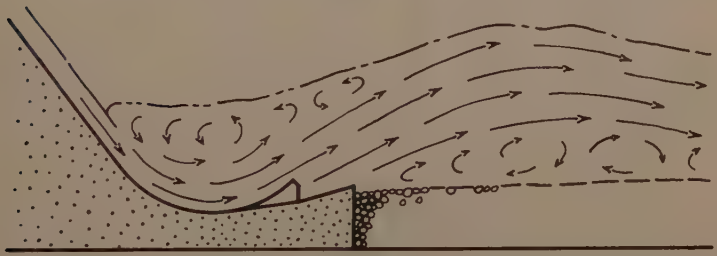

C. q = 4 c.f.s., Tailwater depth = 2.30 feet.

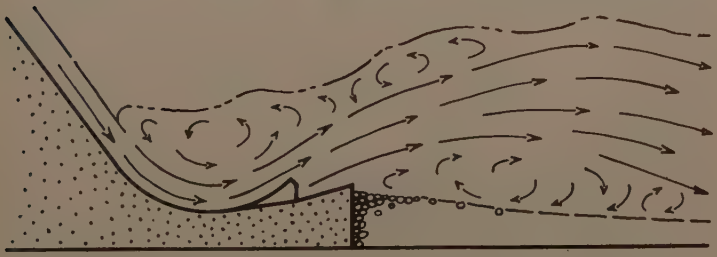

D. q = 5.5 c.f.s., Tailwater depth = 2.45 feet
(Design capacity)

(Bed level 0.9-inch below apron lip at start of test.)

18-INCH BUCKET PERFORMANCE

FIGURE 13

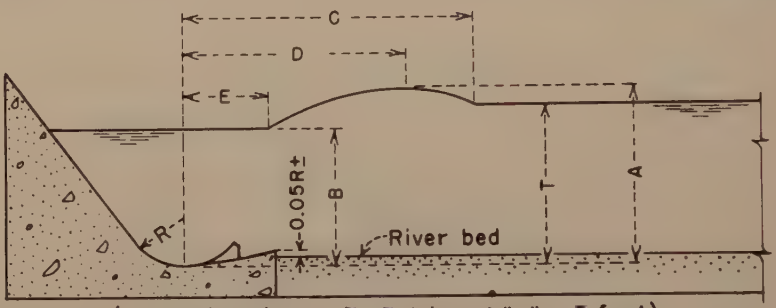

(Crest elevation to bucket invert "x" = 5 feet)

9-INCH BUCKET (R)

Q-cfs	q-cfs	T-ft.	A	B	C	D	E
3.0	1.50	1.85	25	19	45	25	5
3.0	1.50	2.40	32	26	46	27	1
3.50	1.75	1.85	26	19	45	25	5
4.00	2.00	1.85	27	19	46	25	5
4.50	2.25	1.85	28	19	48	28	6
5.00*	2.50	1.85	28	18	50	32	6
5.50	2.75	1.85	29	17	51	31	6
6.00	3.00	1.85	30	16	52	32	6

12-INCH BUCKET (R)

Q-cfs	q-cfs	T-ft.	A	B	C	D	E
5.0	2.5	2.30	32	23	52	35	14
6.0	3.0	2.30	33	22	62	37	11
7.0 *	3.5	2.30	33	21	68	37	9
8.0	4.0	2.30	35	19	70	37	6
12.0	6.0	—	36	7	90	40	1

NOTE: Dimensions A, B, C, D, and E are in inches
* Design capacity

AVERAGE WATER SURFACE MEASUREMENTS

437

Data Analysis

To generalize the design of a bucket from the available data, it is necessary to establish the relation between the variables shown in Figure 14. Figure 8 shows that, for a given height of structure having a particular overfall shape and spillway surface roughness, the sweepout depth, T_S, and minimum tail water depth limit, T_{min}, are functions of the radius of the bucket, R, and the head on the crest, H. The height of structure may be expressed as the height of fall, h, from the spillway crest to the tail water elevation. The overfall shape and H determine the discharge per foot of spillway width and may be expressed as q. Since the spillway surface roughness and the spillway slope had negligible effect on flow in the model, they were not considered in the analysis of model data. The tests showed that the elevation or shape of the movable bed did not affect the minimum tail water limits appreciably. Therefore,

$$T_{min} \text{ or } T_S = f(h, R, \text{and } q)$$

Similarly, the maximum tail water depth limit, T_{max}, is a function of the same variables, but since the slope and elevation of the movable bed with

FIGURE 14

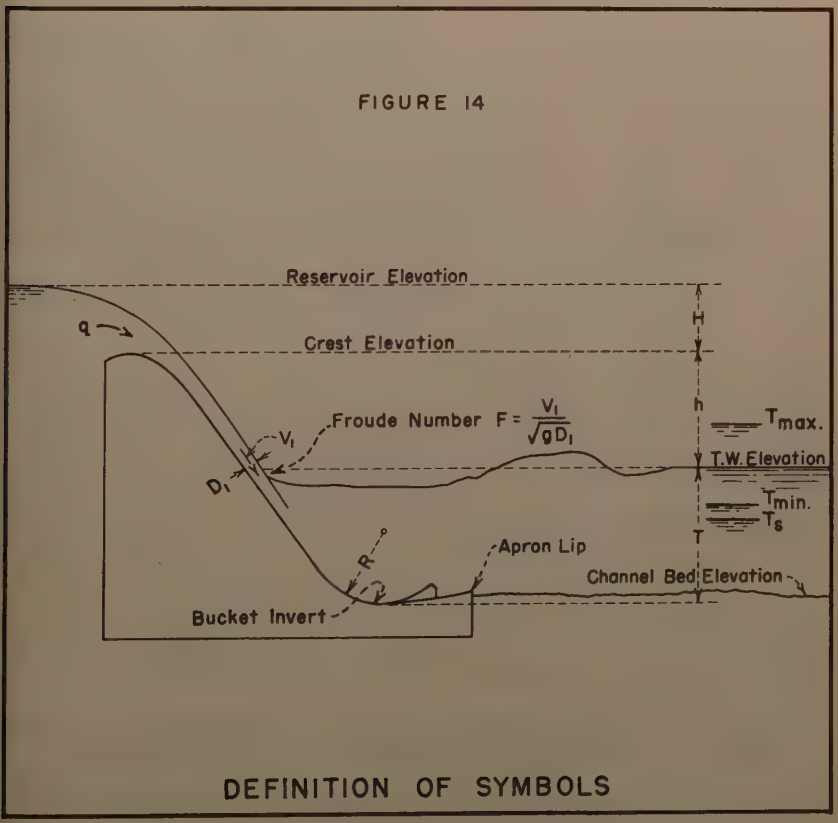

respect to the apron lip does not affect the tail water at which diving occurs

$$T_{max} = f\ (h,\ R,\ q \text{ and channel shape})$$

The maximum capacity of a bucket is a function of discharge and height of fall. Therefore,

$$R_{min} = f\ (h \text{ and } q)$$

The Froude number is a function of velocity and depth of flow and may be expressed

$$F = \frac{V_1}{\sqrt{gD_1}}$$

in which V_1 and D_1 are at tail water elevation, as shown in Figure 14. Since h and q are functions of V_1 and D_1, they may be replaced by the Froude number F. Substituting, then

$$T_{min} \text{ and } T_s = f\ (R,\ F)$$

$$T_{max} = f\ (R,\ F \text{ and channel shape})$$

$$R_{min} = f\ (F)$$

Numerical values for the Froude number were computed from the test data for points on the spillway face corresponding to tail water elevation. Since the Froude number is dimensionless, a numerical value expresses a prototype as well as a model flow condition. To express T_{min}, T_{max}, and R_{min} as dimensionless numbers so that they may also be used to predict prototype flow conditions, T_{min} and T_{max} were divided by D_1; R_{min} was divided by $D_1 + V_1^2/2g$, the depth of flow plus the velocity head at tail water elevation.

To provide data that are useful for determining the minimum bucket radius for a given Froude number, the bucket radius dimensionless ratio $\frac{R}{D_1 + \frac{V_1^2}{2g}}$ is plotted against the Froude number in Figure 15, using only maximum capacity discharge values. The maximum capacity discharge values are plotted for both the sweepout and diving tail water elevations since the Froude number and bucket radius ratio both vary with tail water elevation. For example, the maximum capacity of the 6-inch bucket is q = 1.5 to 1.75 second-feet, and since each discharge has two tailwater limits, four points may be plotted. The two points obtained for each discharge were connected by a dashed line to indicate the trend in bucket size for constant discharge and varying heights of fall to the tail water surface. Eight dashed lines were thereby obtained for the four buckets. A single envelope curve was then drawn, shown as the solid line to the right of the preliminary lines, to indicate the minimum bucket radius. The solid line, therefore, includes a factor of safety which is measured by the distance between the solid line and the test points.

To provide data useful for determining tail water depth limits for a given Froude number, the dimensionless ratios for tail water depth limits, $\frac{T_{min}}{D_1}$ and $\frac{T_{max}}{D_1}$ for each test point, were plotted versus the Froude

number in Figure 16, and each point was labeled with the computed value of the bucket radius ratio. Then, curves were drawn through both the minimum and maximum tail water depth limits having the same bucket radius ratio values. The upper four curves are for the minimum tail water limit and apply

FIGURE 15

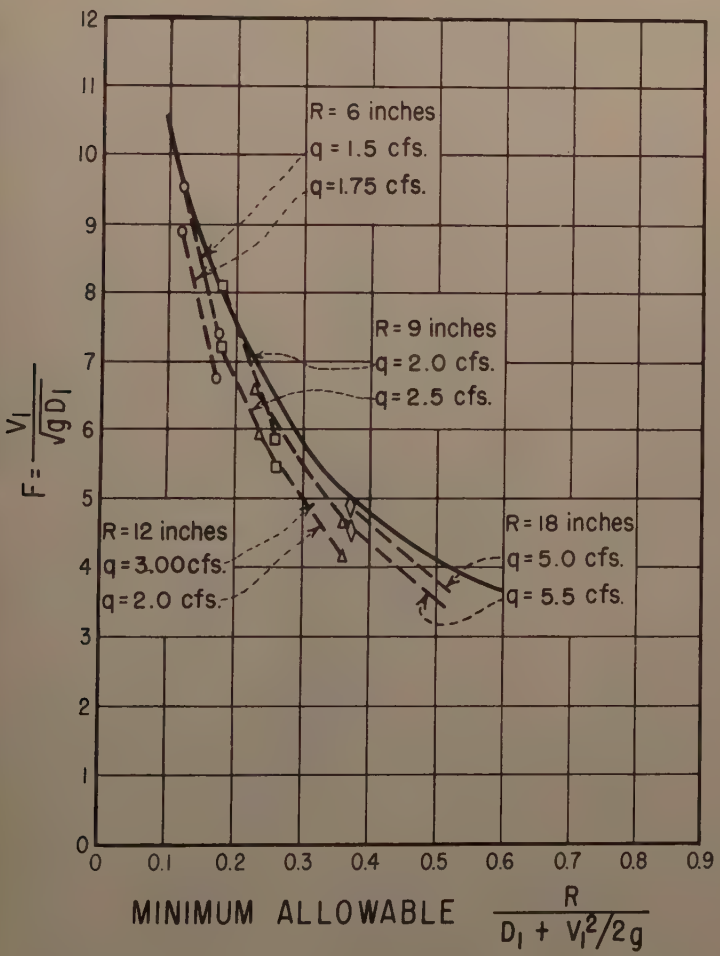

Bed level approximately 0.05R below lip of apron

MINIMUM ALLOWABLE BUCKET RADIUS

FIGURE 1

DIMENSIONLESS PLOT OF MAXIMUM AND MINIMUM TAILWATER DEPTH LIMITS

o any bed arrangement. The ten lower curves apply to the maximum tail vater limitation and have two sets of labels, one for the sloping bed and one or the level bed. Two curves are shown for each value of the bucket radius atio for the upper tail water limit. The upper or solid line curves have an xtra factor of safety included because of the difficulty in obtaining consistent pper tail water limit values. The lower or dashed line curves are a strict nterpretation of the data, including the safety factor incorporated into the ata as previously explained in the discussion of lower and upper tail water imits.

The curves of Figure 16 may be used to determine minimum and maximum ail water limits for a given Froude number and bucket ratio. However, a impler and easier to use version of the same data is given in Figures 17 and 8, which were obtained by cross plotting the curves of Figure 16. The two bscissa scales in Figure 18 differentiate between the sloping bed and the evel bed used in the tests.

The tail water sweepout depth T_S was also expressed as a dimensionless atio $\frac{T_S}{D_1}$ and plotted versus the Froude number in Figure 19, and a curve or each bucket size was drawn. These curves were then cross plotted in Figure 20 to provide more convenient means for determining the sweepout epth.

To aid in determining approximate water surface profiles in and downtream from the bucket, the data of Figure 13 and values scaled from photoraphs of other bucket tests were analyzed and plotted. Refinement of the urves obtained resulted in the curves of Figure 21. The height of the boil bove the tail water may be determined from the Froude number and the atio $\frac{R}{X}$, where X is the height of the spillway from crest to bucket invert.

he depth of water in the bucket, Dimension B in Figures 13 and 21, was ound to remain fairly constant over most of the design operating range, bout 80 to 85 percent of the Dimension T. For minimum recommended tail ater, the percentage dropped to 70 percent, while for high tail water, the alue increased to 90 percent, approximately.

ractical Application

ample problems

To illustrate the use of the methods and charts given in this paper, a step-y-step procedure for designing a slotted bucket is presented. Data from rand Coulee Dam spillway will be used in an example so that the resulting lotted bucket may be compared with the solid bucket individually determined om model tests and now in use at Grand Coulee Dam. The calculations are ummarized in Table 3.

For maximum reservoir elevation 1291.65, the spillway discharge is 000,000 second-feet. Spillway crest elevation is 1260, and head is 31.65 et. The width of the bucket is 1,650 feet; the unit discharge is 606 second-et, and maximum tail water is at elevation 1011. The theoretical velocity ead of the flow entering the basin is the difference between tail water eleva-on and reservoir elevation or 280.65 feet. Then, the theoretical velocity, T, entering the tail water is 134.4 feet per second; $V_1 = \sqrt{2g(H + H)}$. See igure 14.

FIGURE 1

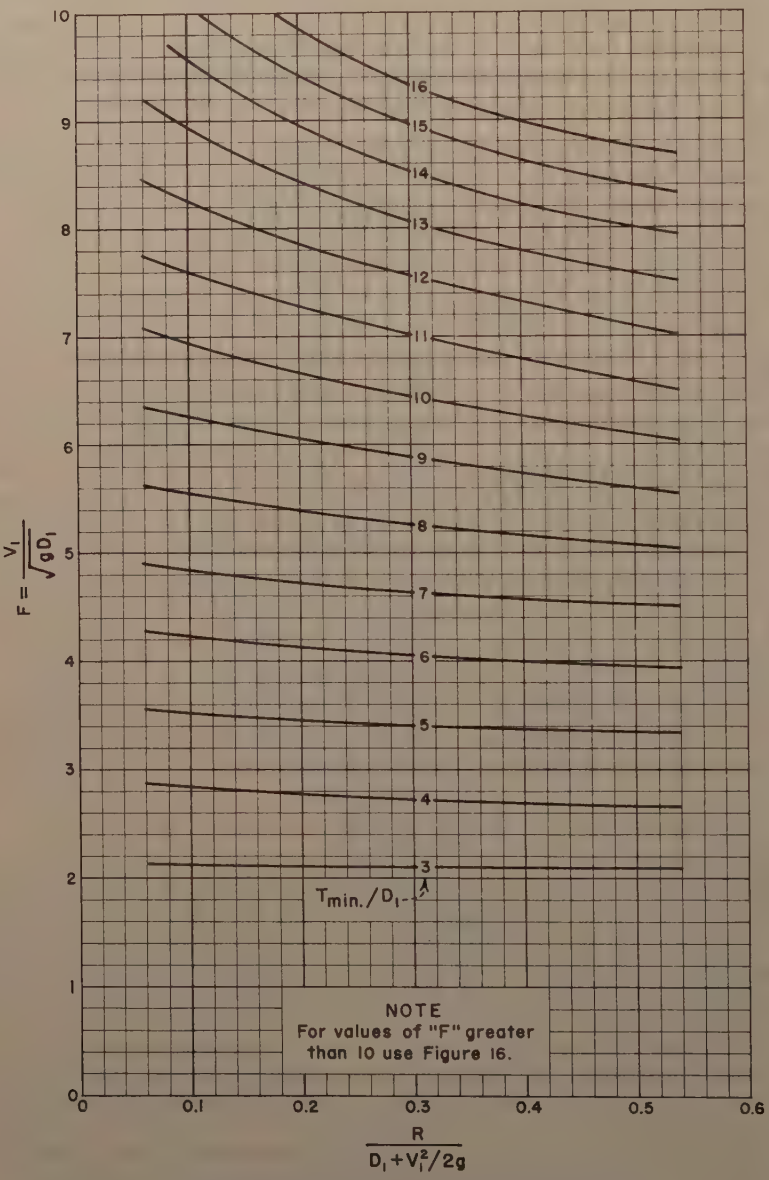

MINIMUM TAILWATER LIMIT

437

FIGURE 18

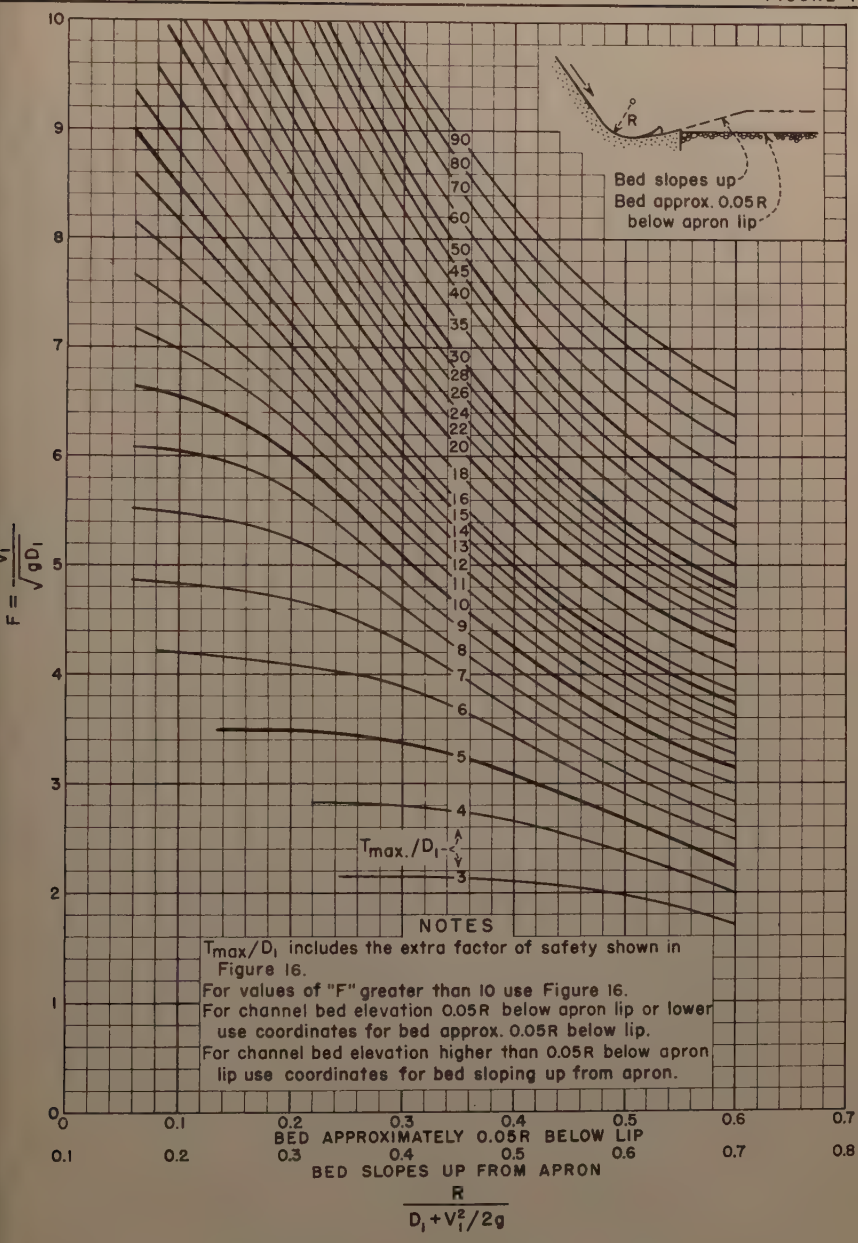

MAXIMUM TAILWATER LIMIT

FIGURE 19

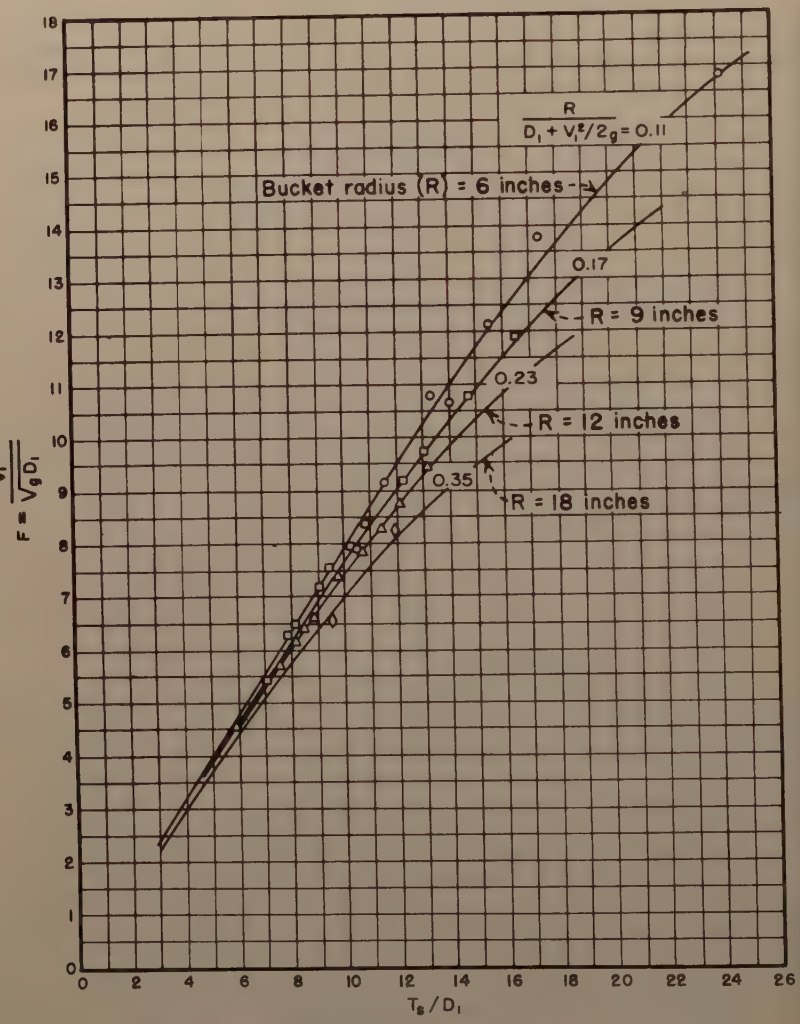

Note: Bed arrangement not critical for sweepout condition

TAILWATER DEPTH AT SWEEPOUT

437

FIGURE 20

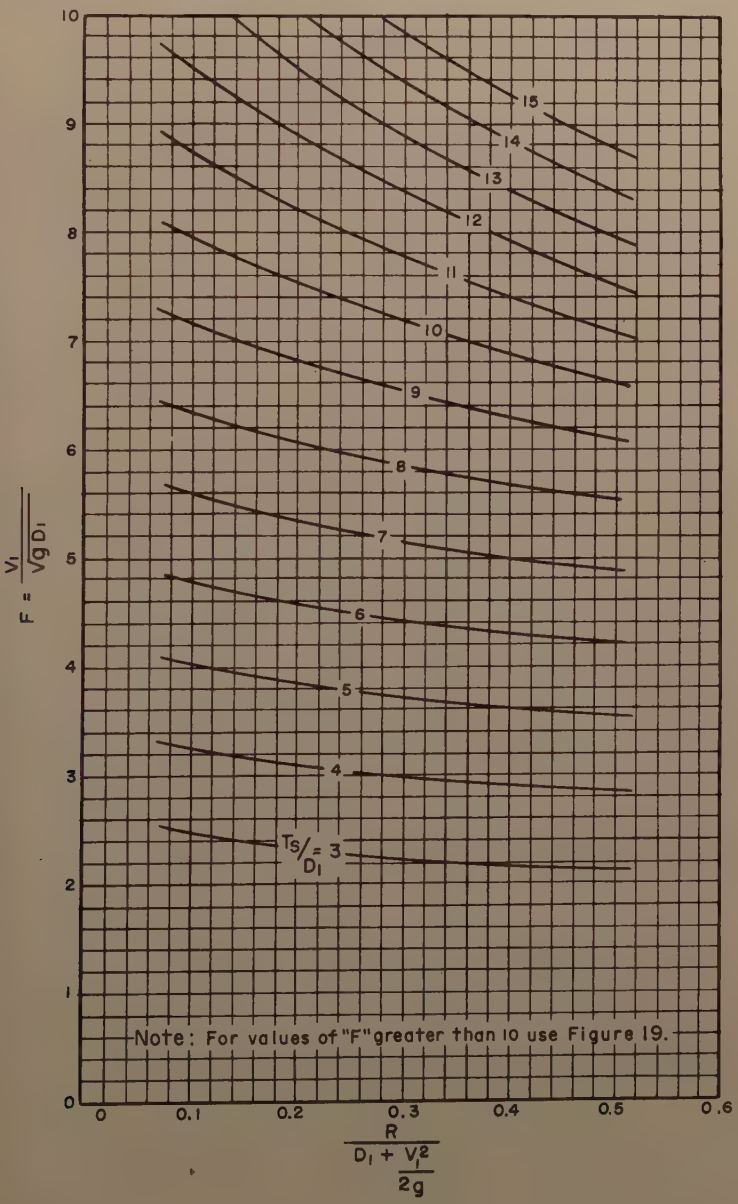

TAILWATER SWEEPOUT DEPTH

437

FIGURE 21

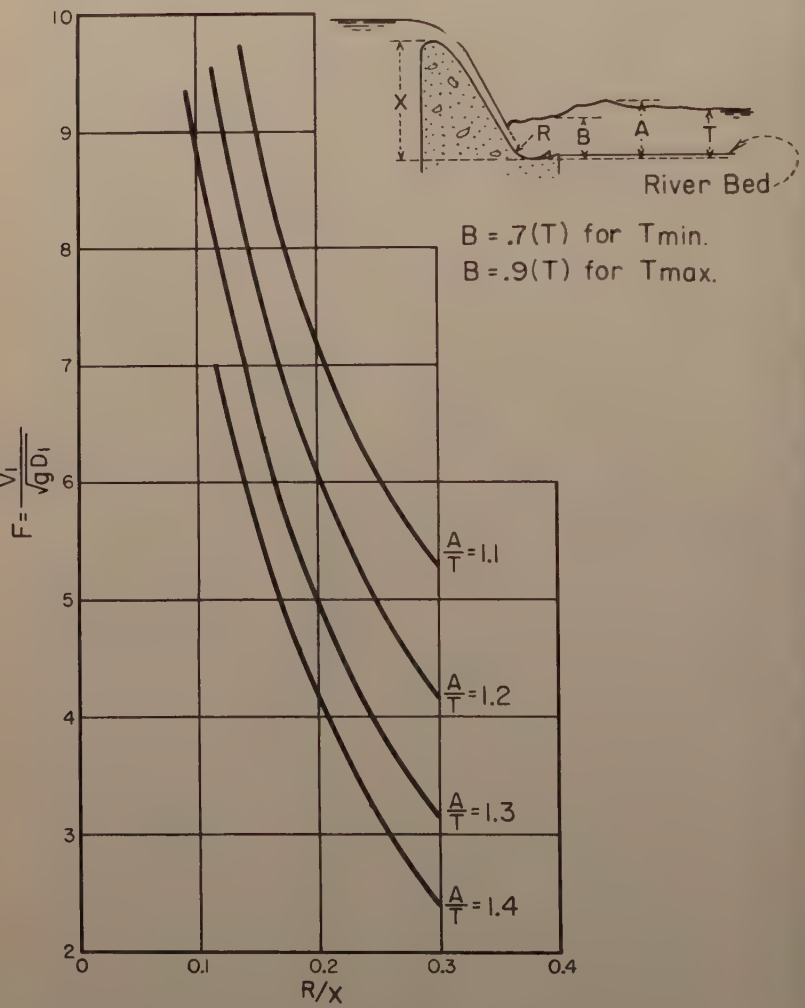

WATER SURFACE PROFILE CHARACTERISTICS
(FOR SLOTTED BUCKETS ONLY)

Table 3

EXAMPLES OF BUCKET DESIGN PROCEDURES

	Angostura Dam				Grand Coulee Dam	Trenton Dam	Missouri Diversion Dam
Q (1,000 cfs)	247	180	100	40	1000	133	90
HW Elev	3198.1	3191.0	3181.5	3170.4	1291.65	2785	2043.4
Crest Elev	3157.2	3157.2	3157.2	3157.2	1260	2743	2032
H	40.9	33.8	24.3	13.2	31.65	42	11.4
W	274	274	274	274	1650	266	644
q	901	657	365	146	606	500	140
TW Elev	3114	3106	3095	3084	1011	2700.6	2018.3
*$\frac{V_1^2}{2g}$	84.1	85.0	86.5	86.4	280.65	84.4	25.1
*V_1 (ft/sec)	73.6	74	74.6	74.5	134.4	73.7	40.2
**$\frac{V_1}{V_1}$	0.98	0.98	0.97	0.93	0.91		0.98
**V_1	72.2	72.5	72.4	69.3	122.4	66.3	39.4
**$\frac{V_1^2}{2g}$	80.9	81.6	81.4	74.6	233.0	68.3	24.1
D_1	12.48	9.06	5.04	2.11	4.95	7.54	3.55
F	3.61	4.25	5.68	8.42	9.70	4.25	3.70
$D_1+\frac{V_1^2}{2g}$	93.38	90.66	86.44	76.71	237.95	75.84	27.65
$\frac{R}{D_1+\frac{V_1^2}{2g}}$	0.50	0.43	0.30	0.16	0.12	0.43	0.49
R	47	39	26	12	28.5	33	14
R (recom'd)	40	40	40	40	30	35	12.5
$\frac{R}{D_1+\frac{V_1^2}{2g}}$	0.43	0.44	0.46	0.52	0.13	0.46	0.45
$\frac{T_{min}}{D_1}$	5.4	6.5	9.1	15.3	14.7	6.5	5.6
T_{min}	67	59	46	32.5	73	49	20
$\frac{T_{max}}{D_1}$	5.7	7.9	17.6	100	23	13.0	8.9
T_{max}	71	72	89	210	114	98	32
$\frac{T_s}{D_1}$	5.0	6.0	8.2	14.4	12.6	6.0	5.2
T_s	62	54	41	30	63	45	18

Note: See Figure 14 for definition of symbols.
Dimensions are in feet unless otherwise noted.
*Theoretical velocity. **Actual velocity.

The actual velocity is less than theoretical at this point, because of frictional resistance on the spillway face. Using Figure 22, the actual velocity is found to be 91 percent of theoretical. Figure 22 is believed to be reasonably accurate, but since only a limited amount of prototype data were available to develop the chart, information obtained from it should be used with caution. The actual velocity, V_A, in this example is 91 percent of 134.4, or 122.4 feet per second. The corresponding depth of flow D_1 on the spillway face is $\frac{q}{V_1}$ or 4.95 feet. Having determined D_1 and V_1, the Froude number is computed to be 9.7.

Entering Figure 15 with Froude number 9.7, the dimensionless ratio for the minimum allowable bucket radius is found to be 0.12 from the solid line curve, from which the radius is computed to be 28.5 feet. In round numbers, a 30-foot bucket radius probably would be used. This is smaller than the 50-foot radius of the solid type bucket that was actually used at Grand Coulee. For the 30-foot radius, the dimensionless ratio would be 0.13. Entering Figure 17 with the dimensionless ratio and the Froude number, $\frac{T_{min}}{D_1}$ is found to be 14.7, from which T_{min} is 73 feet. Similarly, from Figure 18, $\frac{T_{max}}{D_1}$ for the bed elevation below the apron lip is found to be 23, from which T_{max} is 114 feet.

From Figure 20, the sweepout dimensionless depth ratio is 12.6, from which the sweepout depth is 63 feet. Thus, the minimum tail water depth limit of 73 feet provides 10 feet of margin against flow sweeping out of the bucket at the maximum discharge.

Tail water elevation 1011 at Grand Coulee provides 111 feet of tail water depth above riverbed elevation 900. Therefore, the bucket invert should be set no lower than 3 feet below riverbed elevation or more than 38 feet above. In the latter position, there would be no bed scour, and the water surface would be as smooth as possible. However, this location may not be practical, and it may be necessary to set the bucket on bedrock so that the invert is more than 3 feet below the riverbed.

The data in Figure 13 and the curves of Figure 21 may be used to obtain an approximate water surface profile if the bucket invert is placed near channel bed elevation 900. For F = 9.7 and $\frac{R}{X} = \frac{30}{360} = 0.093$; $\frac{A}{T} = 1.3$. The maximum height of boil A is then 1.3×111, or 144 feet above the bucket invert and 33 feet above the tail water. In the bucket, the depth of water B would be 90 percent of 111 feet, or approximately 100 feet. The maximum difference (A-B) would be about 44 feet for the design tail water. The length and location of the boil may be estimated from the data in Figure 13.

Another solution would be to use a larger bucket radius. For a 50-foot radius bucket, which is the radius of the solid bucket actually used at Grand Coulee, the tail water depth limits are 78 and 183 feet, and sweepout depth is 67 feet. Thus, the bucket invert can be placed below the riverbed, but the apron lip should be set about 0.05R, or 2.5 feet above riverbed elevation. If the 50-foot radius bucket is placed below riverbed elevation so that the bed slopes upward from the apron lip, the ratio $\frac{T_{max}}{D_1}$ is 20.5, Figure 18, and

FIGURE 22

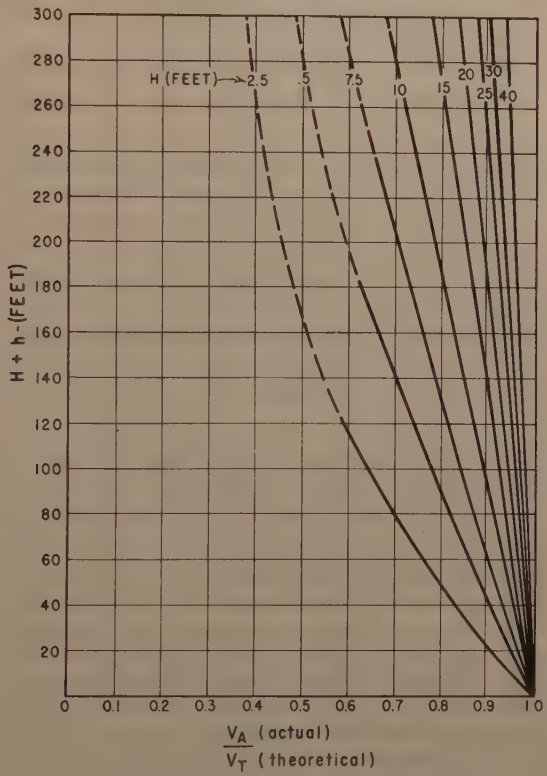

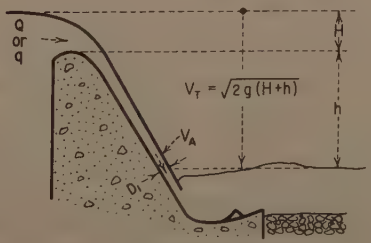

CURVES FOR DETERMINATION OF VELOCITY ENTERING BUCKET FOR STEEP SLOPES 0.8:1 TO 0.6:1

the upper depth limit is computed to be only 101 feet. In this case, the flow from the apron might scour the channel bed because the tail water depth above the bucket invert is greater than the maximum limit, and a still larger bucket radius would be required.

If the invert of the 50-foot radius bucket is placed at bed elevation to provide 111 feet of tail water, $\frac{R}{X} = 0.14$ and $\frac{A}{T} = 1.1$. The height of the boil then would be about 122 feet above the bucket invert, or 11 feet above tail water. The water in the bucket, 80 percent of 111, would be 89 feet deep. The 50-foot bucket would provide a smoother water surface profile than the 30-foot bucket as is shown by comparing the 11-foot high boil with the 33-foot high boil.

Before adopting a design, all factors which might affect the tail water range should be investigated; i.e., large or sudden increases in spillway discharge and effects of discharges from outlet works or powerplant. Tail water elevations for flows less than maximum should also be examined. If V_1 is more than 75 feet per second, pressures on the teeth should be investigated on a hydraulic model.

Discharges for maximum design and less than maximum were investigated for the Angostura installation in Table 3, using the methods presented in this paper. These computations show that the bucket radius obtained for the maximum flow is larger than necessary for the smaller flows and that the tail water depth range for satisfactory performance is greater for smaller flows than for the maximum flow.

The Angostura analysis in Table 3 shows, too, that the bucket radius determined from the Angostura model study is smaller than the radius shown in the table, indicating that the methods presented in this paper provide a factor of safety. This is a desirable feature when hydraulic model studies are not contemplated. On the other hand, hydraulic model studies make it possible to explore regions of uncertainty in particular cases and help to provide the absolute minimum bucket size consistent with acceptable performance.

Other examples in Table 3 include an analysis using the data from Trenton Dam spillway, which utilizes a long flat chute upstream from the energy dissipator. Friction losses are considerably higher than would occur on the steep spillways for which Figure 22 was drawn. In this example, actual velocity measurements taken from a model were used.

Tail water requirements for bucket versus hydraulic jump

In general, a bucket-type dissipator requires a greater depth of tail water than a stilling basin utilizing the hydraulic jump. This is illustrated in Table 4 where pertinent data from Table 3 are summarized to compare the minimum tail water depth necessary for a minimum radius bucket with the computed conjugate tail water depth D_2, for a hydraulic jump. Line 6 shows T_{min} for the buckets worked out in the section Practical Applications. Line 7 shows the conjugate tail water depth required for a hydraulic jump for the same Froude number and D_1, determined from the equation

$$\frac{D_2}{D_1} = 1/2 \sqrt{1 + 8F^2} - 1 .$$

Table 4

COMPARISON OF TAIL WATER DEPTHS REQUIRED FOR BUCKET AND HYDRAULIC JUMP

		Angostura Dam	Angostura Dam	Angostura Dam	Angostura Dam	Grand Coulee Dam	Grand Coulee Dam	Trenton Dam	Missouri Diversion Dam (not built)
1	Q in thousands cfs	247	180	100	40	1,000	1,000	133	90
2	V_1 ft/sec	72	72	73	70	122.4	122.4	66	39
3	D_1 ft	12.5	9.1	5.0	2.1	5.0	5.0	7.6	3.6
4	F	3.6	4.3	5.7	8.5	9.7	9.7	4.2	3.7
5	T_{max} ft	71	72	89	210	114	183	98	32
6	T_{min} ft	67	59	46	32	73	78	49	20
7	T_{conj} ft	57	52	38	24	66	66	40	16
8	Bucket radius ft	47	39	26	12	30	50	35	12.5

Note: If a larger than minimum bucket radius is used, the required minimum tail water depth becomes greater, as shown for the two Grand Coulee bucket radii.

SUMMARY

The slotted bucket, Figure 1B, may be used as an energy dissipator at the base of an overfall. Tests showed the slotted bucket to be superior to the solid bucket in all respects. Wherever practicable, the higher teeth recommended in Design Modification II, Figure 6, should be used.

A simplified version of the seven steps required to design a bucket is given below. The letter symbols refer to Figure 14.

1. Determine Q, q (per foot of bucket width), V_1, D_1; compute Froude number from $F = \frac{V_1}{\sqrt{gD_1}}$ for maximum flow and intermediate flows. In some cases, V_1 may be estimated from Figure 22.

2. Enter Figure 15 with F to find bucket radius ratio from which minimum allowable bucket radius, R, may be computed.

3. Enter Figure 17 with bucket radius ratio and F to find minimum depth limit ratio from which minimum tail water depth limit, T_{min}, may be computed.

4. Enter Figure 18 as in Step 3 above to find maximum tail water depth limit, T_{max}.

5. Set bucket invert elevation so that tail water curve elevations are between tail water depth limits determined by T_{min} and T_{max}. Keep apron lip

and bucket invert above riverbed, if possible. For best performance, set bucket so that the tail water depth is nearer T_{min}. Check setting and determine factor of safety against sweepout from Figure 20 using methods of Step 3.

6. Complete the design of the bucket using Figure 1 to obtain tooth size, spacing, dimensions, etc.

7. Use Figures 13 and 21 to estimate the probable water surface profile in and downstream from the bucket. The sample calculations in Table 3 may prove helpful in analyzing a particular problem.

ACKNOWLEDGMENTS

The bucket tests described in this paper are of recent origin although bucket tests in general have been made since about 1933. Some of the early tests were valuable in this study in that they helped to point the way for the later tests and eliminated certain bucket schemes from further consideration. These early tests were conducted by J. H. Douma, C. W. Thomas, J. W. Ball, and J. N. Bradley. Later tests were made by R. C. Besel, E. J. Rusho, and J. N. Bradley under the laboratory direction of J. E. Warnock. The final tests to develop the slotted bucket and generalize the design were made by G. L. Beichley under the supervision of A. J. Peterka and J. N. Bradley and laboratory direction of H. M. Martin. Some of the material contained in this paper was submitted by G. L. Beichley, as a thesis for the degree of Master of Science, University of Colorado. All tests and analyses were conducted in the Bureau of Reclamation Hydraulic Laboratory, Denver, Colorado.

Journal of the
HYDRAULICS DIVISION
Proceedings of the American Society of Civil Engineers

PERFORMANCE OF FLOOD PREVENTION WORKS DURING THE 1957 FLOODS[a]

Charlie M. Moore,[1] M. ASCE

SYNOPSIS

The hydrologic and structural performance of watershed protection and flood prevention works of the Soil Conservation Service in Arkansas, Oklahoma and Texas during the severe storms and floods of April, May and June, 1957 is discussed in this paper. The design and construction of upstream floodwater retarding structures, the new concept of utilization of vegetated earth spillways in combination with reservoir storage in the design of structures of this type is introduced; and the actual tests of the structures during the storms are evaluated.

INTRODUCTION

The watershed protection and flood prevention work of the Soil Conservation Service is done in cooperation with Soil Conservation Districts and other State subdivisions such as Watershed Districts, Conservancy Districts, Water Control and Improvement Districts, Levee Districts, Drainage Districts, Irrigation Districts, and others. A watershed protection and flood prevention program includes proper land use and treatment in combination with structural works of improvement such as floodwater retarding structures, floodways, channel improvement, floodwater diversions, and sediment control and grade stabilization structures.

Watershed protection and flood prevention work is being carried on under three different authorizations. The Flood Control Act of 1936 included authorization for works of improvement in the Washita River watershed in Texas and Oklahoma, and the Trinity and Middle Colorado River watersheds

Note: Discussion open until March 1, 1960. To extend the closing date one month, a written request must be filed with the Executive Secretary, ASCE. Paper 2201 is part of the copyrighted Journal of the Hydraulics Division, Proceedings of the American Society of Civil Engineers, Vol. 85, No. HY 10, October, 1959.

a. Presented at the October, 1958, ASCE Convention in New York, N. Y.

1. Head, Design and Construction, Eng. and Watershed Planning Unit, SCS, Fort Worth, Tex.

Texas. A "pilot" watershed program, implemented by an item in the 1954 Appropriation Act, included the Six Mile Creek watershed, Arkansas; Double Creek watershed, Oklahoma; and the watersheds of Green, Calaveras and Escondido creeks and Cow Bayou, Texas. Expansion of watershed activities nationwide was authorized by Public Law 566, enacted in 1955, but operations had only started in a few watersheds in this area by the time of the 1957 storms.

Hydrologic Conditions

For 77 months, October 1950 through February 1957, Oklahoma and Texas suffered the most severe drouth of recorded history. Normal or above-normal rainfall was recorded for only 16 months during the drouth period in Texas. Consequently, watershed cover conditions were far below normal over much of the area when the 1957 spring storms occurred.

Excessive rainfall began on April 19 and continued through most of June. Rainfall exceeding 150 percent of normal occurred in Texas, Oklahoma and western Arkansas during April and May. Storm conditions of this intensity and frequency had not been approached since 1908.

During this critical storm period from 35 to 40 inches of rainfall were recorded at several locations. In the Upper Trinity and Brazos Rivers watersheds, many sub-watersheds had from 20 to 35 inches of rain in the 36-day period. The average annual long-time rainfall records for this area range from 27 to 38 inches. The mean depth of rainfall over the three states was 19 inches. This is equivalent to 445 million acre-feet of water, or enough to fill the flood control pool of Lake Texoma 165 times.

Maximum daily rainfall generally ranged from 4 to 10 inches. The maximum 2-day rainfall of 20 inches occurred at Hennessey, Oklahoma. Monthly maximums recorded were 20.48 inches at Glenfawn, Texas; 22.38 inches at Hennessey, Oklahoma; and 19.07 inches at Sparkman, Arkansas. The weighted rainfall on the Honey Creek watershed was 30.5 inches in 37 days, April 19 to May 26.

Fig. 1 shows an isohyetal map of rainfall for the 3-month period. Fig. 2 shows the location of a number of watershed projects in which works of improvement for watershed protection and flood prevention had been completed or were in progress.

Total runoff for the 3-month period far exceeded previous records for both large and small drainage areas. Table 1 shows a comparison, for several watersheds, of the 1957 April-May-June runoff with the mean runoff for that period.

The runoff from the series of storms inundated 11,575,000 acres of flood plain lands along the tributary streams in the 3-state area, causing damages estimated at more than $156,800,000. Ten lives were lost in creek floods in Texas; 4 in Oklahoma.

Before proceeding further with the performance of the floodwater retarding structures during the storms it might be well to discuss the general design and function of such a structure and its spillways.

Structure Design

Floodwater retarding structures, as the name implies, are of the retarding not the retention type. Constructed in compliance with State laws, they releas

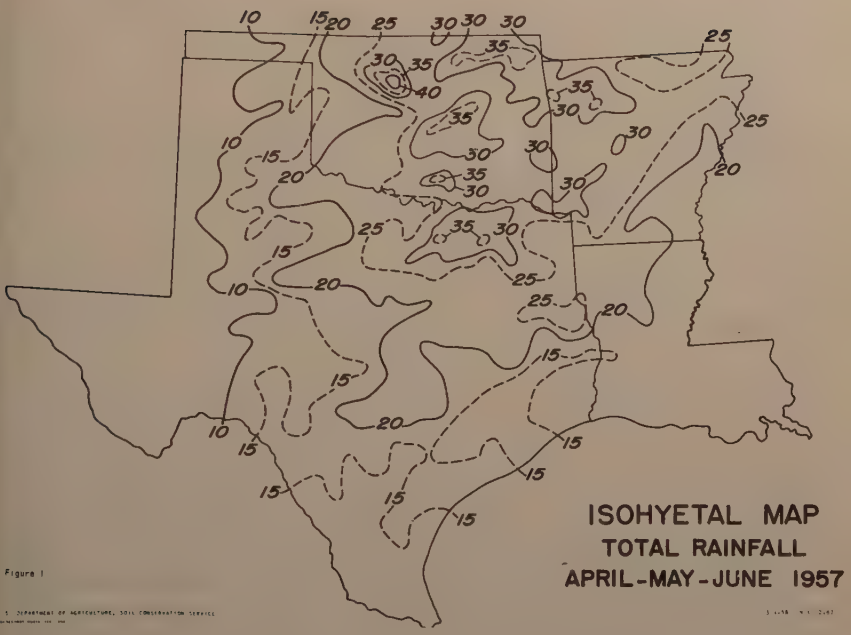

Figure 1

U. S. DEPARTMENT OF AGRICULTURE, SOIL CONSERVATION SERVICE

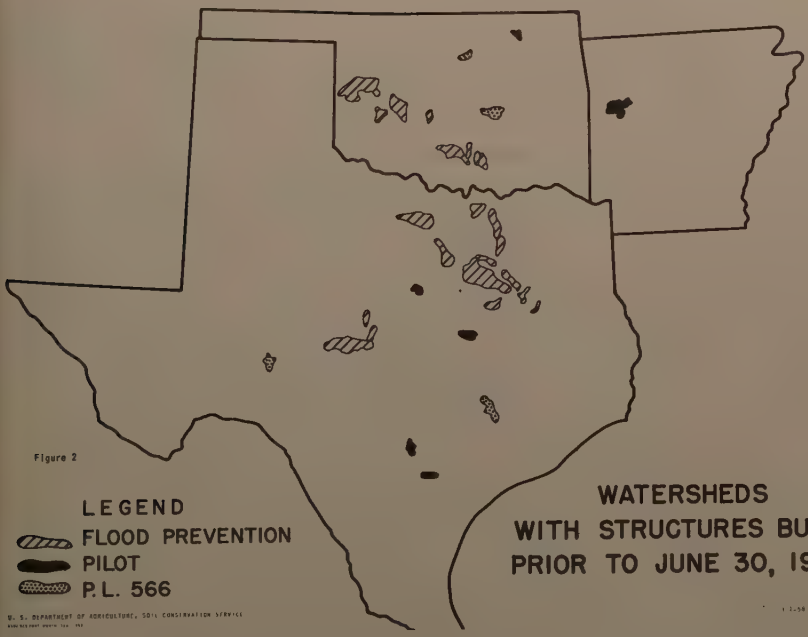

Figure 2

U. S. DEPARTMENT OF AGRICULTURE, SOIL CONSERVATION SERVICE

TABLE 1

April-May-June Runoff
Watershed-Inches

Watershed	1957	Mean
Little River (Horatio, Ark.)	20.0	7.4
East Fork, Trinity River (Lavon Res.)	16.7	---
Trinity River (Dallas, Tex.)	11.5	1.6
Red River (Fulton, Ark.)	11.4	2.1
Washita River (Durwood, Okla.)	5.8	1.5
Cimarron River (Perkins, Okla.)	3.1	0.5

floodwaters automatically through a concrete pipe principal spillway, at a rate designed to prevent flooding of the stream channel below. Fig. 3 is a section of a typical floodwater retarding structure. In general, the criteria for design of the detention pool storage of these structures for protection of agricultural areas range from approximately 3 inches of watershed runoff in western Texas to over 6 inches in eastern Texas; from 3 inches in western Oklahoma to about 5 inches in eastern and southern Oklahoma; and about 4.5 inches in northwest Arkansas. The average total storage for the structures built to date in this area is approximately 1000 acre-feet, with approximately 800 acre-feet being detention storage and 200 acre-feet sediment storage. They are designed to have a 50-year life before the sediment encroaches on the detention storage pool.

Usually the emergency spillways of these structures are earthen and are protected with vegetation adapted to the area in which the dams are located. Generally, this is Bermuda grass sod, which gives very satisfactory results in most of the watersheds of this part of the country. In western Texas and Oklahoma, native grasses and King Ranch bluestem have proved to be satisfactory. Some spillways are founded in rock and vegetation is not required.

To function properly, the spillways must be designed to prevent excessive velocities. Experimental studies at the Outdoor Hydraulics Laboratory of the Agricultural Research Service at Stillwater, Oklahoma, and tested by field application over wide areas, have determined the limitations that must be placed on each kind of vegetation used in channels and spillways. For example, Bermuda grass sod will stand velocities up to 8 feet per second on erosion-resistant soils and 6 feet per second on the less erosion-resistant soils. King Ranch bluestem, a bunch grass, will stand velocities up to 3.5 feet per second without damage. The spillways are designed to have flow depths and widths commensurate with permissible velocities. Much higher velocities are permissible in rock spillways. The maximum velocities pertain to intermittent flows of only a few hours duration.

The emergency spillways are designed to have a 50-foot level crest control section and a straight exit channel below the control section. Any

necessary curvature in the spillway is placed in the entrance or forebay section leading to the control section. The forebay is excavated 2 to 3 feet below the elevation of the crest, or is reverse-graded from the crest to the forebay entrance.

Generally, the widths vary from a minimum of 50 feet to a maximum of 400 feet with a flow depth not exceeding about 4 feet under extreme storm conditions. The side slopes of the spillway generally range from 2:1 to 3:1, except in rock excavation where much steeper slopes can be used. Fig. 4 illustrates the various features of the emergency spillway design.

The exit channel of the spillway is extended to a point where it is considered safe to release the water. Safe velocities are maintained in the exit channel by properly proportioning the spillway as to width, depth of flow, and gradient. Erosion may occur beyond the end of the exit channel, but with good maintenance in this area the exit channel should be stable.

It might be noted here that the use of vegetated earth spillways for flood prevention structures with capacities up to several thousand acre-feet is a material divergence from the accepted principles employed by the engineering profession in past design. Detention dam operation, involving a controlled outlet and temporary storage to reduce frequency of operation of emergency spillways to the point where vegetated spillways will function satisfactorily, has been used with good success. This principle of design has resulted in significant reductions in the cost of floodwater retarding structures with very little sacrifice in safety or permanence of the installation.

The structure embankments in this area generally range from 25 to 50 feet in fill height, the average being about 40 feet. The embankment volumes range from about 26,000 cubic yards to slightly over 300,000 cubic yards, the average being about 97,000 cubic yards. The average cost to date of $38,000 per structure, including all appurtenances, is about 40 cents per cubic yard of embankment.

Fig. 5 is a completed floodwater retarding structure of less than average size, showing vegetated embankment and spillway and partially filled flood pool. The structure is Site No. 11, located in the Pilot and Sister Grove Creek watersheds of the Trinity River near Dallas, Texas. It is 25 feet high and contains 87,000 cubic yards of embankment. The drainage area is 1224 acres, with 530 acre-feet of flood storage and 187 acre-feet of sediment storage space.

Although the embankments are generally homogeneous compacted fills it is necessary at times to use earth sections with rock blankets to fully utilize the material where rock is encountered in the emergency spillway. A typical section of this type of embankment is shown in Fig. 6. This structure is 49 feet high and contains 52,865 cubic yards of embankment. It has a drainage area of 1920 acres with 720 acre-feet of flood storage and 85 acre-feet of sediment storage space.

Dams with this type section are more numerous in the northwestern part of Arkansas and in the western and southwestern parts of Texas, because rock formations are more prevalent in these areas. Economics of design and construction require the utilization of all suitable materials available on the site. Rock from emergency spillways has been used in rock blankets on the upstream and downstream slopes. The rock is placed in lifts along with the impervious section. The larger size rock is pushed to the outer edge of the embankment by means of a rock rake attached to the front of a bulldozer. Gradation is accomplished by smaller rock fragments and spalls sifting

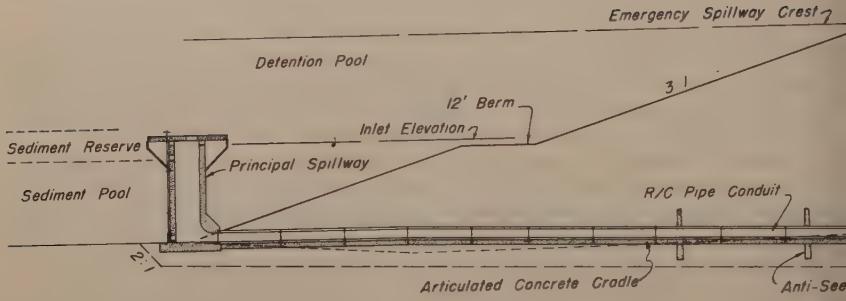

U. S. D. A. SOIL CONSERVATION SERVICE, FORT WORTH, TEXAS
USDA SCS FORT WORTH TEX 1959

TYPICAL SECTIO

through the teeth, thus leaving the finer material closer to the impervious section. In addition, a designed filter is placed between the compacted impervious section and the rock blanket.

Figs. 7 and 8 illustrate the construction of rock-fill blankets and toe section for Site No. 8, Green Creek Watershed, near Dublin, Texas. The dam is 48 feet high and contains 228,655 cubic yards of material. It has a flood pool storage of 2069 acre-feet and a sediment reserve pool of 294 acre-feet. The drainage area is 6880 acres.

Often it is necessary to install foundation drains and relief wells for control of the phreatic line, seepage under the embankment, and piezometric pressures in the foundation. Fig. No. 9 illustrates the location and installation of a drainage system in the foundation of Site No. 17, Barnitz Creek Watershed, Washita River, Oklahoma. This drain consists of 6-inch diameter perforated helicor pipe surrounded with a designed filter material. It is located approximately one-third of the distance upstream from the toe of the embankment to the centerline of the dam. The depth of the drain below normal ground line ranges from 6 feet near the right abutment to about 8 feet at the outlet end near the stream channel. The drain discharges into the outlet channel for the principal spillway, where frequent discharges will prevent silting of the drain outlet.

Where relief wells are needed they are located downstream from the toe of the embankment. The wells are installed using galvanized pipe and well screens with designed filters. They are spaced horizontally as needed and provide relief from piezometric pressures in the deeper underlying aquifers. The wells are connected by means of a collector line which also discharges at the end of the principal spillway.

Construction specifications and designs are based on thorough geologic site investigations and soil mechanics laboratory analyses. Standard construction methods are used in placement of embankment material. Compaction control is based on laboratory analyses. Construction methods are adapted where necessary to fit the equipment generally available for this type of construction.

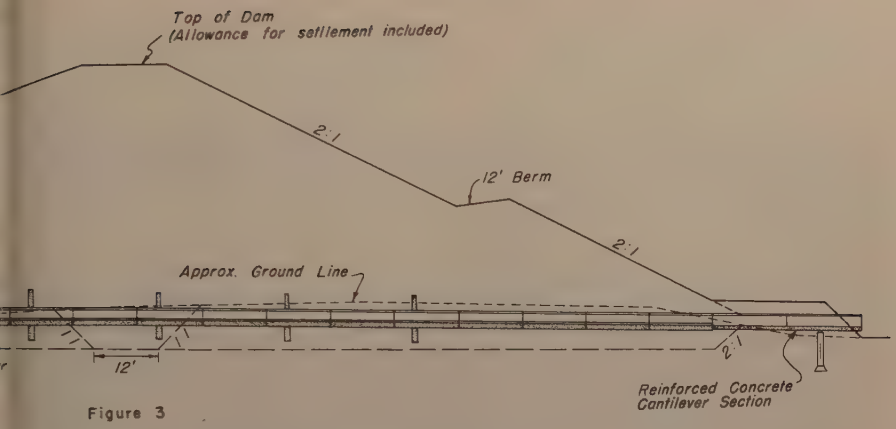

Figure 3

A FLOODWATER RETARDING STUCTURE

Not to Scale

8-27-58 4-R-12612

Performance of Structures

There were 367 upstream floodwater retarding structures in operation in this area by April, 1957, with a combined flood detention capacity of about 285,200 acre-feet. Of these, 195 were in Texas, 149 in Oklahoma, and 23 in Arkansas. Through the process of filling, releasing and refilling during the storm period the structures detained and released in an orderly manner about 534,800 acre-feet of floodwater. If all feasible tributary watershed work for flood prevention had been completed, it is estimated that 33 million acre-feet of detention storage would have been available to control 62 million acre-feet of floodwater.

Of the 367 structures mentioned only 99 had flow through the emergency spillways. Three spillways flowed 4 times, 8 flowed 3 times, 23 flowed twice, and 65 flowed once. The maximum duration of flow was about 14 days. The depth of flow ranged from a few tenths of a foot to as much as 2.3 feet at the control section.

Of the 99 spillways which flowed, 62 were undamaged and 23 others required only slight repair. Moderate repairs ($500 to $1200) were needed on 9 spillways, and 5 (four of which were not yet vegetated) required extensive repairs averaging about $5,000. At the time of the flows 53 spillways had fair to good vegetative cover; the cover was poor on 36 spillways; and 5 newly-completed spillways were unprotected. The severe drouth was the principal cause of below-normal spillway cover conditions. The total cost of spillway repairs amounted only to 1.05 percent of the total construction cost of structures installed in the subwatersheds in Texas where 69 of the spillway flows occurred. This cost was very nominal considering the fact that these structures were subjected to storms exceeding a 100-year frequency. The total cost of repairs was even less in Oklahoma and Arkansas.

The spillways which sustained the greatest damage had inherently bad soil conditions and adequate vegetative cover had not yet been established. For instance, the spillway on Cow Bayou Site 4 near Waco, Texas was underlain

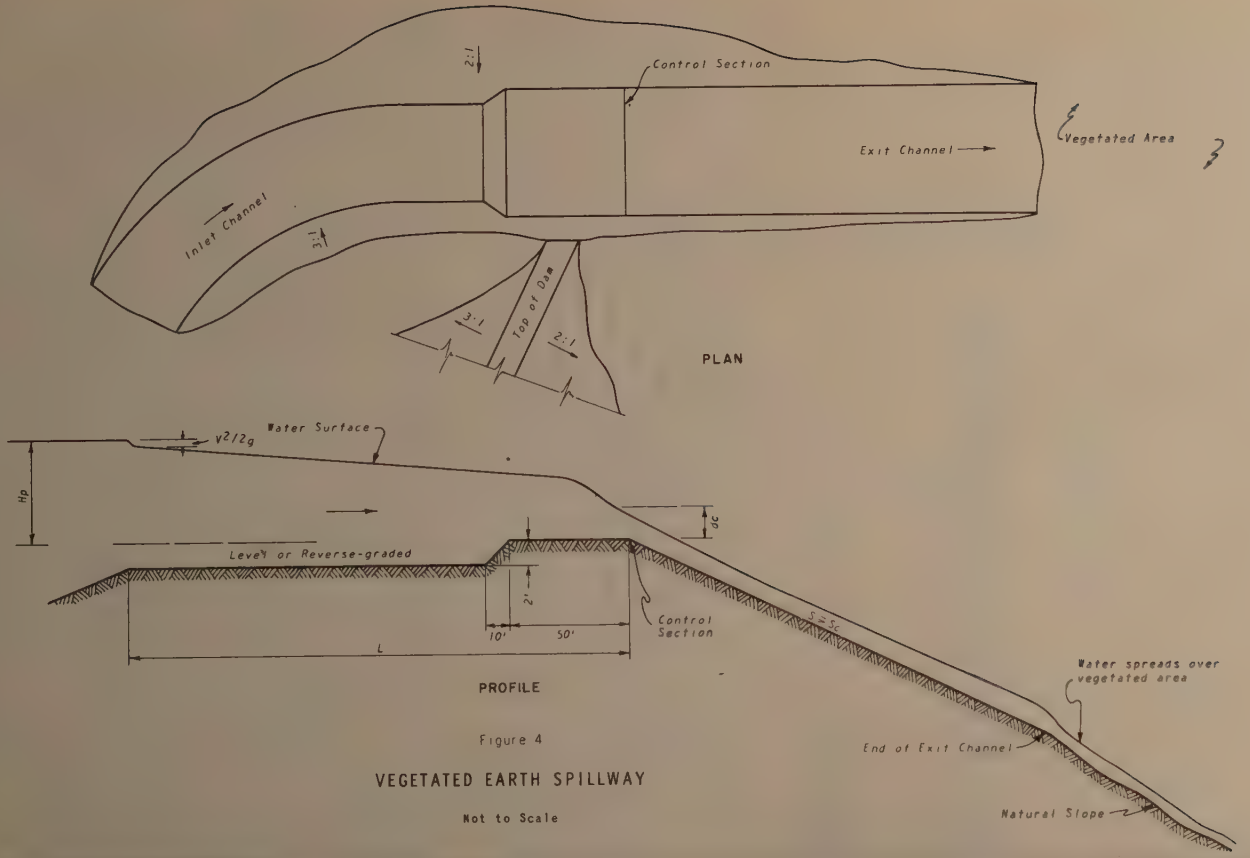

Figure 4

VEGETATED EARTH SPILLWAY

Not to Scale

U S D A SOIL CONSERVATION SERVICE FORT WORTH, TEXAS
USDA-SCS FORT WORTH TEX -1959

Figure 5

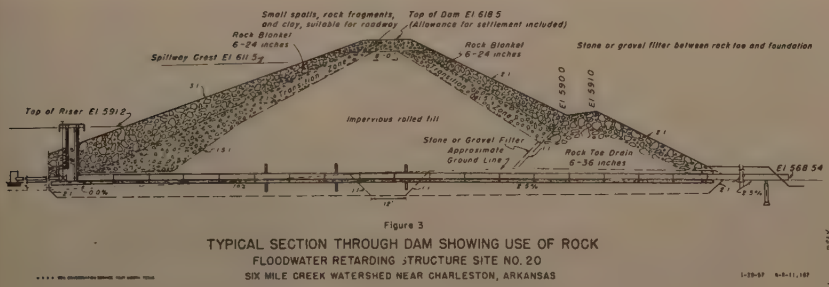

Figure 3
TYPICAL SECTION THROUGH DAM SHOWING USE OF ROCK
FLOODWATER RETARDING STRUCTURE SITE NO. 20
SIX MILE CREEK WATERSHED NEAR CHARLESTON, ARKANSAS

Figure 6

in part by the Eagle Ford Shale formation. It was very difficult to core this material during geologic investigations due to its hardness. In the same spillway it was necessary to use compacted fill in a 15-foot deep gully, extending up the center of the exit channel. During the continuous flow over a period of several days the hard shale became soft and eroded very badly, whereas the compacted fill carried the flows without any appreciable damage.

The spillway on Honey Creek Site No. 8 was ended on the hillside above deep black alluvium. Severe damage was sustained due to the erodibility of the black soil and the abrupt overfall downstream over which the discharge passed after leaving the spillway.

Figure 7

Figure 8

Based on these and other observations future spillway location and design will avoid this type of shale, will include extension of the exit channel through alluvium to stabilized grade, and will perhaps utilize a greater thickness of compacted fill in the exit channels than previously thought desirable.

Figure 9

Returning to the hydrologic features of the storms, Figure 10 shows the inflow and outflow hydrographs for the floodwater retarding structure at Site 6, Six Mile Creek, Arkansas, for the storm of April 27, 1957.

Rain began on April 18 and continued daily through April 24, amounting to 3.53 inches. Another 2.4 inches fell on April 26 and the runoff (2.2 inches) filled the structure detention pool nearly to the emergency spillway crest. Pool inflow continued during the 9-hour interval between rains, and the 1.8 inches of runoff from the 2.0 inches of rain on April 27 produced the hydrographs shown. Although the detention pool was full when the storm began and emergency spillway flow reached a momentary depth of 1.45 feet, the peak discharge was only about 40 percent of the peak rate of inflow. The automatic release from the drop inlet principal spillway remained virtually constant at 24 second-feet.

Fig. 11 illustrates the effect of floodwater retarding structures on peak discharge. The first two examples show that even when there is a large spillway flow the peak discharge is reduced by approximately 50 percent, due to the effect of spillway storage in the pool. When there is no spillway flow, as in the last two examples, the reduction in peak discharge is very high.

For the 3-month storm period Figure 12 shows, for three representative structures, the relationship between the total volume of runoff; the runoff volume actually detained; and the designed floodwater retarding capacity of each structure.

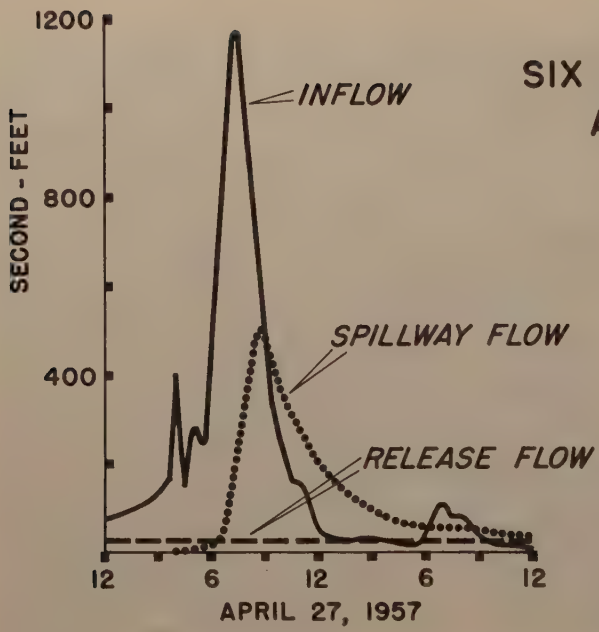

Figure 10

U. S. DEPARTMENT OF AGRICULTURE, SOIL CONSERVATION SERVICE

3-1-58 4-L-12189

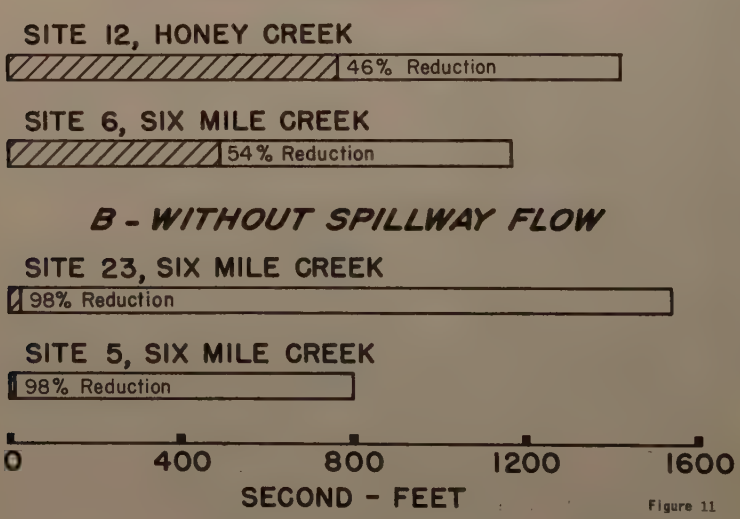

Figure 11

U. S. DEPARTMENT OF AGRICULTURE, SOIL CONSERVATION SERVICE

3-1-58 4-L-12189

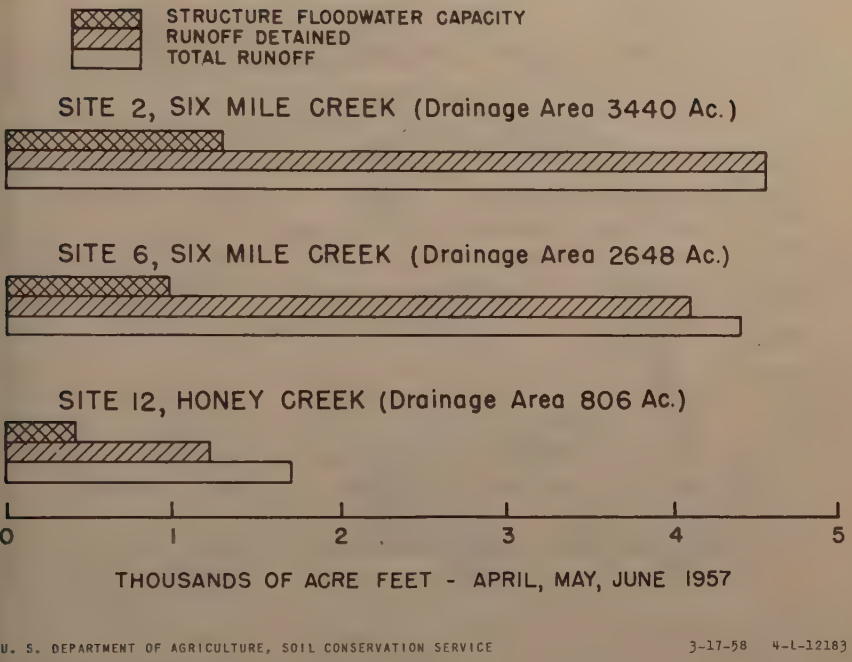

Figure 12

Since there was no emergency spillway flow at Site 2, Six Mile Creek watershed, the structure detained the total runoff, amounting to 3-1/2 times the designed floodwater retarding capacity. The structure at Site 6, Six Mile Creek, detained 94 percent of the total runoff, or more than 4 times the detention pool capacity. At Site 12, Honey Creek, where the emergency spillway flowed twice for a total of about 10 days, the structure detained 71 percent of the runoff, or almost 3 times the capacity of the detention pool.

Fig. 13 is a structure operation graph for Site 12, Honey Creek, for the 3-month period. Amounts of rainfall by days also are shown.

The graph shows that on April 24 the elevation of the water surface in the detention pool reached a point 3 feet below the emergency spillway crest, and that it did not fall more than 4 feet below spillway crest for 42 days. Automatic release of water through the principal spillway continued from April 19 through June.

The effectiveness of watershed protection and flood prevention work in preventing flood damages is illustrated in Fig. 14. Except in the Chigley Sandy Creek example, which is only for one storm, the data covers the 3-month period. For four typical watersheds the chart contrasts estimated flood damages without and with a complete watershed program. Other benefits resulting from the works of improvement were not considered in this analysis.

Studies of flood damages during and following the 1957 spring floods indicated that if no watershed protection and flood prevention work had been done the total flood damages in creek watersheds in Arkansas, Oklahoma and

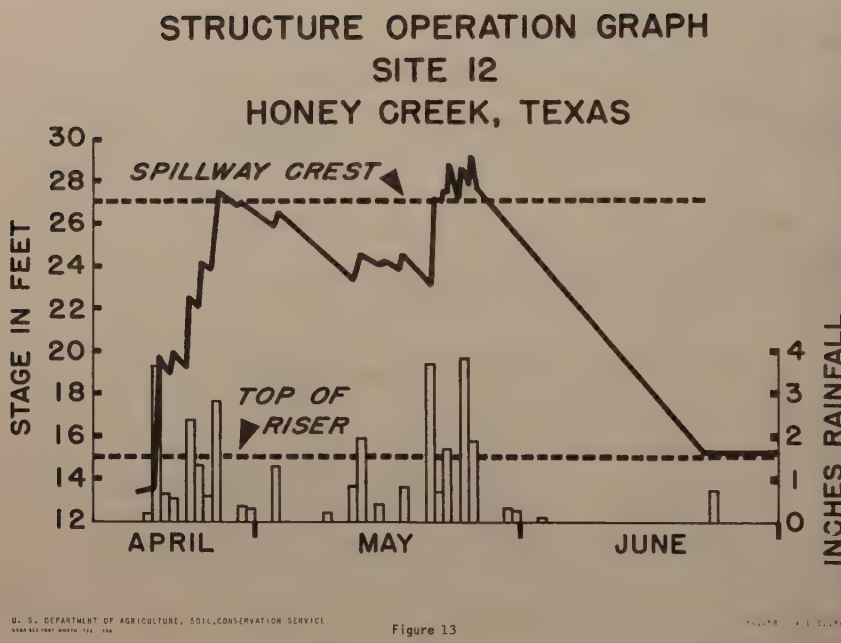

Figure 13

Texas would have amounted to $159,208,000. It was estimated that the work which had been done prevented $2,162,000 in flood damages.

Further analysis indicated that if similar work had been completed in all creek watersheds in the 3-state area in which it appears to be feasible, a total of $109,320,000 of flood damages would have been prevented, or a reduction of about 70 percent. Also, it appears that flood peaks would have been reduced sufficiently to have prevented the loss of the 14 lives.

A high percent of the needed conservation measures and practices had been applied in watersheds where improvement programs are under way. However, the severe and extended drouth had seriously reduced the amount and quality of vegetative cover in most of Texas and Oklahoma. As a result, during the April storms upland sheet erosion was widespread, and severe in many areas. Cover conditions improved rapidly throughout the area during the storm period, and a reduction in the amount of sheet erosion from the storms in late May and June was very evident.

Studies were made in Texas to determine the effect of cover and soil condition on the depth of moisture penetration during the storm period. In April and May 133 paired borings were made on conservation-treated and unprotected areas with otherwise similar conditions, on cropland, range and pasture. Although there was wide variation in the depth of penetration under the different land use, soil and rainfall conditions, the average was twice as great on protected land as on unprotected.

The performance of the watershed protection and flood prevention work exceeded expectations during this unprecedented series of intense storms,

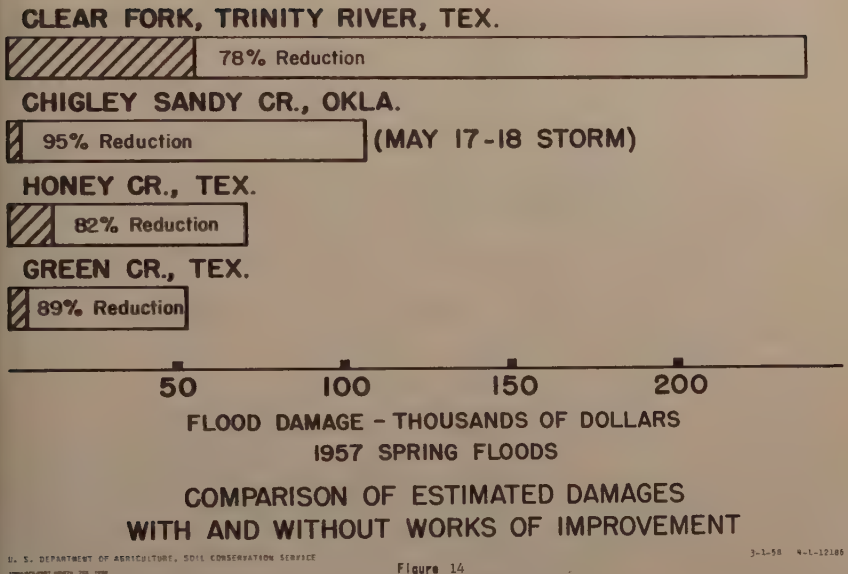

Figure 14

and no major changes in methodology or design criteria appear to be needed. A large amount of valuable technical data was collected, and from its analysis it is hoped to develop worthwhile refinements and improvements in planning and design procedures.

The 1957 spring storms in Arkansas, Oklahoma, and Texas provided a severe test of watershed protection and flood prevention work, and fully demonstrated the effectiveness of protection measures in reducing flood damages.

SUMMARY

The spring storms of 1957 fully tested a great number of upstream floodwater retarding structures and provided a large scale field test by which the hydrologic, design and construction criteria could be evaluated. The evaluation confirmed the fact that vegetated earth spillways for flood prevention structures can be safely used in connection with detention dam operation, involving a controlled outlet and temporary storage to reduce frequency of operation of emergency spillways. This principle of design resulted in significant reductions in the cost of the structures and at a very low relative cost for maintenance following spillway operation.

The effectiveness of watershed protection and flood prevention work in preventing flood damages has been demonstrated, and the effects of similar work in all creek watersheds in the 3-state area in which it appears to be feasible has been pointed out. Through the process of filling, releasing and refilling during the storm period the structures detained and released in an orderly manner almost twice the volume of floodwater as the combined flood detention capacity for which the structures were designed. If all feasible tributary watershed work for flood prevention had been completed, it is estimated that 33 million acre-feet of detention storage would have been available to control 62 million acre-feet of floodwater.

Journal of the
HYDRAULICS DIVISION
Proceedings of the American Society of Civil Engineers

WAVE-INDUCED MOTION OF BOTTOM SEDIMENT PARTICLES[a]

P. S. Eagleson,[1] A.M. ASCE and R. G. Dean,[2] A.M. ASCE

ABSTRACT

Theoretical analyses are presented yielding expressions for incipient motion and net velocity of single spherical bottom sediment particles under oscillatory waves.

These relationships are verified by experiment and are extended to the prediction of equilibrium relationships between local wave characteristics, bottom slope and median particle diameter found on natural beaches.

SYNOPSIS

The problem under study is the mechanics of the motion of sedimentary beach materials, particularly as it applied to their sorting due to selective onshore, offshore transport by shallow-water waves.

A theoretical analysis is presented which yields an equation for the net velocity of a single spherical sediment particle as a function of a resistance coefficient, C_D, the fluid mass transport velocity near the bottom and the beach slope. The equation is verified by laboratory measurements.

Measurements of the incipient motion condition are correlated with Reynolds number by means of a derived resistance coefficient.

By means of existing boundary layer theory both the net sediment velocity and incipient motion expressions are extended separately to the prediction of the equilibrium relationships between local wave characteristics, bottom slope and median particle diameter found on natural beaches. Agreement

Note: Discussion open until March 1, 1960. To extend the closing date one month, a written request must be filed with the Executive Secretary, ASCE. Paper 2202 is part of the copyrighted Journal of the Hydraulics Division, Proceedings of the American Society of Civil Engineers, Vol. 85, No. HY 10, October, 1959.

a. Presented at meeting of Hydraulics Div., ASCE, Massachusetts Institute of Technology, Cambridge, Mass., August, 1957.

1. Assistant Prof. of Hydr. Eng., Hydrodynamics Lab., Dept. of Civ. and Sanitary Eng., Massachusetts Institute of Technology, Cambridge, Mass.
2. Research Assistant, Hydrodynamics Lab., Dept. of Civ. and Sanitary Eng., Massachusetts Institute of Technology, Cambridge, Mass.

with natural beach data was found to be good in both cases but no conclusion was reached with respect to the conditions in nature under which each is applicable.

List of Notations

a	Instantaneous acceleration of fluid or sediment particle, ft./sec.^{2}
A,B,E,P, Q	Coefficients associated with kinematic wave properties, as specified
C	Wave celerity, ft./sec.
C_D	Coefficient of drag
C_L	Coefficient of lift
C_M	Coefficient of virtual mass
C_{Rx}	Coefficient of rolling friction
d	Still water depth, ft.
D	Diameter of sediment particle, mm. or ft., as specified
D_e	Sediment diameter as determined from "equilibrium" criterion, ft. or mm.
D_i	Sediment diameter as determined from "incipient" criterion, ft. or mm.
e	Base of natural logarithms, 2.718. . . . .
——f	Subscript "f" referring to effective kinematic fluid quantity or to physical property of fluid
f	Coefficient associated with kinematic wave properties
F_D	Drag force on sediment particle, lbs.
F_F	Fluid force on sediment particle, resultant of viscous resistance forces, lbs.
F_G	Gravitational force on sediment particle, lbs. (buoyant weight)
F_L	Lift force on sediment particle, lbs. (non-viscous)
F_P	Pressure force on sediment particle, lbs.
F_R	Reaction force on sediment particle, lbs.
F_{RX}	Rolling frictional force on sediment particle, lbs.
F_{VM}	Virtual mass force on sediment particle, lbs.
g	Gravitational constant, 32.2 ft./sec.^{2}
H	Wave height, crest to trough, ft.
——j	Subscript "j" referring to property at elevation, j
j	Distance normal to channel bottom at which maximum fluid mass transport velocity occurs, origin at plane through top of bed roughness particles, mm, or ft. as specified.

k	Mean diameter of roughness particle, mm or ft., as specified
L	Wave length, ft.
M	Moment of forces on sediment particle, ft. lbs.; particle mass, slugs.
$\_\_o$	Subscript "o" referring either to kinematic conditions in region of potential flow or to deep water wave geometry.
R_D	Reynolds number based on net relative fluid-sediment particle velocity.
R_I	Reynolds number, based on instantaneous relative fluid-sediment particle velocity.
$\_\_s$	Subscript "s" referring to sediment
s	Specific gravity of fluid or sediment, as indicated.
t	Time coordinate, sec.
T	Wave period, sec.
$\overline{U}(y)$	Longuet Higgins' fluid mass transport velocity at elevation y ft./sec. or ft./min. as specified.
$\overline{U}_f$	Effective fluid mass transport velocity, ft./sec. or ft./min. as specified.
$\overline{U}_o$	Stokes' theoretical fluid mass transport velocity evaluated near the bottom of the channel, ft./sec. or ft./min. as specified.
v	Instantaneous velocity, ft./sec.
$\overline{V}_s$	Net sediment velocity, ft./sec. or ft./min., as specified.
$\_\_x$	Subscript "x" referring to coordinate direction.
x	Coordinate parallel to beach, positive in direction of wave propagation, origin arbitrary, ft.
$\_\_y$	Subscript "y" referring to coordinate normal to beach.
y	Coordinate normal to channel bottom, positive upwards origin at upper edge of roughness particle, ft.
α	Angle of beach with horizontal, radians
β	A measure of the extent of viscous effects under a wave $(ft.)^{-1}$
γ	Specific weight, $lbs./ft.^3$
ϵ	Coefficient of rolling frictional resistance
θ	Wave phase angle, radians, origin 90° behind wave crest
ν	Kinematic viscosity of fluid, $ft.^2/sec.$ or $cm.^2/sec.$
π	3.1415 . . . .
ρ	Mass density, $slugs/ft.^3$
σ	Angular frequency, rad./sec.
Σ	Symbol indicating summation of quantities.

ϕ Angle between normal to beach and element of sediment particle reaction cone in plane of wave particle motion, radians.

Φ Functional symbol

λ Angle between resultant viscous force and face of beach, radians.

INTRODUCTION

As an oscillatory wave advances into shoaling water, a depth is eventually reached at which the unsteady fluid particle motion caused by the wave reaches the bottom. Shoreward of this point, as the depth decreases and the wave steepens, the particle displacement and velocity increase in magnitude. This unsteady fluid motion at the bottom produces hydrodynamic forces on the sediment particles comprising the beach. Under the proper conditions, these forces may be of sufficient magnitude to initiate and maintain motion of the sediment particles. For sediment densities near that of the fluid, the net sediment motion approaches the mass transport of the fluid.

It is recognized that other wave-induced phenomena such as rip and littoral current, breakers and bed fluidization can cause local motion of bottom sediments, but it is the general motion due to wave passage that is examined here as a possible explanation of the observed banding of sediment properties parallel to many natural beaches.

Ippen and Eagleson[1] made extensive laboratory observations of the behavior of discrete spherical sediment particles under wave action. It is the aim of the present study to expand the theoretical basis of the previous investigation through re-evaluation of existing data and through additional related experiments in order to present the data in terms of familiar physical relationships which may be justifiably extrapolated to natural beach conditions.

Ippen and Eagleson[1] divided the observed motion into two classifications:

1. Incipient sediment motion - an instantaneous condition reached when the resultant of all the active forces on the particle intersects the line connecting the bed-particle contact points.

2. Established sediment motion - an oscillatory or quasi-oscillatory condition of motion reached when for some portion of each wave cycle the moment of the instantaneous active forces exceeds that value necessary to initiate motion. The instantaneous hydrodynamic forces are oscillatory in nature and due to wave asymmetry, their net value (temporal average over one wave period) is always in the onshore direction. Gravity, however, provides an unidirectional offshore force. Thus, the particular local sediment, wave and beach characteristics will determine an offshore gravity force and a net onshore hydrodynamic force, the difference between which will lead to onshore, offshore or no net sediment motion.

This paper will take up these two classifications in the order listed and finally will apply the results of both investigations to natural beaches.

Theoretical Considerations

The details of this development are presented in Reference (2): only the briefest outline of steps is included here.

A. Forces Acting

Figure (1) shows the instantaneous forces acting on a discrete spherical sediment particle on a plane beach roughened with spherical particles of uniform diameter.

The individual forces are defined under LIST OF NOTATIONS.

B. Incipient Motion

Incipient motion has been described above as a condition of unstable equilibrium in which the obliquity of the resultant active force must equal the slope of an element (lying in a plane normal to the wave crests) of the polyhedron bounded by the reaction forces.

For a bed composed of irregular sand grains, the number, inclination and angular orientation of the reaction forces may have infinite variation, the average of which defines a mean, right circular "stability cone" the elements of which make angle ϕ with the cone's axis.

If the viscous resistance and apparent mass forces are assumed to act through the upper edge of the particle and all others through the particle center (see Fig. 1), and if moments are taken about the point of bed particle contact, the conditions of incipient motion may be written:

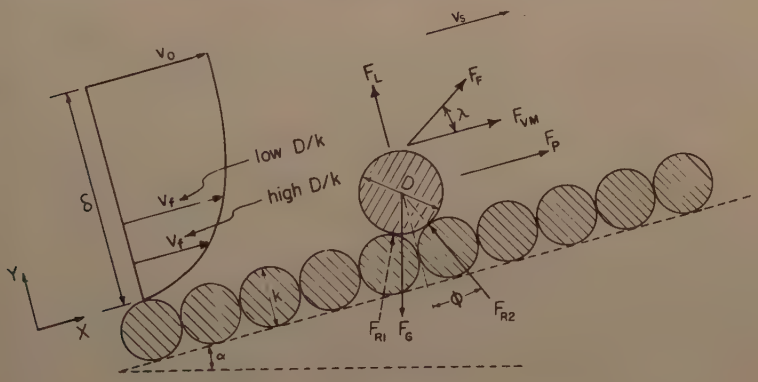

FIG. 1 FORCES ACTING AND IDEALIZED BED-PARTICLE GEOMETRY

$$\Sigma M = 0 = \underbrace{\rho_f \frac{\pi D^3}{16} v_f^2 [C_D(1+\cos\phi)+C_L \sin\phi]}_{\text{Viscous Resistance and Lift}} + \underbrace{\rho_f \frac{\pi D^4}{12}[C_M a_f(1+\cos\phi)+a_o\cos\phi]}_{\text{Apparent Mass and Pressure}} - \underbrace{\rho_f \frac{\pi D^4}{12} g\left(\frac{S_s}{S_f}-1\right)\sin(\alpha+\phi)}_{\text{Gravity}} \quad (1)$$

in which the combined viscous and non-viscous normal forces ($F_F \sin\lambda$ and F_L respectively) are expressed in terms of a lift coefficient, C_L.

C. Established Sediment Motion

Equation of Motion

Assuming that the sediment particle is in motion throughout the entire wave cycle, the established motion condition is expressed by summing all forces parallel to the bottom. For waves shoaling with normal incidence, this is

$$\underbrace{M_s a_s}_{\text{Inertia}} = \underbrace{M_f a_o}_{\text{Pressure}} + \underbrace{C_M M_f (a_f - a_s)}_{\text{Apparent Mass}} + \underbrace{C_D \rho_f \frac{\pi D^2}{8}(v_f - v_s)|v_f - v_s|}_{\text{Drag}} \underbrace{- g(M_s - M_f)\sin\alpha}_{\text{Gravity}} \underbrace{- \epsilon[F_G\cos\alpha - F_F\sin\lambda - F_L]\frac{v_s}{|v_s|}}_{\text{Bottom Resistance}} \quad (2)$$

The following assumptions are now made:

1. The drag force and the bottom frictional force are both linear functions of the relative instantaneous velocity, $(v_f - v_s)$.

2. Convective accelerations of the sediment particles are negligible.

3. The elevation at which the instantaneous velocity and acceleration are applied is independent of time.

4. The instantaneous fluid particle velocities at the edge of and within the bottom boundary layer are given respectively by expression of the form

$$v_o = \sigma A_o \sin\sigma t + 2\sigma B_o \sin 2\sigma t + E_o \quad (3)$$

$$v = A_f \sin\sigma t + B_f \sin 2\sigma t + P_f \cos\sigma t + Q_f \cos 2\sigma t + E_f \quad (4)$$

where the quantities A, B, P, Q, and E are independent of time and $\sigma t = \pi/2$ under the wave crest.

5. The coefficient of apparent mass is constant with time.

Net Sediment Motion

The net sediment velocity may now be obtained by integration of Eq. (2) over one complete wave cycle to yield:

$$\underbrace{C_D \rho_f \frac{\pi D^2}{8}(\overline{U}_f - \overline{V}_s)^2}_{\text{DRAG}} + \underbrace{C_{Rx} \rho_f \frac{\pi D^2}{8}(\overline{U}_f - \overline{V}_s)^2}_{\text{BOTTOM RESISTANCE}} = \underbrace{g(M_s - M_f)\sin\alpha}_{\text{GRAVITY}} \quad (5)$$

where C_D and C_{Rx} are inversely proportional to the relative velocity, $\overline{U}_f - \overline{V}_s$. A detailed derivation of Eq. (5) is presented in Reference (2).

As was pointed out in Reference (1) both $\overline{U}_f$ and $\overline{V}_s$ are the residue of a cyclic integration of much higher instantaneous velocities. $\overline{U}_f$ and $\overline{V}_s$ are thus to be considered as indicative of the remainder of intense instantaneous action and not, in general, as capable of significant dynamic action of their own. Nevertheless, in a region of linear drag (as in the assumption here) the relative net velocity as determined by the difference between these two residues is identical with the average relative instantaneous velocity. The difference between the two net velocities, therefore, does have dynamical significance.

In order to verify Equation (5), it was necessary to determine, experimentally, values of $\overline{V}_s$, $\overline{U}_f$, C_D and C_{Rx} for given beach, wave and sediment properties.

Experimental Equipment and Procedures

In keeping with the aim of the study, simplifications were made which allowed concentration on primary variables.

The experimental facilities consisted of a 100 foot long, 2-1/2 foot wide and 3 foot deep glass-walled wave channel in one end of which an artificially roughened, fixed plane beach of variable slope was installed. Waves were generated at the other end by a horizontally reciprocating piston actuated by a hydraulic servomechanism with continuously variable speed and stroke.

The range of variables tested was:

Incident Waves

Characteristics of the incident waves in the constant depth portion of the channel are given in Table I.

Beach Slope

Two slopes were used:

$$\tan \alpha_1 = 1/14.8 = 0.0675$$

$$\tan \alpha_2 = 1/22.4 = 0.0447$$

Beach Roughness

The beach surfaces were coated with a uniform layer of immovable sand

TABLE I. Characteristics of Test Waves Before Transformation

Wave No.	H Ft.	L Ft.	T Sec.	d Ft.	d/L	H/L	H_o/L_o Approx.
1	0.186	8.92	1.43	1.75	0.196	0.0209	0.018
2	0.265	11.16	1.68	1.75	0.157	0.0237	0.020
3	0.354	8.42	1.39	1.75	0.208	0.0420	0.039
4	0.234	5.91	1.10	1.75	0.296	0.0396	0.041
5	0.230	4.36	0.94	1.75	0.401	0.0528	0.054
6	0.440	7.20	1.24	1.75	0.243	0.0611	0.061
7	0.357	5.99	1.11	1.75	0.293	0.0598	0.060
8	0.114	30.16	4.04	1.50	0.050	0.0038	0.001
9	0.235	16.22	2.33	1.50	0.093	0.0145	0.009

grains whose mean diameter, as determined by sieving, was:

$k_1 = 1.83$ mm. $k_2 = 0.79$ mm.

In addition, a smooth, uncoated surface was used yielding a roughness of assumed mean height:

$k_3 = 0$ mm.

Spherical Sediment Particles

Characteristics of the movable sediments are given in Table II.

Wave Characteristics

Local wave characteristics were determined by means of capacitance type wave profile wires in conjunction with a recording oscillograph.

Incipient Sediment Motion

Definition of incipient motion was accomplished by gradually varying the local wave characteristics until stationary sediment particles tipped out of their roughness hollows and continued to oscillate.

Unfortunately, it was not possible to obtain a reliable indication of the wave phase at which this condition was reached but note was made of the direction of initial motion.

Established Sediment Motion

The net velocity of single spherical particles was determined by timing their net movement over successive six inch increments on the beach.

TABLE II. Characteristics of Movable Sediments

No.	Nominal Size D mm. (Ft.)	Specific Gravity through Fall Velocity	D/k	
			k = 0.79 mm.	k = 1.83 mm
1	2 (.0066)	1.29	2.62	1.09
2	3 (.0098)	1.19	3.93	1.64
3	3.17 (.0104)	1.28	4.17	1.73
4	5 (.0164)	1.24	6.56	2.74
5	2.3 (.0075)	2.63	3.00	1.25
6	3 (.0098)	2.44	3.93	1.64
7	4 (.0131)	2.17	5.24	2.19
8	5 (.0164)	2.13	6.56	2.74
9	6 (.0197)	2.12	7.88	3.29
10	4.37 (.0143)	7.00	5.72	2.39

In order to get a statistically valid picture of net particle velocity at any beach position this single particle technique was repeated 10 times which gave a 95% confidence interval of $\pm$ 10%.

Fluid Mass Transport Velocities

In order to determine $\overline{U}_f$, the fluid mass transport velocity effective in the motion of a given size sediment under a given wave, globules of a fluid immiscible with and slightly heavier than water were introduced on the smooth beach surface. Measurements of the mean net globule velocity were then made under the same test waves as described above for sediment particles.

To define the distribution of net mass transport velocity through the boundary layer, measurements of the net velocity of a range of globule sizes

were made under each of several wave conditions. The net globule velocity was assumed to be that of the fluid at its center.

It is recognized that bottom roughness will modify the near-bottom distribution of instantaneous fluid velocity however its effect on the net (mass transport) velocities was assumed negligible.

Resistance Coefficients

Because of the difficulty of evaluating the coefficient of rolling friction, C_{Rx}, its effect was approximated by including it implicitly in the definition of the drag coefficient, C_D, as was done by Carty[3] in an experimental study of the resistance coefficients of spheres on a plane boundary. The study was performed in the manner of a "fall velocity" determination by timing the steady-state rolling velocity of various spheres on an inclined smooth plane boundary submerged in fluids of different viscosity.

Presentation and Discussion of Results

Net Sediment Velocities, $\overline{V}_s$

A complete tabulation of the net sediment motion data has been published elsewhere[2] thus only a sample will be given here.

In Fig. 2 the average net velocities obtained for various sediment particles under waves No. 2 and 3 are plotted with respect to position on the beach. Following the motion of the 3 mm. glass particle on the smooth beach a helpful summary of general observation is obtained:

A point of zero net velocity may be seen at approximately Sta. 48 where the sediment is in oscillating equilibrium. This same particle introduced offshore of the equilibrium point will move offshore under the predominant driving force of gravity. As the particle moves offshore it moves continually into a weaker fluid velocity field. Eventually the maximum local effective instantaneous fluid velocity under the crest may fall below that value required for incipient particle motion and a quasi-oscillatory sediment motion containing only the offshore cycle may result. With progress into still deeper water, even this motion will vanish and the sediment will come to complete rest.

Onshore of the point of oscillatory equilibrium, the effective fluid velocities provide the predominant driving force and since they increase sharply in the direction of motion, they produce a considerable net convective particle acceleration.

In the vicinity of the breaker, the onshore motion is more and more opposed by the backrush from the preceding waves and the sediments come to another point of oscillatory equilibrium.

Effective Fluid Mass Transport Velocity, $\overline{U}_f$

Longuet-Higgins[4] presents a theoretical solution for the mass transport velocity distribution in a closed channel which satisfies continuity. Within the bottom boundary layer this solution is given by:

$$2\frac{\overline{U}(y)}{\overline{U}_o} = 5 - 8\,e^{-\beta y}\cos\beta y + 3\,e^{-2\beta y} = \Phi \qquad (6)$$

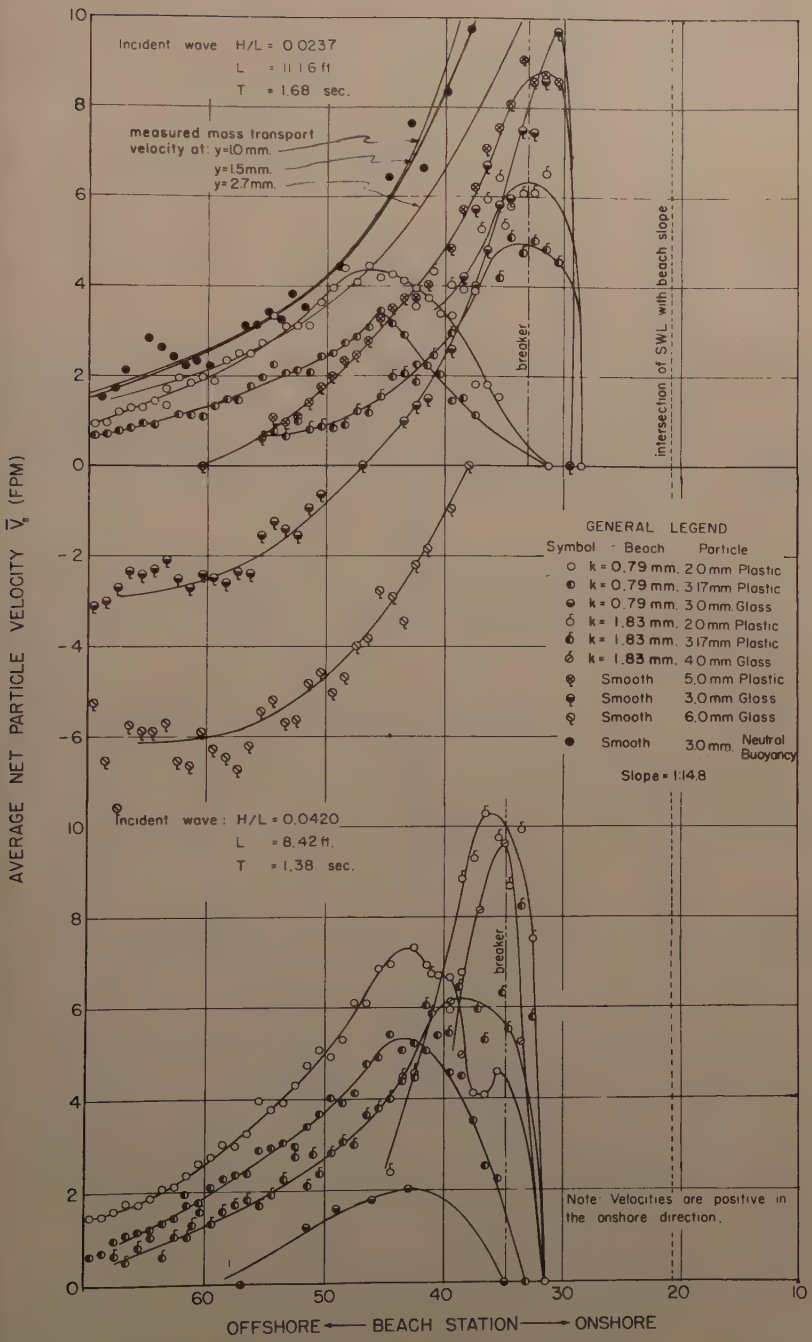

FIG.2 TYPICAL VARIATIONS IN NET SEDIMENT AND WATER PARTICLE VELOCITY WITH POSITION ON BEACH

in which

$$\overline{U}_o = \frac{1}{2}\left(\pi \frac{H}{L}\right)^2 \frac{C}{\sinh^2 \frac{2\pi d}{L}} \tag{7}$$

and

$$\beta^{-1} = \sqrt{\frac{2\nu}{\sigma}} \tag{8}$$

A sample set of measured distributions of net velocity at three separate points on the smooth, 1 to 15 slope under a given wave is shown in Fig. 3. Because of the difficulty of determining the true net boundary layer limit due to the presence of the return flow, the more readily distinguishable point of maximum net velocity was chosen as the reference dimension, j, for dimensionless comparison of the velocity distributions.

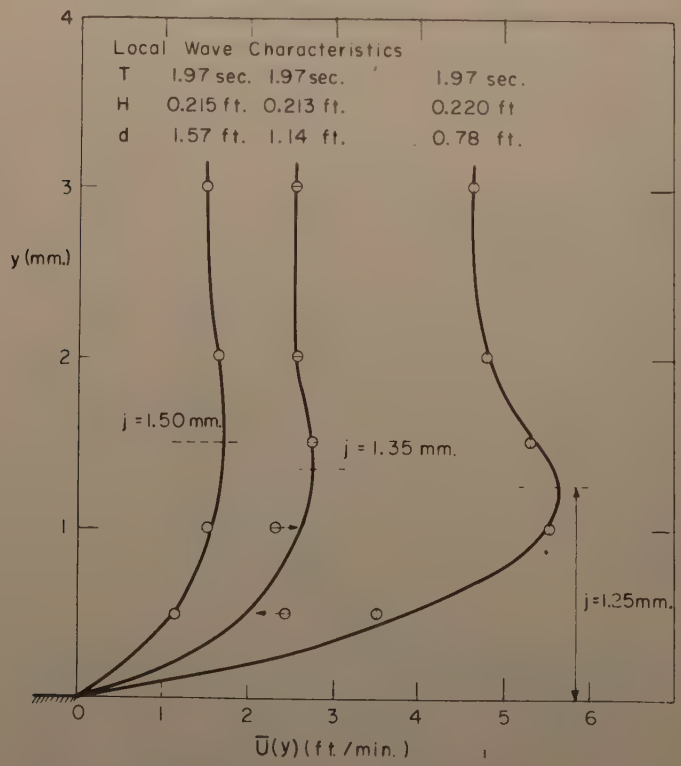

FIG. 3 SAMPLE DISTRIBUTIONS OF NET FLUID VELOCITY WITHIN THE BOUNDARY LAYER ON A SMOOTH BOTTOM

All the experimental velocity distributions are presented on this basis in Fig. 4 where they are compared with the Longuet-Higgins theory Eq. (6).

Measured values of the quantity, j, are compared in Fig. 5 with the theory which is given by the first maximum of Eq. (6) to be:

$$j_{theor.} = 2.306\sqrt{\frac{2\nu}{\sigma}} = 1.30\sqrt{\nu T} \qquad (9)$$

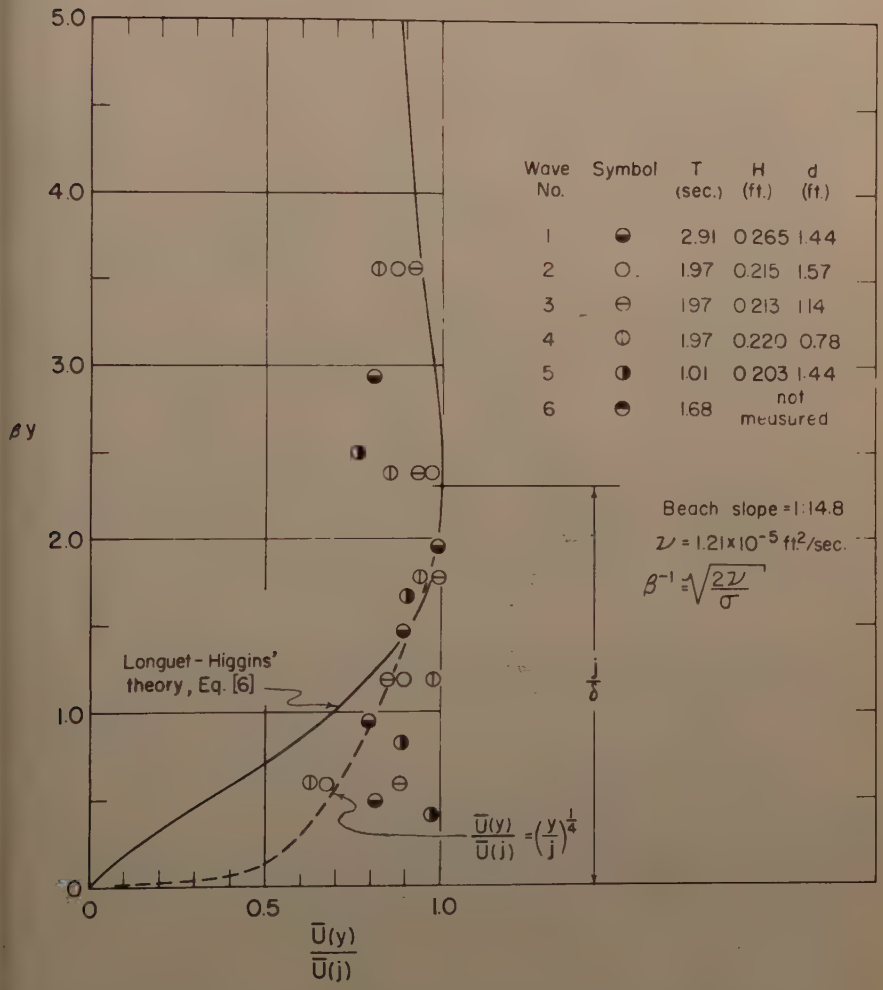

FIG. 4 DISTRIBUTION OF NET FLUID VELOCITY WITHIN THE BOUNDARY LAYER ON A SMOOTH BOTTOM

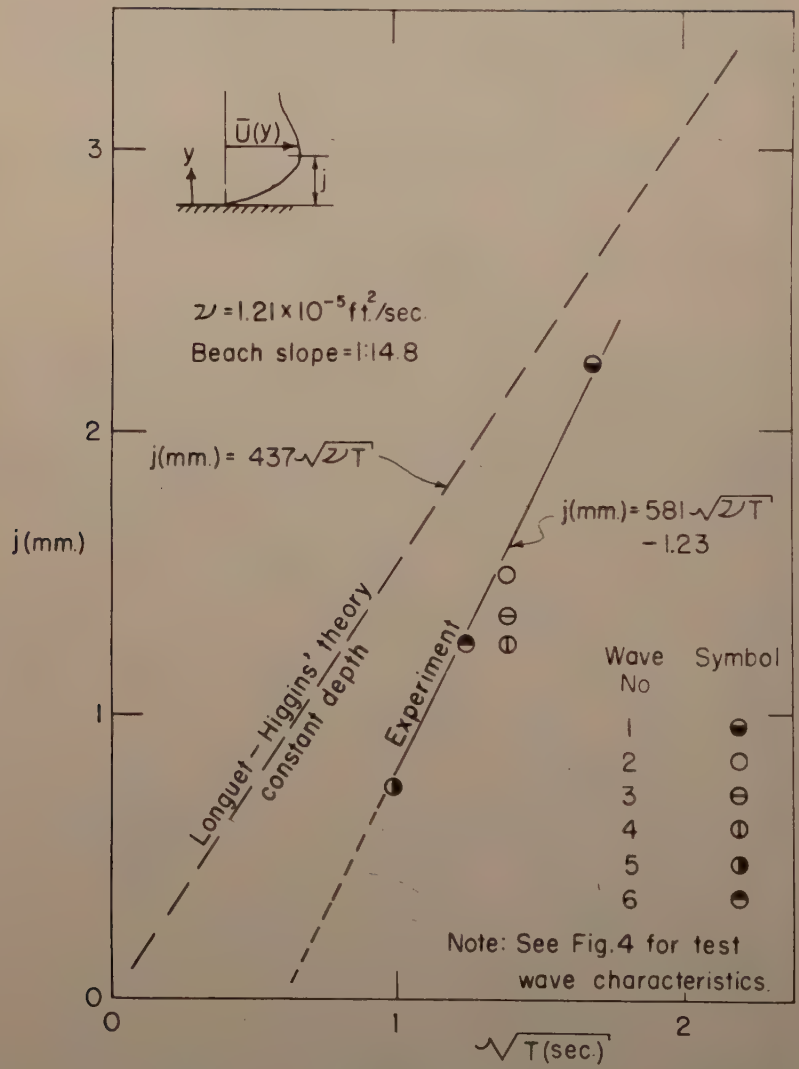

FIG. 5 ELEVATION OF MAXIMUM MASS TRANSPORT VELOCITY WITHIN THE BOUNDARY LAYER ON A SMOOTH BOTTOM

It should be remembered when studying the comparisons of Figs. 4 and 5 that the theory was developed for a constant depth while the experimental bottom had a 1 to 15 slope. For waves 1, 2 and 5, velocity distributions were measured close to the toe of the beach where the wave possessed essentially its constant depth characteristics. The extent of the variation caused by depth change is indicated by the distributions for waves 2, 3 and 4 which were measured at three progressively shallower depths in the transformation of a single wave. It would seem that any effect of bottom slope would increase with decreasing depth to wave length ratio d/L. However, experiment approaches theory with increasing wave period (decreasing d/L in this case) as may be seen from the measurements of j in Fig. 5.

It is thus reasoned that the discrepancies noted between theory and experiment are not primarily a result of the sloping bottom but may be due to some inadequacy of the theory for high frequency waves. For these waves a simple "power law" distribution such as the 1/4th power curve indicated in Fig. 4 may provide a more accurate description of velocity variation close to the bottom. It is interesting that recent unpublished experiments by the senior author have indicated instantaneous bottom shearing stresses to be several times greater than theory for waves comparable in frequency to these.

Because of this apparent inaccuracy in the theory when applied to laboratory waves the mass transport velocity effective in the motion of a given sediment was measured as described under Experimental Procedures. Some of these data are shown in the sample data presentation (Fig. 2). The similarity in the curves of net sediment and net fluid velocity indicates the analogous nature of the two phenomena.

Resistance Coefficients, C_D and C_{Rx}

By evaluating the drag coefficient for spheres rolling down an inclined, smooth plane boundary from the relation:

$$C_D \rho_f \frac{\pi D^2}{8} v_s^2 = F_G \sin\alpha \qquad (10)$$

Carty[3] has included implicitly in C_D at least a partial effect of rolling friction. His coefficients are presented as a function of Reynolds Number, R_D, in Fig. (6) where they may be compared with those for spheres in an infinite fluid.

The conventional reference velocity, "v_o," used in drag computations is the root mean square freestream velocity. In this case the component of peripheral velocity in the direction of translation (relative free stream velocity) varies linearly from zero at the bed to twice the translational velocity, v_s, at the upper edge of the particle. The root mean square relative free stream (evaluated over the projected area of the particle) velocity may be shown to be 1.12 times the translational velocity which was used by Carty to define his parameters.

The resistance curve for spheres rolling on a plane boundary was corrected for this velocity effect as shown in Fig. (6).

As mentioned above the experimental resistance coefficients include implicity, the effect of rolling friction. Since this frictional force is a function of F_G, the degree to which Fig. (6) determines C_D uniquely as a function of R_D defines the importance of this neglected force. The small scatter of

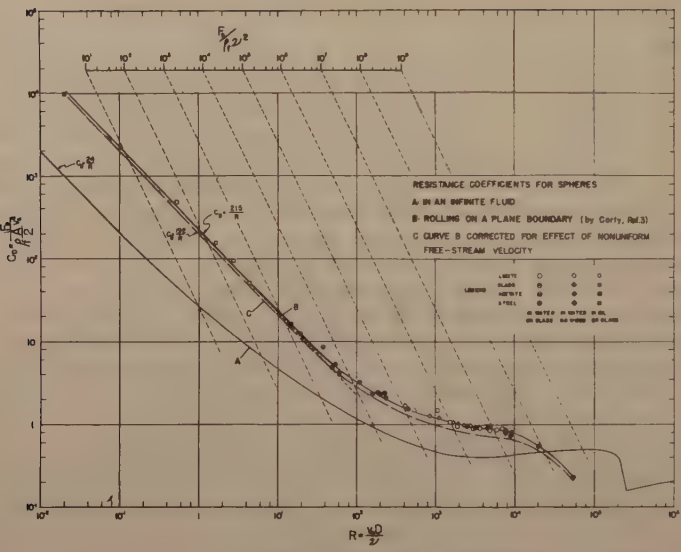

FIG 6 RESISTANCE COEFFICIENTS FOR SPHERES

the experimental points thus indicates the effect of rolling friction to be quite small.

It should also be noted that there is a basic hydrodynamic difference between the gravity-induced motion studied by Carty and the fluid-induced net sediment motion which is of prime concern here. This difference lies in the sense of particle rotation with respect to the direction of the relative translational velocity. The effect of this reversed flow picture on the resistance coefficient is zero in an infinite fluid and has not been determined in the presence of a solid boundary.

Absorbing the effect of bottom friction in the resistance coefficient, Equation (5) may be written:

$$C_D \rho_f \frac{\pi D^2}{8} (\overline{U}_f - \overline{V}_s)^2 = F_G \sin\alpha \qquad (11)$$

In order to demonstrate the validity of Equation (11) it was used to compute resistance coefficients using measured relative net velocities. Data from shoreward of the point of maximum net convective acceleration (i.e. inflection point of the curves such as in Fig. 2) were excluded due to the action of forces not included in Equation (11). All other data for a given value of the drag force, $F_G \sin\alpha$ and for each boundary geometry D/k, were averaged and the resulting coefficients are compared with the Carty curve in Fig. 7. Each plotted point represents the average of from 2 to 9 individual sets of data, each under different wave conditions. Excellent agreement is obtained where the boundary geometries are similar, that is at high D/k. A scattering of points from rough surfaces shows a trend to consistently lower coefficients at the same Reynolds number as the ratio D/k decreases. The effect of low D/k is two-fold. The first is to modify the exposed particle area and

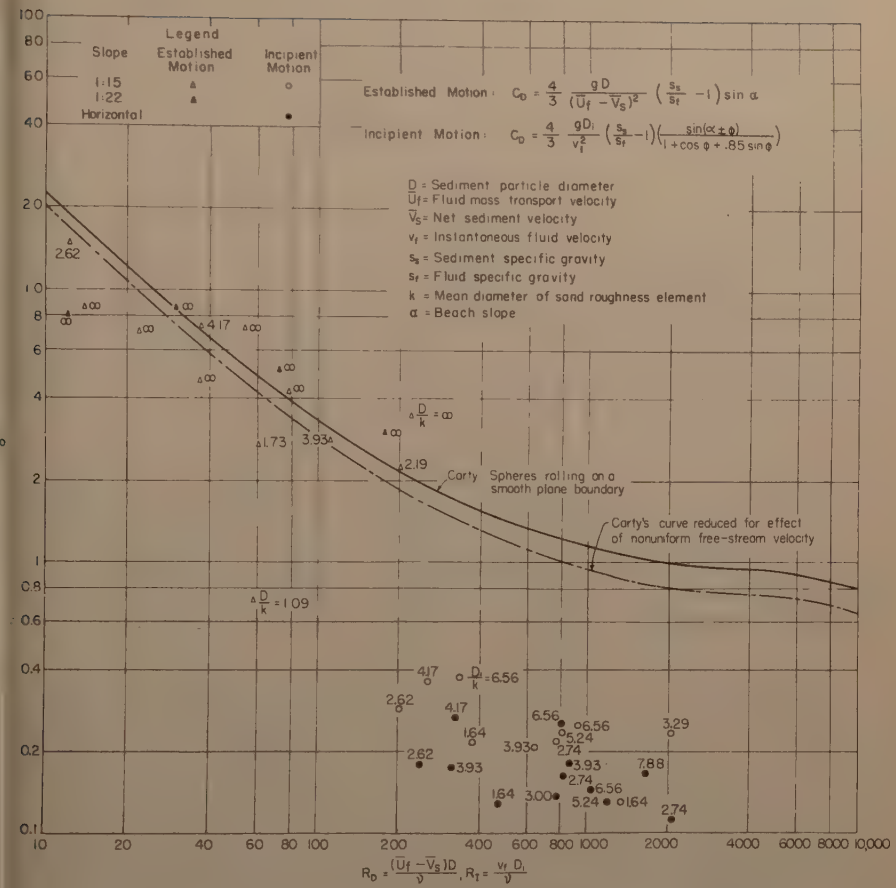

FIG. 7 RESISTANCE COEFFICIENTS DEFINING INCIPIENT AND ESTABLISHED MOTION

consequently the streamline configuration. The second is to introduce a larger bottom resistance which leads to smaller net sediment velocities. Under the definition of Equation (11) both effects should lead to lower coefficients at the same $F_G \sin \alpha$.

If the percentage difference between resistance coefficients for different D/k's is assumed independent of Reynolds number, the effect of bed-particle geometry may be shown as in Fig. 8, for established motion.

Incipient Motion

Equation (1) describes the instantaneous moment acting on a stationary sediment particle. It will be assumed that incipient motion occurs for a given D/k, W_b and α at the wave phase angle at which the hydrodynamic portion of

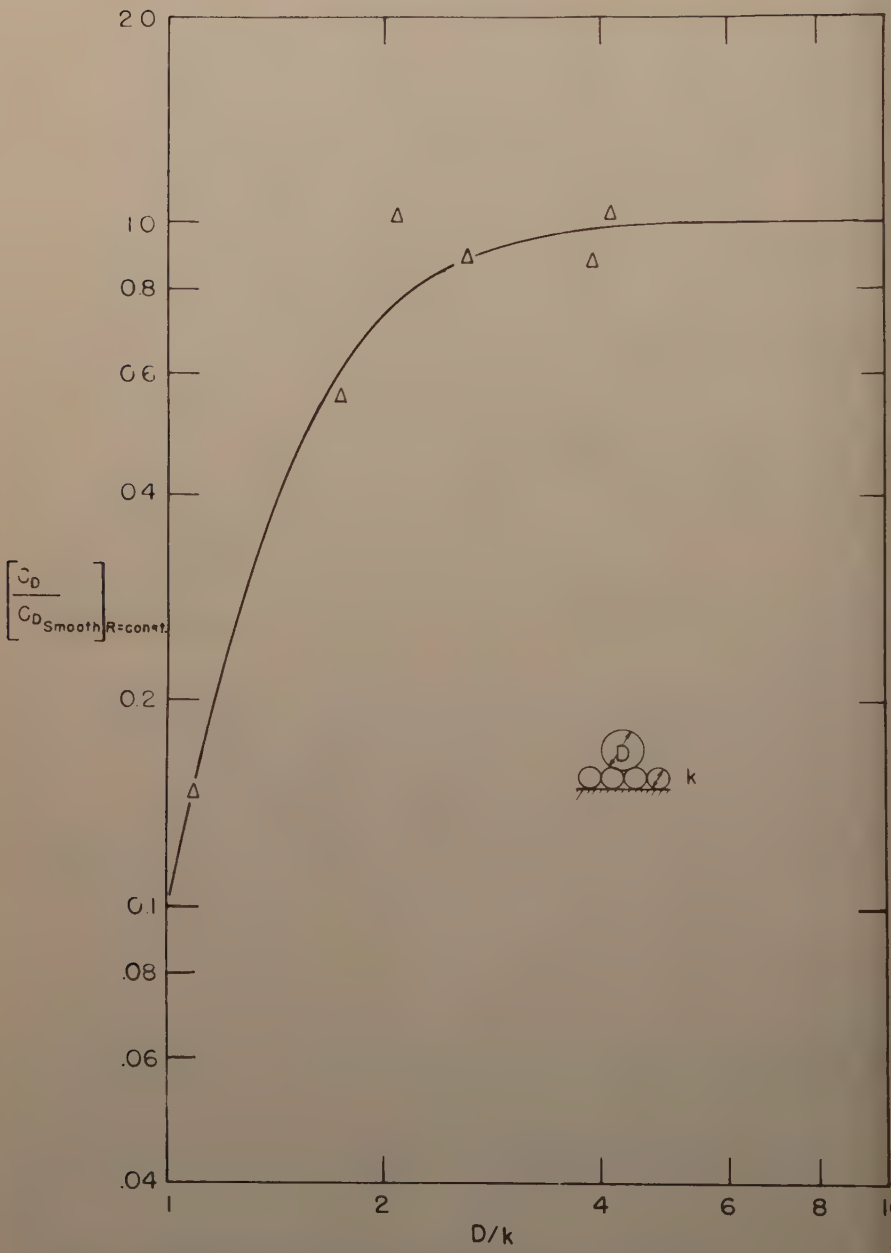

FIG. 8 EFFECT OF BED-PARTICLE GEOMETRY ON THE RESISTANCE COEFFICIENTS OF SPHERES

this moment has its maximum value. Because the moment is composed of drag and inertial components which are 90° out of phase, the value of this phase angle is not immediately obvious.

For long waves Lamb(5) gives the near-bottom velocity distribution as:

$$v_f = \frac{f}{\sigma}\left[\sin\theta - e^{-\beta y}\sin(\theta-\beta y)\right] \tag{12}$$

where

$$\frac{f}{\sigma} = \frac{H}{2}\,\frac{\sigma}{\sinh\frac{2\pi d}{L}} \tag{13}$$

Equation (12) and its first time derivative are now substituted into Eq. (1) with the additional assumptions.

$$1.\quad v = v_f \quad \text{when } y = D \tag{14}$$

$$2\quad a = a_f \quad \text{when } y = D \tag{15}$$

Differentiation of the first two terms of Eq. (1) in order to obtain the location of the maximum hydrodynamic moment then yields:

$$\frac{d\Sigma M}{d\theta} = 0 = \frac{d}{d\theta}\left[\frac{3}{4}\frac{v_f^2}{\sigma D}\left[C_D(1+\cos\phi)+C_L\sin\phi\right] + C_M\frac{dv_f}{d\theta}(1+\cos\phi)+\frac{dv_o}{d\theta}\cos\phi\right] \tag{16}$$

C_M is assumed equal to 0.6 as given by Streeter(6) for a sphere on a smooth plane boundary in potential flow and C_L is assumed equal to 0.85 C_D as given by Chepil.(7) Then:

1. If C_D is assumed constant at the appropriate value determined for established motion at high R - then, as might be expected, the drag and lift forces predominate for all βD and the phase angle for incipient motion is close to 90°.

2. If C_D is assumed inversely proportional to R with the constant of proportionality taking on the appropriate value determined for established motion at low R - then for a large βD (these laboratory data) inertia forces will predominate and the phase angle θ of maximum force will be close to 0° while for small βD (most natural beaches) drag and lift forces will govern as in case 1 above.

Multiple regression statistical techniques were applied to the laboratory data in an effort to obtain independent determinations of C_D, C_M and incipient θ. Due presumably to the scatter of the data, wildly varying results including imaginary and negative coefficients were obtained and the technique was abandoned.

An approximate evaluation of these data may be obtained under the assumption that all accelerative effects may be ignored. With this assumption the condition of incipient motion is given by Eq. (1) rewritten to yield:

$$C_D = \frac{4}{3}\frac{\beta D}{v_f^2}\left(\frac{S_s}{S_f}-1\right)\left(\frac{\sin(\alpha\pm\phi)}{1+\cos\phi+.85\sin\phi}\right) \tag{17}$$

The effective velocity, v_f, is given by Eqs. (12) and (14) evaluated at $\theta = 270°$ or 90° depending upon whether the initial motion was observed to be in the offshore or onshore direction respectively.

The tangent of the angle of repose ($\tan \phi$) for the various bed-particle combinations was determined experimentally by tilting an immersed roughened plane supporting the particular particle until motion ensued. These data are presented in Fig. 9 in comparison with the theoretical relationship for an idealized bed-particle geometry. It should be remembered that the values of ϕ determined in this manner apply to incipient motion in a moving fluid only when the resultant active force acts through the particle center. Due to the effect of bottom roughness in elevating the point of application of the drag force this assumption becomes poor as D/k becomes small.

The resistance coefficients calculated on the basis of these velocities and repose angles are presented in Fig. 7 as a function of the instantaneous Reynolds number, R_I. Each point shown represents the average of from 1 to 10 separate determinations (each under different wave conditions) of incipient motion for each separate combination of F_G, D/k and α.

Since in all probability the critical phase angle is somewhat less than 90° the drag and lift forces and Reynolds number will be less and the resistance coefficient correspondingly higher.

These data should not be expected to agree completely with those for established motion however since for low D/k at least the latter include an appreciable effect of rolling friction.

It is possible to conclude only that there is no qualitative disagreement between the theory and experiment.

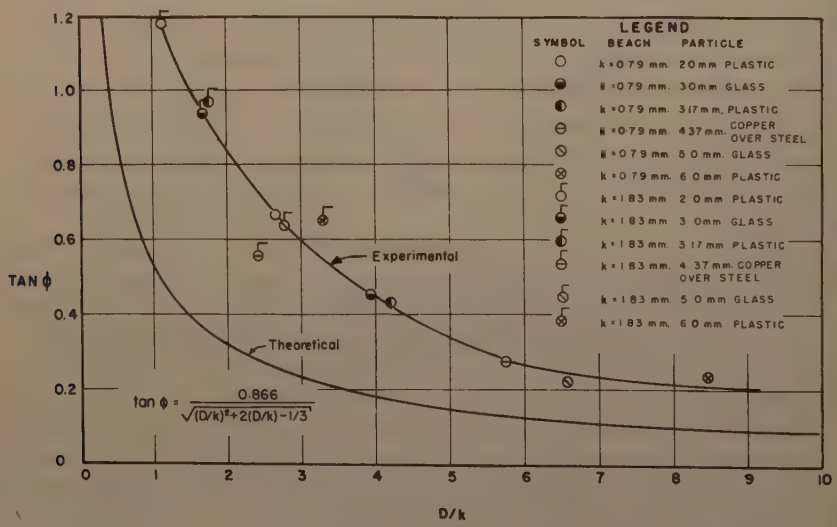

FIG. 9 ANGLE OF REPOSE AS A FUNCTION OF BED-PARTICLE GEOMETRY

Extrapolation of Results to Natural Beaches

Although the type of sediment motion dealt with here may be obscured by any one of several others on natural beaches, certain phenomena of sediment distribution may be explained qualitatively on the basis of the findings reported.

Observations of many natural beaches show the median sediment size to be distributed from coarse to fine in the offshore direction and the skewness of the local size distribution to increase consistently in the same direction.

Two of the laboratory-observed phenomena reported yield a qualitative explanation of these variations. These phenomena are:

1. The equilibrium condition of established sediment motion.
2. The condition of incipient sediment motion.

These conditions will be discussed separately.

Equilibrated Established Motion

As long as instantaneous fluid velocities exceed the incipient value at some time during each wave cycle, the sediment will be in the condition herein referred to as established motion.

In the laboratory, due to the constant experimental slope, the condition of oscillating equilibrium producing zero net motion is a condition of unstable equilibrium as far as any single particle is concerned. This is true with any wave train of essentially constant form since any irregularity which forces the sediment particle off its equilibrium location moves it into a zone of net motion leading away from the equilibrium position.

A typical natural beach, on the other hand, has a slope which varies from mild to steep in the onshore direction, a fact which causes the condition of oscillating equilibrium to be one of stable equilibrium. Any irregularity in the wave train will produce a net hydrodynamic force on the particle which tends to move it away from its equilibrium position. Due to the slope variation this particle displacement brings into play a modified gravity force which acts to restore the particle to its equilibrium position.

Considering the condition D/k = 1 to most nearly represent the bed-particle geometry of equilibrium natural beaches, the resistance coefficient may be written for the range of interest as:

$$C_D = \frac{19.2}{R_D} \tag{18}$$

from Figures (6), (7) and (8).

Substituting Eq. (18) into Eq. (11) and simplifying for the case of interest, i.e. $\overline{V}_s = 0$;

$$\frac{g D^2}{\nu \overline{U}_f}\left(\frac{s_s}{s_f} - 1\right)\sin\alpha = 14.4 \tag{19}$$

For sand in sea water:

a. $s_s = 2.65$

b. $s_f = 1.03$

c. $\nu = 1.45 \times 10^{-5}$ ft/sec.

thus

$$D^2 \sin\alpha = 4.13 \times 10^{-6} \bar{U}_f \tag{20}$$

In order to define $\bar{U}_f$ for natural beaches the velocity distribution of Longuet-Higgins,[4] Eq. (6), is used.

Near the bottom Eq. (6) may be approximated by:

$$\beta y = 0.32 \Phi^{7/8} \tag{21}$$

thus

$$\Phi = 2 \frac{\bar{U}(y)}{\bar{U}_o} = 3.68 (\beta y)^{8/7} \tag{22}$$

On a very rough bottom (D/k = 1) the sediment particle is partially embedded in the beach and the fluid velocities acting on the remainder of the lower portion are so weak that their contribution to dynamic pressures is probably quite small. For this reason the fluid velocity effective in motion of these natural sediments will be assumed to act at the upper edge of the particle.

$$\bar{U}(y) = \bar{U}_f \quad \text{when} \quad y = D \tag{23}$$

The effect of this shielding on the particle area exposed to drag is implicitly in the drag coefficients given in Fig. 8.

Using (22) and (23), (20) becomes:

$$D_e^2 \sin\alpha = 7.60 \times 10^{-6} (\beta D_e)^{8/7} \bar{U}_o \tag{24}$$

in which D is in feet and $\bar{U}_o$ is in ft. per sec.

Eq. (24) describes the equilibrium relationship between particle size, beach slope and local wave characteristics under the assumption that the equilibrium condition of established sediment motion is the controlling mechanism.

Incipient Motion

If, on the other hand, the sediment size which satisfies the conditions for oscillating equilibrium at all locations cannot be moved by the maximum local instantaneous fluid velocity, then the median remaining size will be governed by incipient motion conditions.

Suppose a beach which initially had the same normal distribution of sand sizes at each location is subjected to a given incident wave until the sorting process has reached equilibrium. In the deeper water, only the smallest of the sediment particles will be put into motion with some moving onshore and some offshore. At stations further onshore the size just capable of being moved by the maximum local instantaneous fluid velocity (called the incipient particle size) increases thereby producing an absence of a larger and larger percentage of the smaller sizes. This effect will move the median remaining size to increasingly larger diameters with distance in the onshore direction.

As before considering the conditions D/k = 1 to be most representative of the beach conditions of interest the resistance coefficient will be given by Eq. (18).

As stated above, for small βD the maximum moment is in phase with the velocity. Under these conditions the effective velocity, v_f, as given by Eqs. (12) and (14) may be approximated by:

$$v_f = 0.86 \frac{f}{\sigma} \beta D \qquad .01 < \beta D < 1.0 \tag{25}$$

Eqs. (18) and (25) may be substituted into Eq. (17) to obtain

$$\frac{g D \sigma}{\nu f \beta} \left(\frac{S_s}{S_f} - 1\right)\left(\frac{\sin(\alpha \pm \phi)}{1 + \cos\phi + .85 \sin\phi}\right) = 12.4 \tag{26}$$

Again for sand in sea water, Eq. (26) becomes:

$$\frac{D_i}{\beta} \sin(\alpha \pm .92) = 8.1 \times 10^{-6} \frac{f}{\sigma} \tag{27}$$

where tan ϕ is obtained from Fig. (9) for D/k = 1.

Eq. (27) describes the equilibrium relationship between particle size, beach slope and local wave characteristics under the assumption that the condition of incipient sediment motion is the controlling mechanism.

An additional important simplification, the quantitative effect of which is indeterminate at this time, results from considering the bed to be permeable. Flow into the permeable natural bed under the wave crest will increase particle stability, but flow out of the bed under the wave trough will reduce the effective particle weight and may in fact put the whole surface of the bed in a "quick" of fluidized condition.

This would normally lead to smaller incipient sizes in a zone of onshore motion and larger incipient sizes in a zone of offshore motion.

It should be remembered that the degree to which the "incipient sediment size" represents the median remaining size depends to a great degree upon the initial distribution of sizes at the locality.

At this time it is not possible to state which of the above criteria governs the formation of equilibrium beaches. It is recognized, however, that wherever the incipient size, D_i, (that maximum size which the local instantaneous fluid velocities are just able to move) is smaller than the equilibrium sediment size, D_e, (that size which would be in oscillating equilibrium under the local fluid velocities) the equilibrium criterion cannot govern the median remaining size. For small beach slopes Eqs. (24) and (27) may be combined to yield a definition of this limiting condition:

$$\frac{D_e}{D_i} = .082 \beta^{1/3} \frac{\sigma}{f} \bar{U}_o^{7/6} \left(\sin\alpha^{-1/6} + 1.3 \sin\alpha^{-7/6}\right) = 1 \tag{28}$$

Comparison with Natural Beach Data

It can be seen from Eqs. (24) and (27) that for a given wave system there is a relationship between the local sediment diameter and the local beach

slope at equilibrium. For a measured set of natural beach and wave characteristics it is possible to test the applicability of this relationship.

Data concerning local depth and median particle size along fourteen ranges of three natural beaches on the Eastern coast of the United States were supplied by the Beach Erosion Board. A sample of the information is shown in Fig. 10.

The significant wave estimated by the Beach Erosion Board to apply to these beaches has an 8 second period and a deep-water height, H_o = 1.5 ft. (H_o/L_o = 0.0046).

Using small amplitude wave transformation theory wave characteristics bracketing those of the estimated wave were introduced into Eqs. (24) and (27) and the resulting expressions were plotted as the solid lines of Fig. (11).

There is considerable variability in the natural beach data and consequently the arithmetic mean of all measurements at constant H_o/d was determined and plotted along with arrows to show the extent of the variation. Excluded from the averages in Fig. 11-a were all data points for which the theoretical diameter ratio, D_e/D_i, was greater than unity as determined from Eq. (28). The small numbers by each plotted point indicate the number of observations determining that mean.

The variations are due in some part to the difficulty of scaling small local slopes accurately from a plotted beach profile.

Agreement of the mean data with theory is remarkable for both theoretical models.

Thus, for known predominant deep water wave characteristics it is possible, using these criteria, to:

1. Predict median sand size distribution knowing the equilibrium beach profile, or

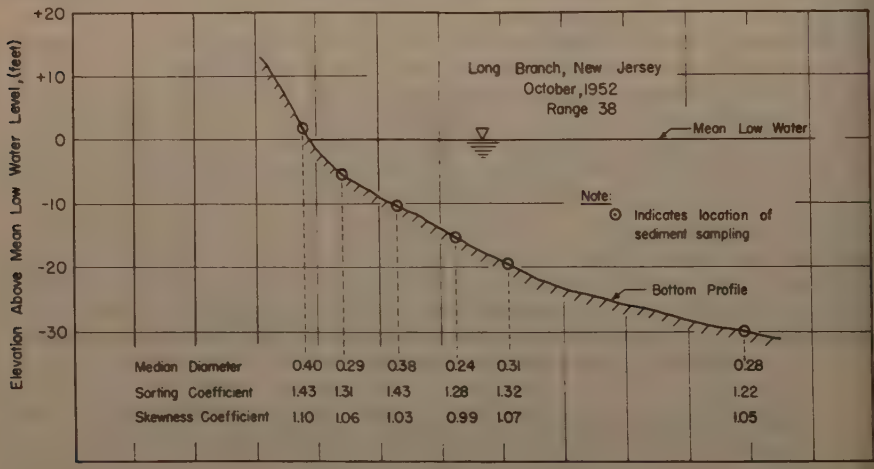

FIG. 10 SAMPLE NATURAL BEACH DATA AS FURNISHED BY THE BEACH EROSION BOARD

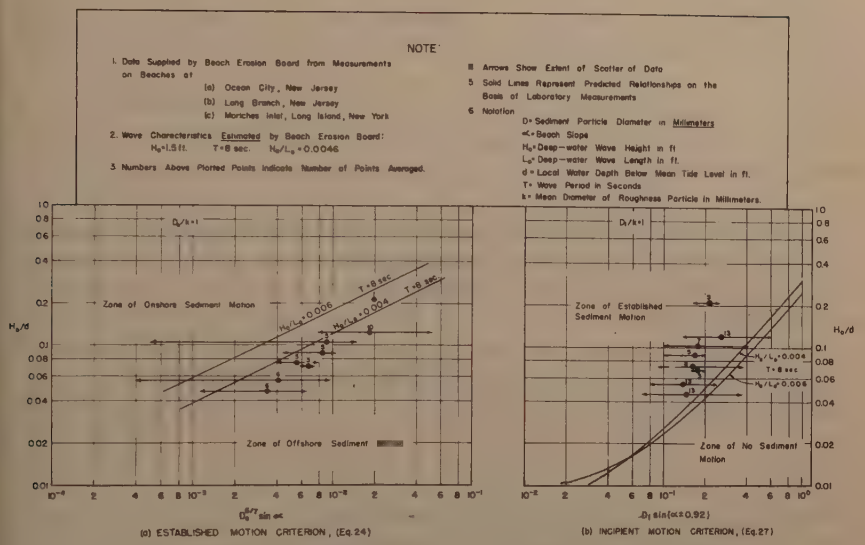

(a) ESTABLISHED MOTION CRITERION, (Eq.24) (b) INCIPIENT MOTION CRITERION, (Eq.27)

FIG. 11 PREDICTED AND OBSERVED EQUILIBRIUM CHARACTERISTICS OF NATURAL BEACHES

2. Predict equilibrium beach profile knowing the distribution of median sand size.

Use of Eq. (11) to describe the rate of sand motion should permit simultaneous determination of both equilibrium slope and sand size distribution starting from known initial, unstable values of these variables. Current investigations are proceeding in this direction.

A complementary laboratory investigation of two-dimensional natural sand beaches is currently underway in the Hydrodynamics Laboratory at M.I.T. under the sponsorship of the Beach Erosion Board. The aims of this study are:

1. To determine to what extent either of the above criteria may be applied or can be modified to apply to the prediction of equilibrium profiles of natural beaches.

2. To determine to what extent the derived equation of net sediment motion can be utilized in the prediction of transient beach behavior following a change in incident wave form.

SUMMARY AND CONCLUSIONS

A series of experiments was made concerning two facets of the wave induced motion of discrete spherical sediment particles: (1) Established net motion on both smooth and artificially roughened beaches (2) Incipient motion on artificially roughened beaches.

An equation of net sediment motion was derived and verified by the laboratory measurements.

Two criteria for the local mean sediment size - beach slope relationship for equilibrium beach profiles were developed and compared with natural beach data.

The following conclusions may be drawn from this set of experiments:

1. The bottom boundary layer under high frequency ($\sigma > 2$) waves is considerably thinner than predicted by available theory.

2. The instantaneous drag force is linearly related to the instantaneous relative fluid-sediment velocity in the usual range of sediment particle Reynolds number (as defined by the instantaneous relative fluid-sediment velocity) encountered in the zone of established motion in both the laboratory and on natural beaches.

3. All phases of established sediment motion exclusive of the effects of the breaker may be described in terms of the relative net fluid-sediment velocity by the equation:

$$C_D \rho_f \frac{\pi D^2}{8} \left(\overline{U}_f - \overline{V}_s\right)^2 = F_G \sin\alpha$$

in which C_D includes the effect of bed resistance and is, by conclusion 2, a linear function of the relative net fluid sediment velocity.

4. Two rational equations have been developed for predicting the relationship between the local characteristics of slope and median sediment diameter on two-dimensional equilibrium natural beaches:

a. On the basis that the median remaining size is indicated by that size which can be maintained in oscillating equilibrium at the point -

$$D_e^{6/7} \sin\alpha = 7.60 \times 10^{-6} \beta^{8/7} \overline{U}_o$$

b. On the basis that the largest particle just capable of instantaneous motion will indicate the median remaining size at the point -

$$D_i \sin(\alpha \pm .92) = 8.0 \times 10^{-6} \frac{f}{\sigma} \beta$$

Comparison of both of these equations with the limited available prototype data is encouraging but it is not yet possible to say with assurance which mechanism controls the natural beach configuration.

ACKNOWLEDGMENT

This investigation was carried out at the Hydrodynamics Laboratory in the Department of Civil and Sanitary Engineering at the Massachusetts Institute of Technology under the sponsorship of the Beach Erosion Board, Corps of Engineers, U. S. Army.

Particular credit is due Mr. Luis A. Peralta who performed much of the early experimental work and data analysis.

1. Ippen, A. T. and Eagleson, P. S., "A Study of Sediment Sorting by Waves Shoaling on a Plane Beach," M.I.T. Hydrodynamics Laboratory Technical Report No. 18, 1955, also published as Beach Erosion Board Technical Memorandum No. 63, Washington, 1955.

2. Eagleson, P. S., Dean, R. G. and Peralta, L. A., "The Mechanics of the Motion of Discrete Spherical Bottom Sediment Particles Due to Shoaling Waves," M.I.T. Hydrodynamics Laboratory Technical Report No. 26, 1957, also published as Beach Erosion Board Technical Memorandum No. 104, Washington, 1958.

3. Carty, J. J., Jr., "Resistance Coefficients for Spheres on a Plane Boundary," Thesis submitted to the Massachusetts Institute of Technology for the degree of B.S., M.I.T., Cambridge, Massachusetts, May, 1957. (Unpublished).

4. Longuet-Higgins, "Mass Transport in Water Waves," Phil. Trans. Roy. Lond. Series A, No. 903, Vol. 245, pp. 535-581, 31 March 1953.

5. Lamb, H., "Hydrodynamics," Dover Publications, New York Sixth Ed., 1932, p. 622.

6. Streeter, V. L., "Fluid Dynamics," McGraw-Hill Book Co. Inc., First Edition, 1948, p. 80.

7. Chepil, W. S., "The use of Evenly Spaced Hemispheres to Evaluate Aerodynamic Forces on a Soil Surface," Trans. A. G. U. Vol. 39 No. 3, June 1958, pp. 397 - 404.

Journal of the
HYDRAULICS DIVISION
Proceedings of the American Society of Civil Engineers

HYDRAULIC CHARACTERISTICS OF GATE SLOTS[a]

J. W. Ball,[1] M. ASCE

ABSTRACT

Flow turbulence within gate slots, and cavitation damage just downstream from gate slots, occur when wheel (or roller) gates and slide gates are operated at small openings under heads in excess of about 35 feet. A discussion of these conditions is given together with a discussion of the investigation which led to a generally applicable, cavitation-free, gate slot design.

INTRODUCTION

There are many factors to be considered in designing gates of the wheel (roller) or slide type. One of the most important factors concerns the grooves or slots in which the ends of the gates are supported (Fig. 1). This paper discusses the hydraulic characteristics of a wide variety of such slot shapes.

Unless gate slots are properly designed turbulence and cavitation will occur to cause the destruction of roller chains and wheels as well as costly damage to flow surfaces (Fig. 2). More extensive damage than that shown in the illustration has occurred in several cases. Turbulent surging within the slots can be controlled by baffle plates attached to the bottoms of the gates, and, to some degree, by shaping the slots. It can also be eliminated by attaching extensions to the bottom corners of the gate leaves to fill the slots. Cavitation can be eliminated only by preventing the occurrence of vapor pressure in or near the slots. This may be quite difficult to accomplish in the high head installations encountered in present day designs. The difficulty of eliminating cavitation pressures therefore reduces the gate slot problem to principally a study of pressure intensity and distribution.

Note: Discussion open until March 1, 1960. To extend the closing date one month, a written request must be filed with the Executive Secretary, ASCE. Paper 2224 is part of the copyrighted Journal of the Hydraulics Division, Proceedings of the American Society of Civil Engineers, Vol. 85, No. HY 10, October, 1959.

a. Presented at the June 1958 ASCE Convention in Portland, Ore.

1. Hydr. Engr., Commissioner's Office, Bureau of Reclamation, Denver, Colo.

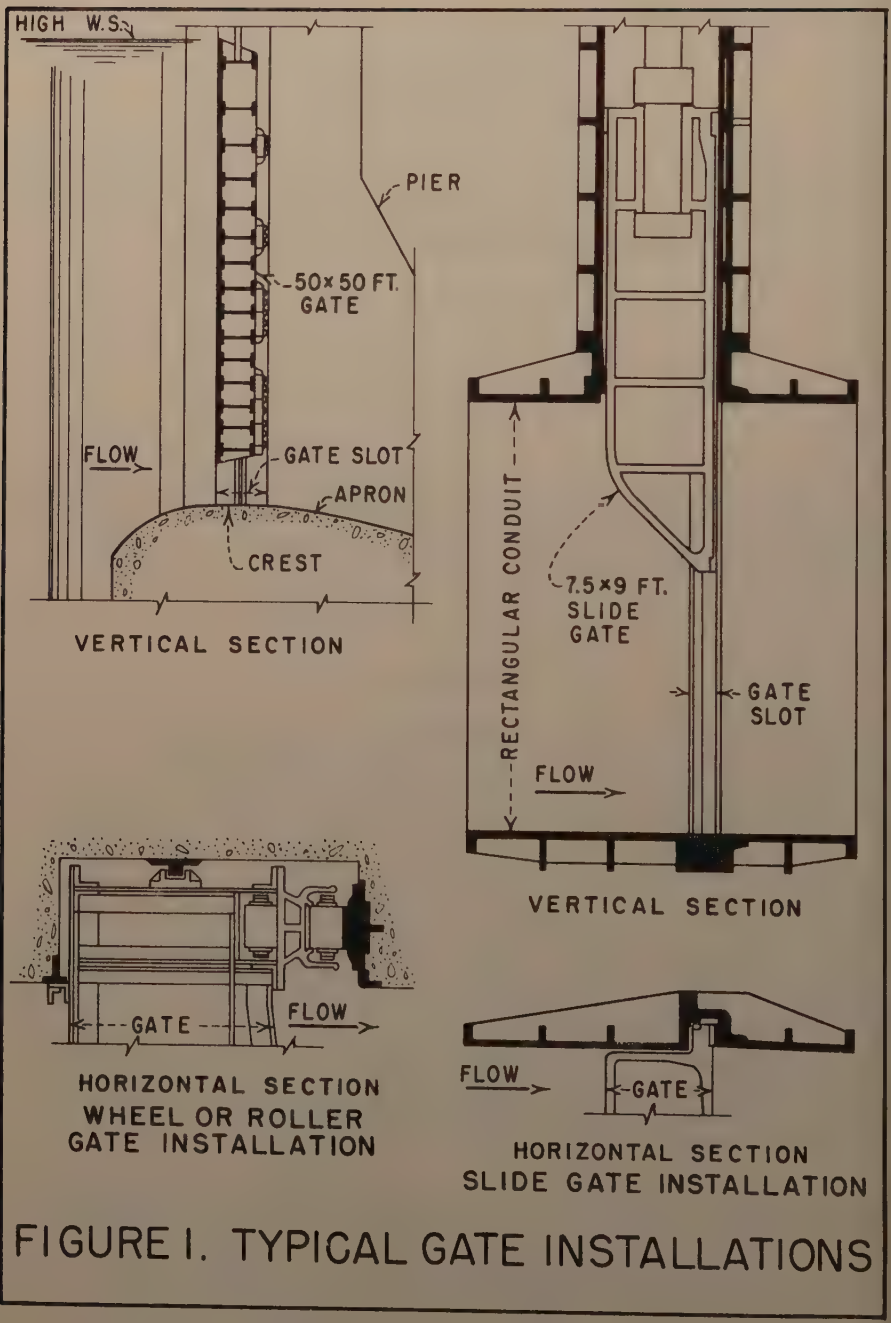

FIGURE 1. TYPICAL GATE INSTALLATIONS

Damage to roller chains by violent turbulence and excessive cavitation erosion on flow surfaces of Bureau of Reclamation Stoney gate installations led, in 1941, to studies of the causes and remedies for the trouble. An appraisal of existing structures, as well as structures under construction and in the design stages, disclosed the need for a four-phase investigation to obtain satisfactory and economical solutions for all the structures. The first phase was an inspection of existing structures to determine whether or not cavitation damage had occurred and under what conditions. The second phase was to develop a means of correcting the trouble at existing structures with a minimum of alteration. The third phase was to evolve a satisfactory slot design that could be constructed within the confines of block-outs provided for second-stage concrete in spillways under construction. The fourth phase was to develop a design which would be generally applicable to future structures. This four-phase investigation concerned specific projects using wide slots for wheel or roller gates that operated under heads of about 50 feet. A discussion of the investigation results is given in subsequent sections of this paper.

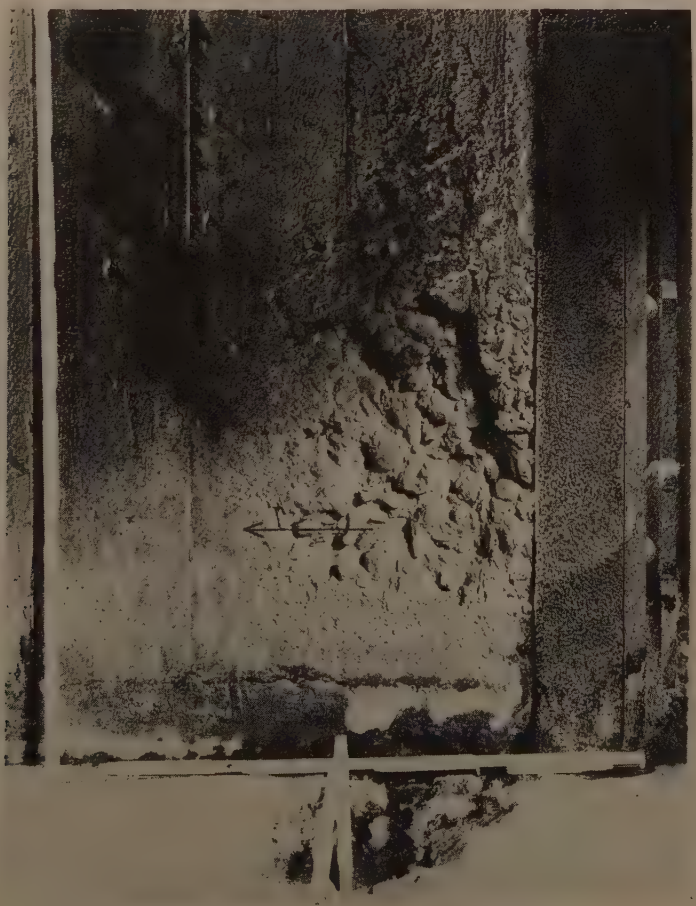

Figure 2

More recent investigations of a more general nature have concerned both wheel and slide gates under much higher heads. Over the years following the tests mentioned above, many different types of outlet structures were built. During this time there was a constant trend toward higher heads and more severe operating conditions, particularly on slide gates. However, it was not until inspections were made in recent years, and severe damage was reported on slide gates, that the problem was again high-lighted and the study of gate slots intensified.

Test Equipment

The first laboratory tests on slots of wheel gates were made on a relatively large-scale, sectional hydraulic model. A gate leaf controlled the flow, and thus the influence of the leaf at various positions was included. In this model, the heads and velocities were low and the discharges were therefore within the capacity of the laboratory pumps. However, when higher heads were considered, the pump capacity was no longer adequate for complete hydraulic models of reasonable size, or for scaled sectional models that included a leaf and a slot of adequate size. Modified sectional models which contained a relatively large slot in one wall of a closed rectangular conduit were therefore used for most of the gate slot tests. Water was used as the flowing medium in the first test facility (Fig. 3). Air was used in a similar apparatus for subsequent tests. Gate leaves were not used in these facilities. A cavitation testing facility recently constructed in the laboratory was used in one special test (Fig. 4).

Discussion of Test Methods

The manner in which the gate leaf affects the flow in the slot, and the influence of this flow on the pressures in and near the slot, are important in the analysis of gate slot problems. The major portion of the tests discussed in

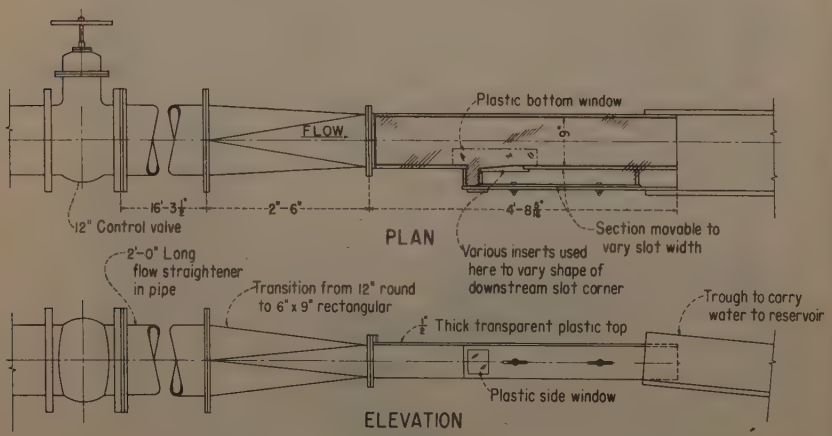

FIGURE 3. HYDRAULIC TEST FACILITY FOR GATE SLOTS

this paper were made on hydraulic and aerodynamic models which represented the gate in the wide open position with the conduit downstream flowing full. At first thought, this method of testing would not seem to cover all the important conditions for the slot. However, an examination of flow conditions during the opening and closing cycles on a gate shows that this method will satisfy nearly all conditions of operation.

As the leaf of a wide open gate is moved toward the closed position, it deflects the flow downward and outward into the slots. This action becomes more pronounced as the leaf moves farther into the flow and it soon prevents aeration of the slot. This "sealing" point varies somewhat with the shape of the slot, but in all cases occurs at or near the wide open position. Tests made on a large hydraulic model illustrated this flow characteristic. The model tested had slots with the downstream corners offset away from the flow approximately 1/3 the slot depth, and walls downstream from the slot corners that diverged at a rate of 12:1.

The flow through this gate cleared the slots and the downstream walls when the leaf was wide open, and during closure of the gate until it reached about 97 per cent open. At the 97 per cent opening a small amount of water was deflected into the slot and a great deal of air was carried with it. This air-water mixture spiraled downward in the slot and flowed back into the stream at the bottom of the body. As the leaf closed to 95 per cent open, more water was directed into the top of the slot, but only the portion of the jet near the top stayed in contact with the walls. As the leaf closed to about 93 per cent open, the slots filled quickly and the sides of the jet contacted and remained in contact with the diverging walls for the full height of the jet. Some air was drawn into the slot at the corner near the gate leaf bottom at 93 per cent open, but no air entered the slot at an opening of less than 92 per cent. The gate opening at which the slots fill will vary with the slot design. On most gates filling of the slots will occur nearer full open than with the tested gate because the offsets in the tested gate were relatively large and the downstream walls diverged.

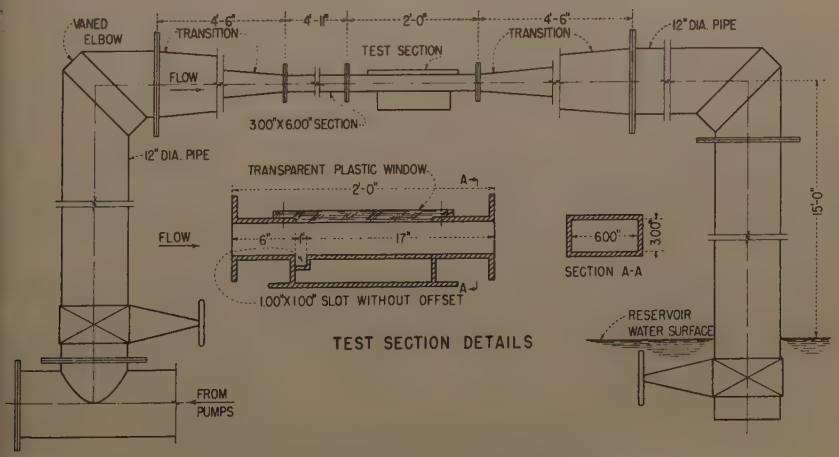

FIGURE 4. CAVITATION TEST FACILITY WITH ORIGINAL GATE SLOT

Because of the filling and sealing actions described above, it is believed that the data presented are generally applicable to the gate slot problem, particularly with the reference pressure taken at the downstream face of the leaf, and the reference velocity taken as the average flow velocity passing the slot. The data would not be applicable at large gate openings where the flow clears the downstream corners of the slots. This condition is not critical. The data would also not be applicable at very small openings with most slot shapes because at these openings the downstream edge of the slot becomes a control and a contraction occurs at the corner. This condition will be discussed in detail in a subsequent part of this paper.

In recent years model studies have been conducted on most of the gate slot types used by the Bureau of Reclamation. These studies were made to keep pace with more severe operating conditions, and because it was desirable to forestall inadequate operation wherever possible. The tests concerned slide gate slots in particular, but the results are applicable also to wheel gates since the main difference in the two types is size rather than shape.

Correlation Problems

It is important to note that the tests discussed in this paper were made over a period of years, that the facilities used were not always the same, and that many equipment and technique changes were made to obtain data which at first did not appear pertinent but later proved important. In light of these factors, the correlation between the results of the various water and air models was considered excellent. However, direct comparison of data presented in this paper must be made with care. One factor which makes comparison difficult is the relative location of piezometers. The steep pressure gradients in critical regions, such as in the slot at the downstream corner, and just below the downstream corner, make relative locations in different models quite important. This was not fully taken into consideration in the earlier tests. Where data are presented for design use, sufficient piezometer coverage was made to define accurately the pressure distribution. The curves present the low pressures in the critical areas using the relationship $\frac{h_x - h_o}{h_v}$; where h_x = pressure at any point, h_o = reference pressure at downstream face of gate leaf, and h_v = velocity head for average velocity past gate slot.

During the analysis of the test data, it was found that if h_x was assumed to be vapor pressure, the relationship, $\frac{h_x - h_o}{h_v}$, did not indicate the true head at which cavitation was known to occur in field installations. The relationship always indicated a much higher head would be needed to produce cavitation than actually existed in the field structures. A slot shape was therefore placed in a cavitation test facility to determine what value of h_x would exist when incipient cavitation occurred at the slot (Fig. 4). In this facility the ambient pressure and velocity could be varied to produce cavitation of different intensity.

Test Results

Early Tests for Wheel Gates

Inspection of Existing Structures

Several Bureau structures were examined in 1941 for signs of cavitation damage after the damage shown on Fig. 2 was discovered. It was found that the structure shown in Fig. 2 was the only one which had incurred serious damage. Two other structures had not operated sufficiently to be damaged, while another, which had operated for moderate periods, showed no damage. It is of interest to note that an inspection made on the latter structure in 1956, some 15 years later, revealed minor cavitation damage near the crest and just downstream from the gate slots.

Tests on Existing (Damaged) Design

A 1:24 sectional model was constructed of the gate design which had incurred damage. Tests showed that turbulent surging was present within the gate slots where the roller chains were located, and that this surging caused movement of loose parts of the chains. The destruction of the prototype roller chains was attributed to this action. Tests showed that the surging could be reduced to reasonable proportions by placing guard plates in the slots at the bottom corners of the leaf.

A number of gate slot shapes were tested in an attempt to eliminate the low pressures which caused the cavitation. The objective at the time was to eliminate all regions of subatmospheric pressure originating from the gate slots. Several treatments accomplished this, but not all were practicable. Some of the most promising designs for various stages of construction are shown in Fig. 5.

Flow lines in the bottom of the slot and on nearby surfaces of the original design at a small gate opening were recorded by paint tests. The tests showed clearly the presence of a separation zone along the wall immediately downstream of the slot, and the presence of complex currents within the slot. A plot of the pressure distribution on the wall downstream from the slot showed severe subatmospheric pressures in the separation zone (A, Fig. 5).

The treatment proposed for the damaged structure, that of placing a deflector at the upstream corner of the slot and a 90 degree circular arc at the downstream corner (B, Fig. 5), was never used. The power units at the project were placed in operation shortly after specifications were prepared for the slot changes, and the requirement of the gates to release large quantities of water frequently was eliminated. Only repairs to the damaged surfaces were deemed necessary and this work was done.

Designs for Structures Under Construction

A slot with a deflector on the upstream corner, an outward offset on the downstream corner, and an inward curve on the downstream wall that connected to the previous, parallel-wall alinement, was developed for the under-construction case (C, Fig. 5). This design has been used on a limited number of structures and there has been no report of damage.

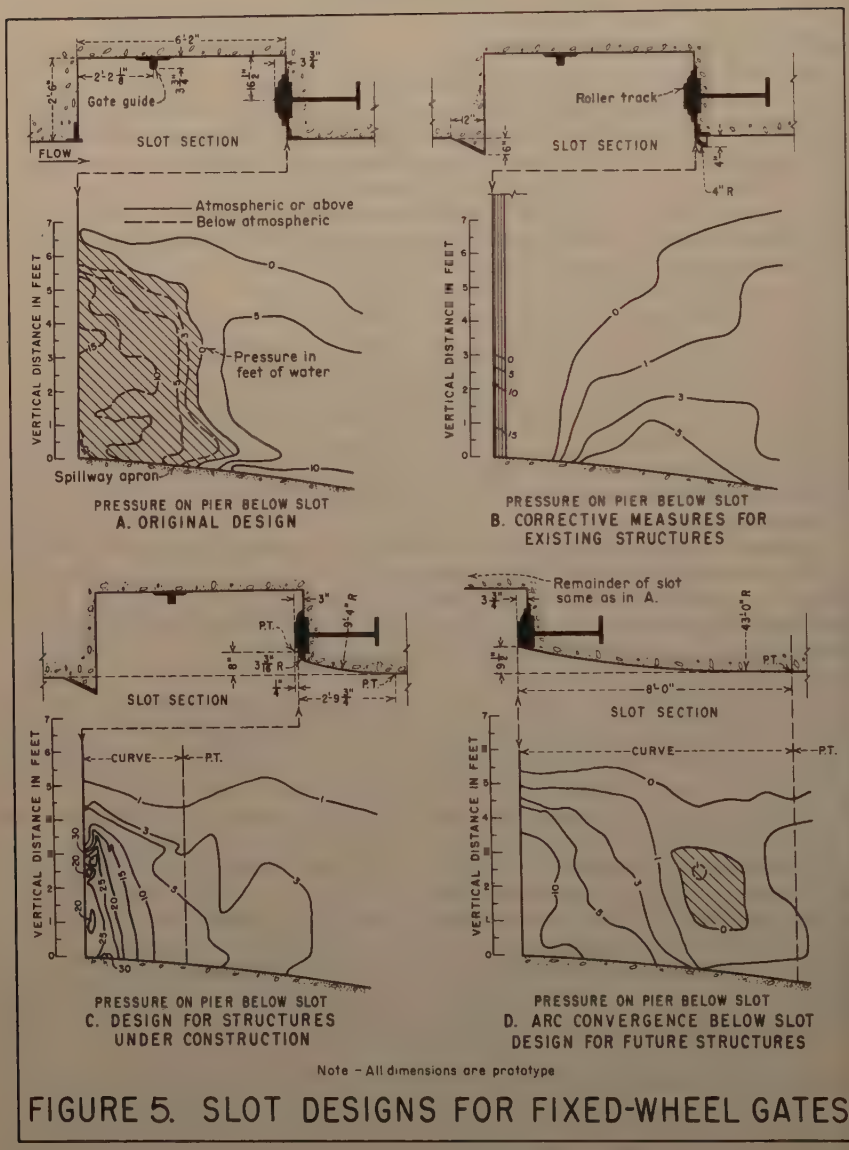

Note – All dimensions are prototype

FIGURE 5. SLOT DESIGNS FOR FIXED-WHEEL GATES

Designs for Structures in Planning Stage

Variations of the design adopted for the under-construction case were considered for future projects. One was similar to that developed later for relatively narrow gate slots (D, Fig. 5). In this slot the offset of the downstream corner was about one-third of the slot depth, considerably more than for the recent design. Paint tests showed the flow to be in contact with the downstream wall with no evidence of separation. Other tests showed the pressure distribution to be entirely satisfactory. The design was not pursued, however, when it was decided to avoid the slot problem by using extensions on the bottom corners of the gate leaves to fill the gate slots.

The slot filler extended down into recesses within the spillway crest when the gate was closed, and rose with the leaf to fill the slot as the gate opened. The filler occupied the full slot section to form smooth, continuous flow boundaries on which no subatmospheric pressures or cavitation could occur.

The ideal design of this type would be one which filled the slots at all gate openings. This was considered impracticable and a length of 6 feet was finally adopted for the one case where the extensions were used because operation at larger openings would be rare. At this point the tests were interrupted by war requirements and work was suspended for several years.

European Experiences

Shortly after the test program was suspended, an article on European experiences was published. (1) The article pointed out that the problem was not a new one, and stated that it was necessary to alter and repair structures built as early as 1885. Some of the solutions used were illustrated. There is a striking similarity between these and some of the shapes developed and used in more recent years. Actually the main difference is that present-day designs have been extended to include slide gates, and refined to handle much higher heads.

Tests for Slide Gates and Wheel Gates

Plans were made to use slide gates at higher heads than those at which damage had already occurred. A series of studies on the standard slide gate showed that severe subatmospheric pressures existed just downstream from the slot. The pressures at high-velocity flows were so low that cavitation damage would surely occur.

Early studies disclosed that low pressures could exist in as many as four locations in and near the slots, depending on the configuration of the slots. This was the case regardless of the type of leaf used.

The research on the water and air models concerned five distinct types of slots, and numerous variations of each type. The types will be referred to as:

1. Original slot with inline upstream and downstream walls (Standard gate).
2. Slot with deflector on upstream corner.
3. Slot with offset downstream corner and parallel downstream wall.
4. Slot with offset downstream corner and divergent downstream wall.
5. Slot with offset downstream corner and convergent downstream wall.

Because tests have shown that a great amount of circulation occurs in slots, and that this circulation seems greater for wide slots than for narrow ones, it is believed that gate slots should be made as narrow as possible. However, in most of the tests made to obtain general data, the slot widths were varied to cover width-to-depth ratios from 0.5 to 2.5. In a few cases the width-to-depth ratio was increased to 5.0.

Standard Slide Gate

Pressure distribution curves for the slot with inline upstream and downstream walls, the shape referred to as the original design, showed a critical pressure area on the wall just downstream from the downstream slot corner. The pressure relationships for critical areas of the slot at various width-to-depth ratios are shown in Fig. 6. The curve for the low pressure within the slot shows that pressures are about the same as the reference pressure, and that there is little change over a wide range of W/D ratios.

The pressures in the slot at the downstream corner are above the reference pressure and increase as W/D increases. The pressure at this point first increases rapidly, and then gradually, indicating that the flow spreads into the slot to cause a pressure build up as the slot widens. The leveling off of the pressure with the wider slots might be expected because the conditions are approaching those for a sudden contaction within a pipe.

The pressures on the surface immediately downstream from the downstream slot corner are the lowest found in this design. Subatmospheric pressures occur at this point for all slot widths tested and become more severe as the slot width increases.

It was noted that the pressure relationship, $\frac{h_x - h_o}{h_v}$, indicated that cavitation pressures would not occur on the surface at this location until a head in excess of 100 feet was reached. Field conditions show that severe cavitation will occur with this design for heads of 50 feet. This suggests that the pressure at this location does not have to reach vapor pressure for cavitation to occur at the slot and that scale effect may be an important factor.

To determine the pressure that would exist just past the downstream slot corner when incipient cavitation occurs this slot shape with a W/D ratio of 1.0 was placed in a special test facility (Fig. 4). Tests were made at several velocities. At each velocity the ambient pressure was adjusted until cavitatio could just be seen clearly at the downstream slot corner. The average value of $\frac{h_x - h_o}{h_v}$, for a piezometer located 0.06 inch from the corner was -0.14. In a typical case the values for h_x, h_o, and h_v, were -18.4, -10.0, and 60.0 feet of water, respectively. Thus the pressure on the surface just downstream of th downstream slot corner need not be of vapor pressure magnitude for cavitation to occur at the slot. This same phenomenon has been observed in studies made on the formation of cavitation in the vicinity of abrupt, into-the-flow offsets on flow boundaries.

From the cavitation tests on this shape it was concluded that there was a critical value of the relationship $\frac{h_x - h_o}{h_v}$ for each slot shape and W/D ratio. However, this relationship is not an appropriate tool for predicting cavitation because it does not include the basic requirement for cavitation, that is, vapo pressure.

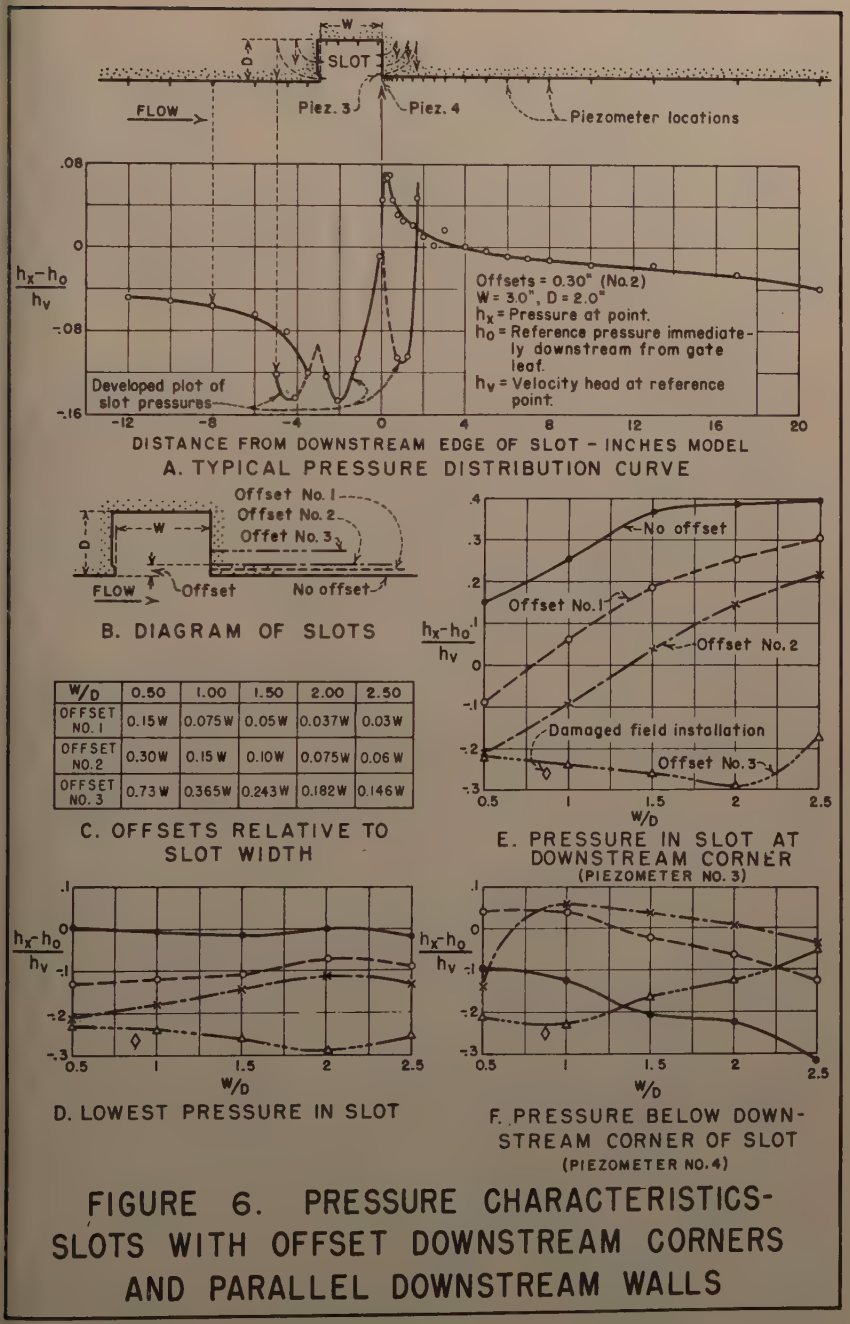

W/D	0.50	1.00	1.50	2.00	2.50
OFFSET NO. 1	0.15W	0.075W	0.05W	0.037W	0.03W
OFFSET NO. 2	0.30W	0.15W	0.10W	0.075W	0.06W
OFFSET NO. 3	0.73W	0.365W	0.243W	0.182W	0.146W

C. OFFSETS RELATIVE TO SLOT WIDTH

FIGURE 6. PRESSURE CHARACTERISTICS-SLOTS WITH OFFSET DOWNSTREAM CORNERS AND PARALLEL DOWNSTREAM WALLS

A better parameter for predicting cavitation at gate slots is the cavitation number, or index for the particular slot, $K = \frac{h_o - H_v}{h_v}$, where, h_o is the computed average pressure in feet of water in the flow passing the slot, H_v is the vapor pressure referred to atmosphere, and h_v is the velocity head corresponding to the average velocity of flow passing the slot. The index for incipient cavitation for the tested slot shape was 0.28.

A program for determining the critical cavitation indexes for particular slot shapes is currently being pursued. Although the data presented in this paper do not provide this means of pin-pointing the cavitation characteristics of the various slot designs, it is extremely valuable for visualizing and comparing the cavitation potential and other hydraulic characteristics of the designs.

Contraction Upstream of Slot

In one gate design, a forced contraction was used to overcome the slot problem (Fig. 7). This large contraction directed the jet away from the slot and provided aeration as the jet issued from the gate. Model studies indicated satisfactory operation with free discharge and with back pressure operation where aeration can occur. Several units of this design have been installed, and no trouble has been experienced after a number of years of operation. The capacity of the design is somewhat less than for the usual slide gate, the discharge coefficient being 0.80 based on the orifice diameter. This compares to about 0.94 for the slide gate.

Deflectors on Upstream Slot Corners

In tests made on a gate for a medium head installation which released flow directly into a stilling basin, the required uniformly distributed flow was obtained by adding small deflectors at the upstream edges of narrow slots, and by eliminating the convex curve on the upstream face of the gate. No pressures were measured in the vicinity of the slots. The deflectors decreased the capacity of the gate, the discharge coefficient being decreased to 0.84 from 0.94.

The design was used in several moderate head installations. Then the need arose for a higher capacity, higher head gate. An extensive investigation was begun to develop a cavitation-free slot which would not seriously affect gate capacity. Two deflector heights for five different slot widths were tested. The deflectors varied from 0.025 to 0.25 times the slot width. In the first series, the downstream slot corner was in line with the upstream wall. The deflector caused a lowering of the pressure within the slot for all widths, but there was a gradual increase in this pressure as the slot widened (Fig. 8). For different deflectors, the higher the deflector, using reasonably small sizes, the lower the pressure becomes within the slot. These trends apparently result from the ejector action induced by the deflected jet as it passes the slot. The lowest pressures within the slots were substantially below the reference pressure at the downstream face of the gate leaf. The pressures were severely subatmospheric in all cases, particularly so for slots with small width-to-depth ratios.

Similarly, the pressures within the slot at the downstream corner were severely subatmospheric, as were the pressures below the downstream corner, for large deflectors and small W/D ratios.

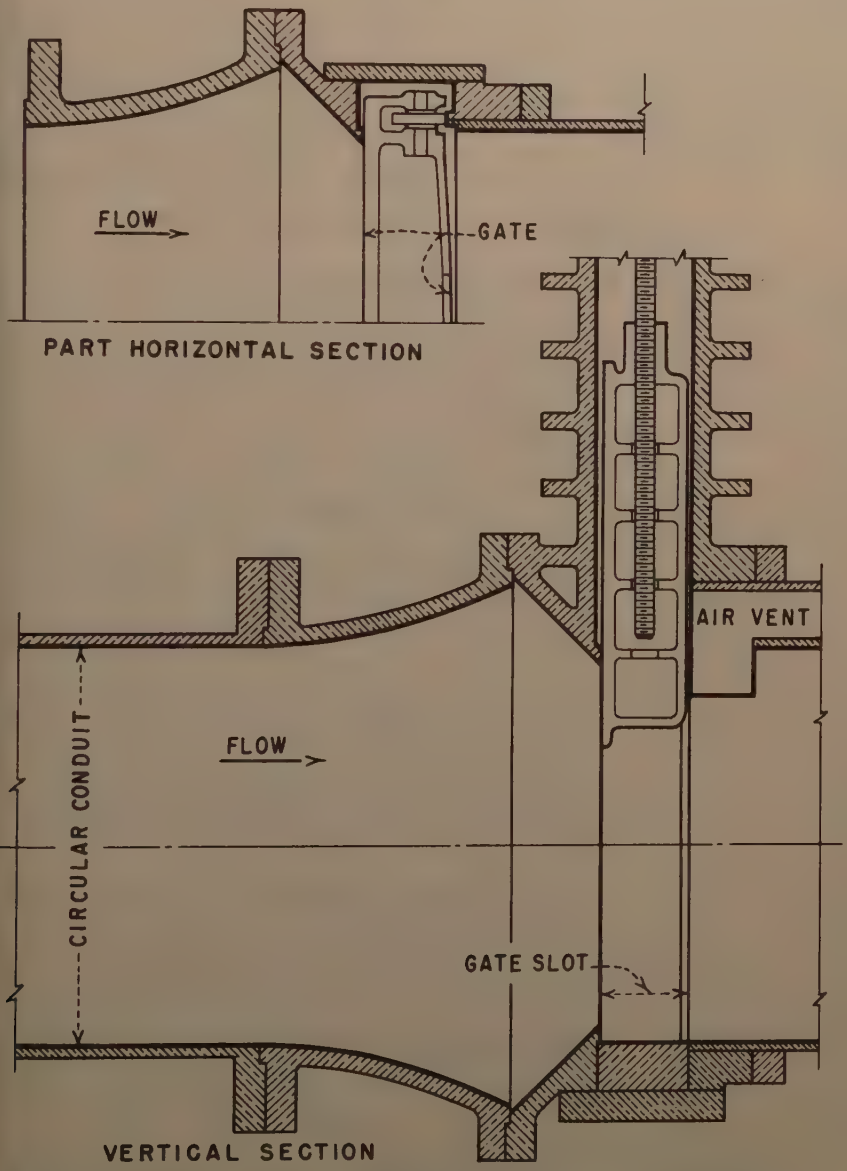

FIGURE 7. GATE WITH LARGE CONTRACTION UPSTREAM FROM SLOT

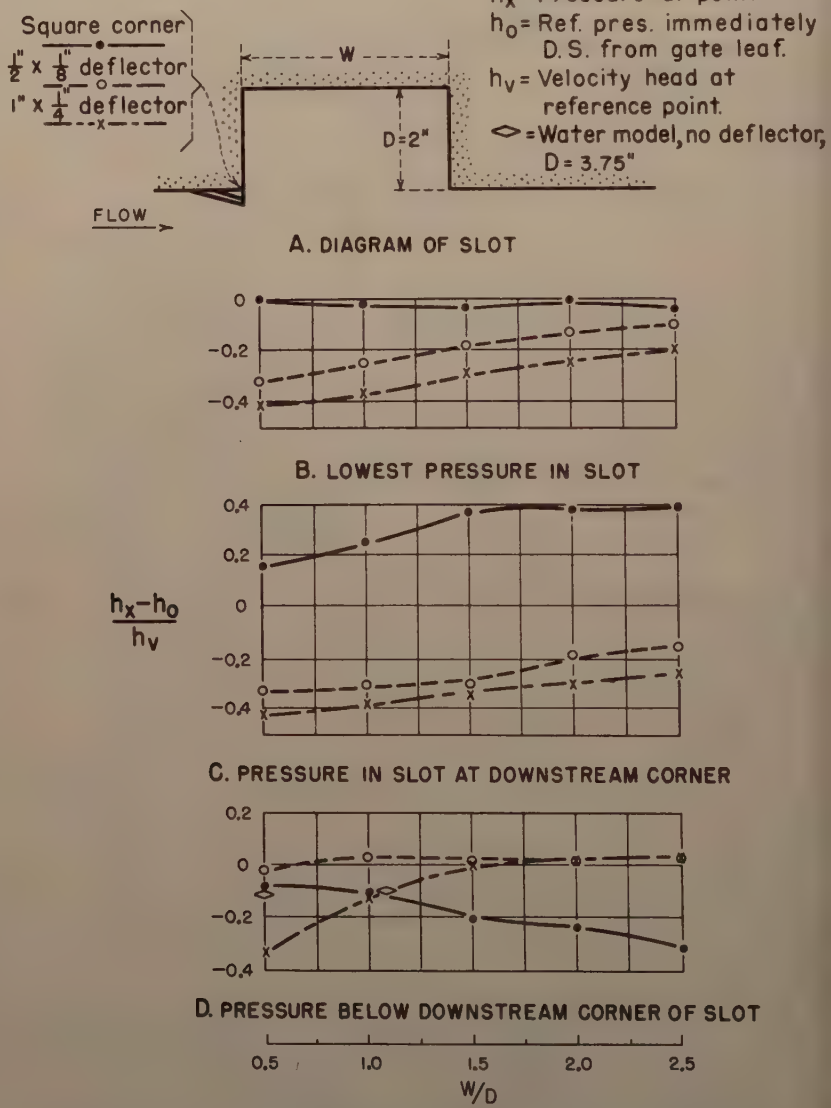

FIGURE 8. PRESSURE CHARACTERISTICS-SLOTS WITH DEFLECTORS AT UPSTREAM CORNERS AND INLINE DOWNSTREAM WALLS

A second series of deflector tests was made with the downstream slot corner offset slightly outward. The results were not greatly different from those with no offset (Fig. 9). No further tests were made using deflectors because they caused the pressures within the slots to go considerably below the reference pressure and appeared to be conducive to cavitation for all but very low heads. Furthermore, they restricted the flow passage too much and reduced the carrying capacity of the gates. Subsequent tests were directed toward developing a slot with the downstream corners offset outward from the flow. The amount of offset and the manner in which the surfaces just downstream from the corners were alined were of particular interest.

Offset Downstream Slot Corner and Parallel Downstream Walls

Offsetting the downstream corners outward and continuing the downstream walls parallel to the axis of the gate was considered. The typical pressure distribution curve for this design shows that critical conditions might exist at three locations (A, Fig. 6). Pressures within the slots were substantially lower than the reference pressure. They would be severely subatmospheric with low back pressure on the gate at all width-to-depth ratios, and would become more severe with increases in W/D. The offset apparently causes an ejector action at the slot that lowers the pressure within the slot.

At small W/D ratios, the pressure within the slot at the downstream corner was severely subatmospheric for all offsets tested. The pressure increased gradually as W/D increased. Subatmospheric pressures would be most severe for the larger offsets, unless effective aeration could be provided.

Pressures immediately below the downstream corner of the slot may be positive or negative, depending upon the offset. Large offsets and wide slots give severe negative pressures.

The wide slot with a large offset is similar to one on which cavitation damage occurred in the field. Pressure relationships obtained from a model of the slot are shown on Fig. 6. These adverse relationships show that the cavitation damage could have been expected.

The pressure characteristics of slots with offset downstream corners and parallel downstream wall indicate cavitation within the slot for all except very small offsets, thus the design was considered undesirable.

Offset Slot Corner and Diverging Downstream Walls

The effect of offsetting the downstream slot corner and continuing the flow passage with divergent walls was investigated. A typical pressure curve for this design is shown on Fig. 10. The pressures within the slot were much below the reference pressure and severely subatmospheric when there was little or no back pressure on the gate. The subatmospheric pressures became more severe as the offset increased. The pressure increased slightly as W/D increased.

Pressures in the slot at the downstream corner at small W/D ratios may be above or well below atmospheric, depending on the amount of offset. There was a pressure build-up at this location for all offsets as W/D increased.

Pressures immediately below the downstream corner may be above or greatly below atmospheric pressure, depending on the amount of offset and the W/D ratio. Primarily the pressures were negative. Generally, the pressure decreased as W/D increased. The pressures became severely subatmospheric as the offset decreased.

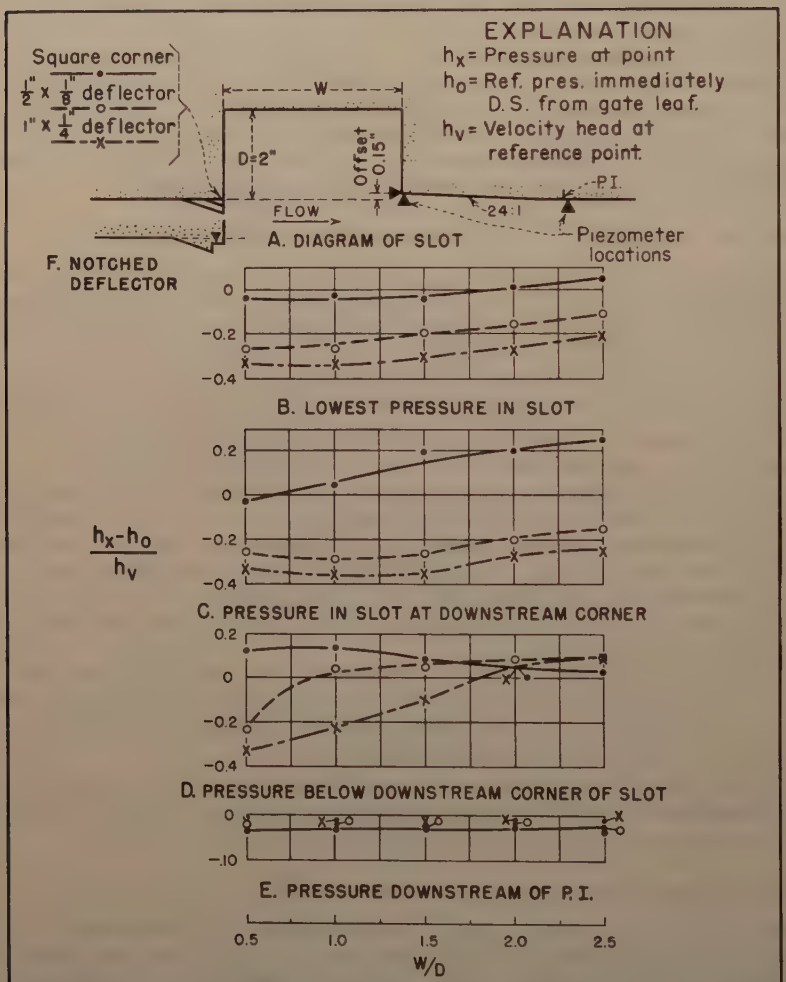

FIGURE 9. PRESSURE CHARACTERISTICS—SLOTS WITH DEFLECTORS AT UPSTREAM CORNERS AND WITH OFFSET DOWNSTREAM CORNERS AND 24:1 CONVERGING DOWNSTREAM WALLS

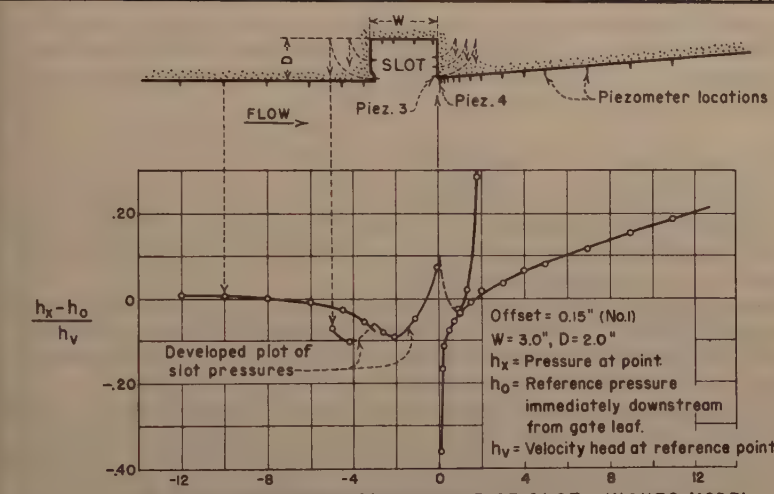

A. TYPICAL PRESSURE DISTRIBUTION CURVE

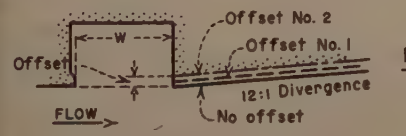

B. DIAGRAM OF SLOTS

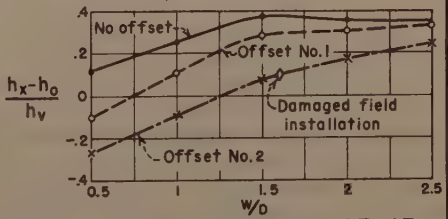

E. PRESSURE IN SLOT AT DOWNSTREAM CORNER (PIEZOMETER NO. 3)

W/D	0.50	1.00	1.50	2.00	2.50
OFFSET NO. 1	0.15 W	0.075 W	0.05 W	0.037 W	0.03 W
OFFSET NO. 2	0.30 W	0.15 W	0.10 W	0.075 W	0.06 W

C. OFFSETS RELATIVE TO SLOT WIDTH

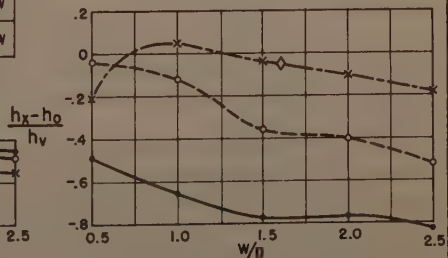

F. PRESSURE BELOW DOWNSTREAM CORNER OF SLOT (PIEZOMETER NO. 4)

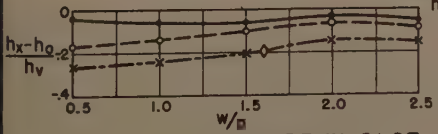

D. LOWEST PRESSURE IN SLOT

FIGURE 10. PRESSURE CHARACTERISTICS- SLOTS WITH OFFSET DOWNSTREAM CORNERS AND 24:1 DIVERGING DOWNSTREAM WALLS

The design with a large offset and diverging walls was similar to one on which cavitation damage was experienced. Pressure relationships obtained from a model approximating the prototype structure are shown in Fig. 10. They indicate that low pressures within the slot were the source of damage. Local irregularities in the concrete, and at concrete-to-metal joints, may have been a contributing factor.

Offset Slot Corner and Converging Downstream Wall

Two distinct types of converging walls were studied. In one type the convergence rate was constant, such as 12:1 and 24:1. In the other type the rate varied, such as a circular arc extending from the offset corner to the point of tangency in line with the upstream wall.

The first tests were made using a hydraulic model. The tests were quite encouraging and one of the shapes was used successfully in two field installations.(2) Later most of the shapes tested with water were reexamined in air and all subsequent tests were made with air.

12:1 Converging Wall.—One design in common use, having a 1-inch offset corner rounded on a 1-1/4-inch radius and a 12:1 converging downstream wall, was among the first examined by model studies. The test shape differed slightly from the prototype shape in that the upstream slot corner of the model was not rounded because it was reasoned that the rounding would cause the flow to expand into the slot rather than to continue past it. This expansion would worsen pressure conditions in the contraction at the downstream corner of the slot. The pressure curve (Fig. 11) obtained with the test shape in a hydraulic model is similar to that previously reported.(3) Negative pressures near the intersection of the 12:1 convergence and the straight wall were severe, more so than indicated in the previously reported tests. The Bureau tests indicated that the outwardly offset, 1-inch-rounded corner with a 12:1 convergence eliminated cavitation pressures near the downstream edge of the slot, but transferred them to the line of intersection of the converging and in-line wall sections (Fig. 11). Field experience shows cavitation below a slot with such a 12:1 convergence.

In tests which followed, the rounded downstream corner was replaced with a sharp one on the basis that earlier exploratory tests indicated no adverse effects. An offset downstream corner followed by a 12:1 convergence was investigated for various slot widths. The offset to width ratio varied from 0.03 to 0.15 (Fig. 12).

The lowest pressures within the slot were slightly less than the reference pressure at the downstream face of the leaf. These pressures approached the reference pressure as the W/D ratio increased. A rising pressure trend was noted within the slot at the downstream corner. The pressure immediately downstream from the corner was above the reference pressure at small W/D ratios and decreased to reach the reference pressure as W/D increased. The pressure immediately downstream from the intersection of the converging and parallel wall sections was below the reference pressure for all W/D ratios, and changed little with changes in this ratio.

24:1 Converging Wall.—The pressure distribution for a slot with a downstream corner offset a small amount and the wall immediately downstream converged at a 24:1 rate was similar to that for the same offset with a 12:1 convergence (Figs. 12 and 13). The lowest pressure within the slot did not differ materially from that for the 12:1 convergence. This pressure was

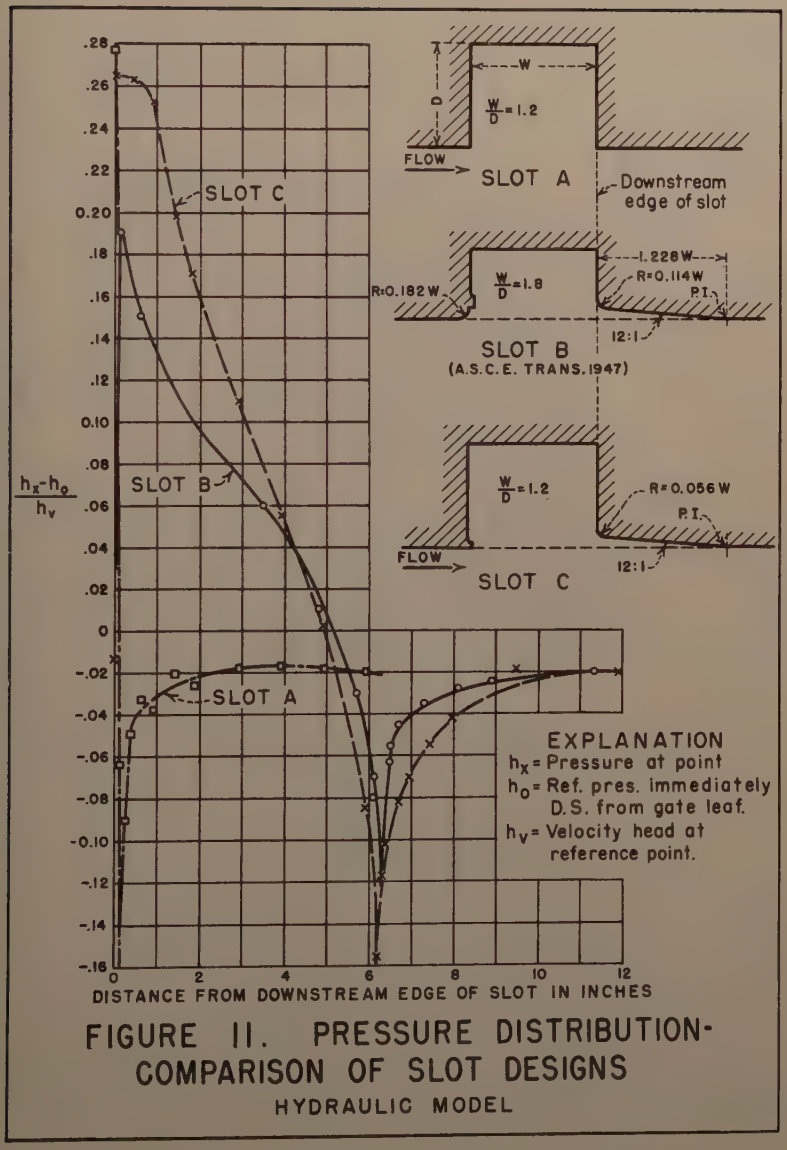

FIGURE 11. PRESSURE DISTRIBUTION-COMPARISON OF SLOT DESIGNS

HYDRAULIC MODEL

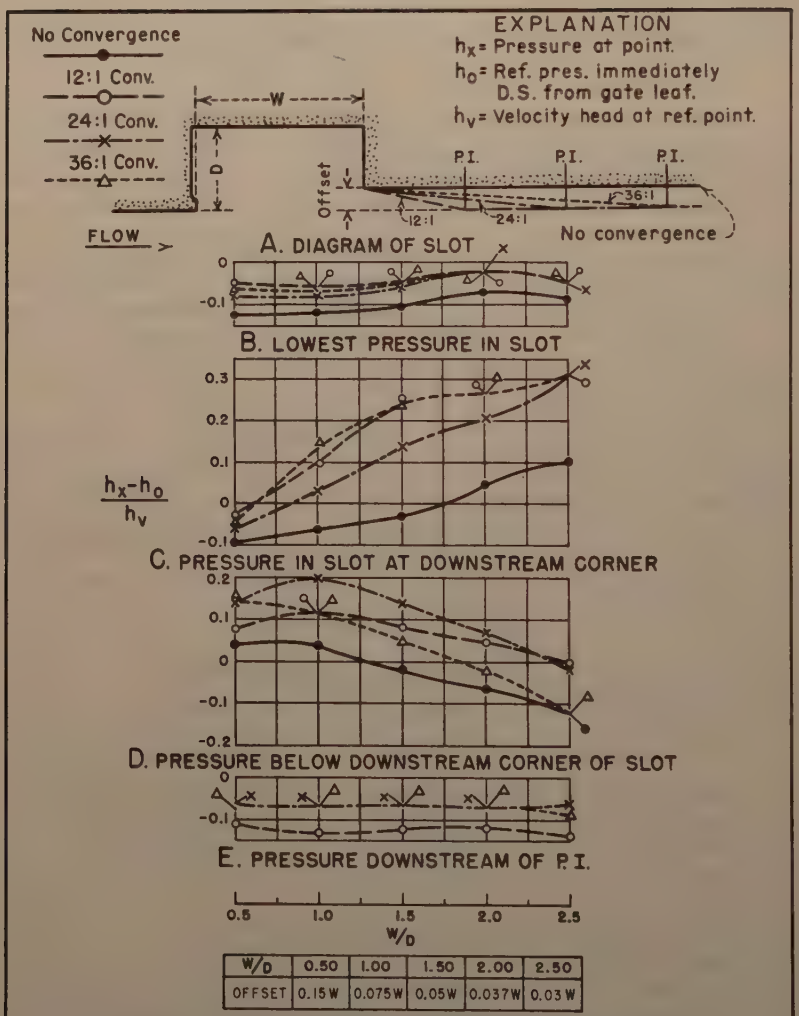

W/D	0.50	1.00	1.50	2.00	2.50
OFFSET	0.15W	0.075W	0.05W	0.037W	0.03W

FIGURE 12. PRESSURE CHARACTERISTICS-SLOT WITH OFFSET DOWNSTREAM CORNERS AND CONSTANT-RATE CONVERGING DOWNSTREAM WALLS

slightly below the reference pressure at the downstream face of the leaf and approached the reference pressure as W/D increased. A comparison of data from the hydraulic and aerodynamic models for a 24:1 convergence shows excellent agreement (Fig. 13).

Pressures in the slot at the downstream corner were below the reference pressure at small W/D ratios and increased rapidly as W/D increased.

Although pressures immediately below the downstream corner decreased gradually as W/D increased, the pressures remained positive until the W/D ratio reached about 2.5.

Pressures downstream from the line of intersection of the converging walls are somewhat below the reference pressure. The pressure relationships are constant for all W/D ratios and are nearer the reference pressure than for the 12:1 convergence. The tests with water indicate slightly lower pressure than the test with air (Fig. 13). This is understandable because the surfaces upstream and downstream of the line of intersection were machined from metal on the hydraulic model, and were hand worked in wood on the air model. A much sharper intersection line resulted in the metal, and the pressures just past this line would be expected to be lower than for the slightly less sharp line in the wood.

In one series of tests, the slot depth was decreased to 1/2 the original depth (Fig. 13). The pressure trends were similar to those for the deeper slot but occurred more gradually. It was concluded that the amount of offset was governed more by the slot width than the slot depth.

36:1 Converging Walls.—A more gradual convergence downstream from the offset corner changed the pressure conditions only slightly. The trend of the lowest pressure in the slot was about the same as for the more rapid convergence with the same corner offset (Fig. 12). This was also true of the pressure within the slot at the downstream corner and the pressure immediately downstream from the offset corner. At W/D = 2.5, the latter pressure was quite low.

Pressures at the line of intersection were slightly higher and, thus, nearer the reference pressure than for the more rapid convergences. However, the change was not sufficient to eliminate the need for rounding the corner at the line of intersection.

Offset Slot Corner and Curved Converging Downstream Wall

The low pressures just downstream from the line of intersection of the converging and parallel walls were cavitation potentials at high heads, and a means of preventing these low pressures was sought. Considerable improvement was obtained by rounding the intersection downstream from the 24:1 convergence, but the amount of rounding used did not eliminate the cavitation potential (Figs. 13 and 14). It appeared that substantial rounding would be required to materially reduce this cavitation potential and it may be just as feasible to make the convergence a continuous curve.

Arc Convergence.—Radii which varied from about 80 to 300 times the corner offset were tested. Pressure-wise this design proved superior to all others tested (Fig. 15).

The low pressures within the slot were slightly below the reference pressures for all arcs when the downstream slot corner was offset. The pressures did not change as the W/D ratio was varied. When no offset was used the pressures were somewhat higher.

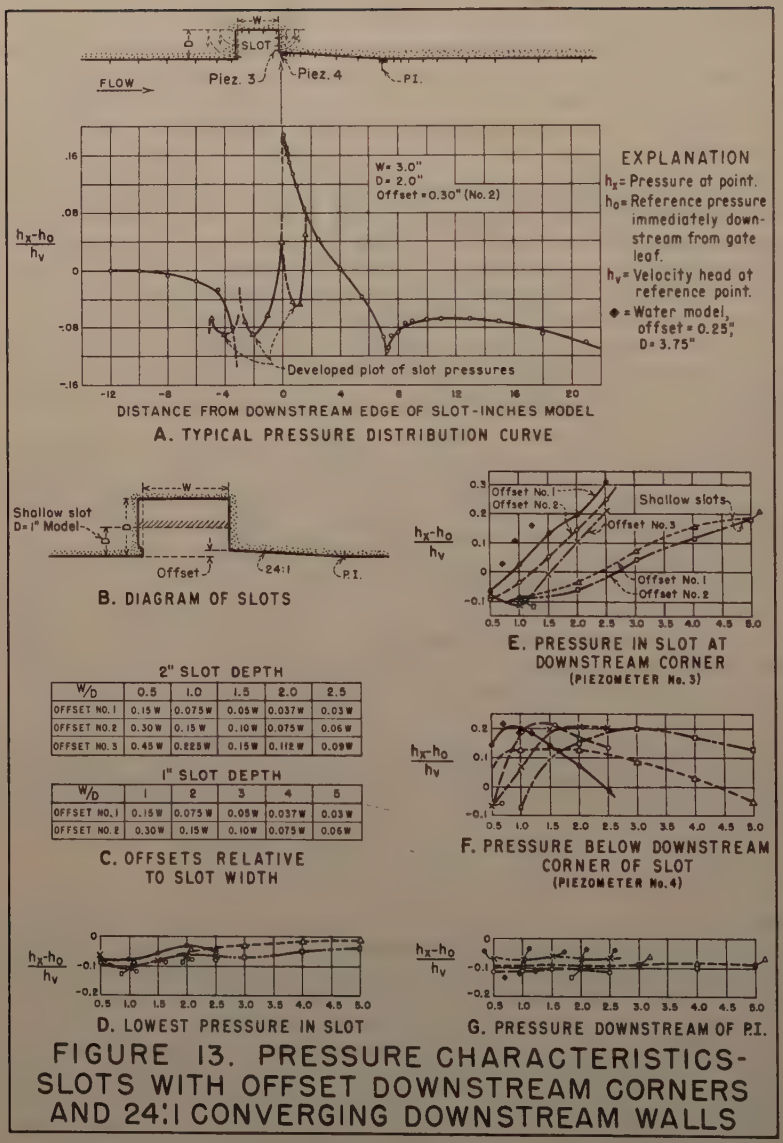

2" SLOT DEPTH

W/D	0.5	1.0	1.5	2.0	2.5
OFFSET NO. 1	0.15 W	0.075 W	0.05 W	0.037 W	0.03 W
OFFSET NO. 2	0.30 W	0.15 W	0.10 W	0.075 W	0.06 W
OFFSET NO. 3	0.45 W	0.225 W	0.15 W	0.112 W	0.09 W

1" SLOT DEPTH

W/D	1	2	3	4	5
OFFSET NO. 1	0.15 W	0.075 W	0.05 W	0.037 W	0.03 W
OFFSET NO. 2	0.30 W	0.15 W	0.10 W	0.075 W	0.06 W

C. OFFSETS RELATIVE TO SLOT WIDTH

FIGURE 13. PRESSURE CHARACTERISTICS- SLOTS WITH OFFSET DOWNSTREAM CORNERS AND 24:1 CONVERGING DOWNSTREAM WALLS

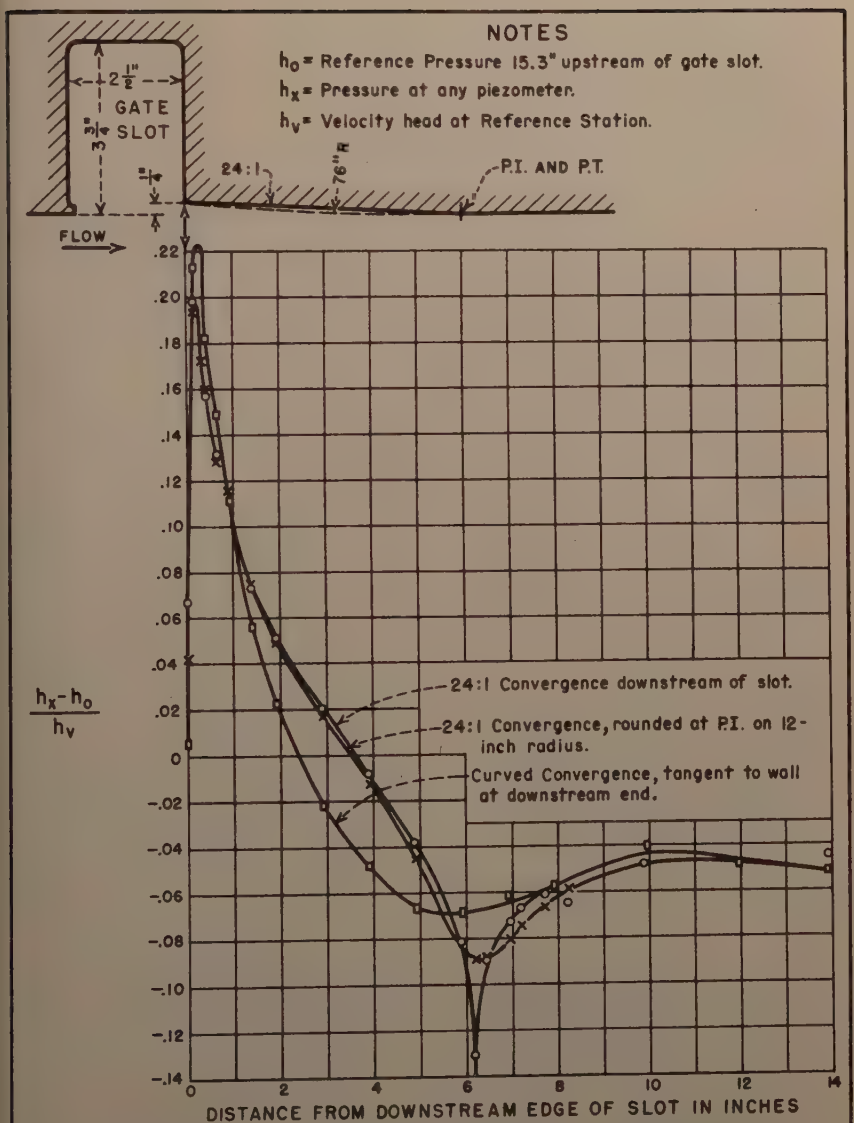

FIGURE 14. COMPARISON OF PRESSURE CHARACTERISTICS–SLOTS WITH OFFSET DOWNSTREAM CORNERS AND CONSTANT AND VARIABLE-RATE CONVERGING DOWNSTREAM WALLS

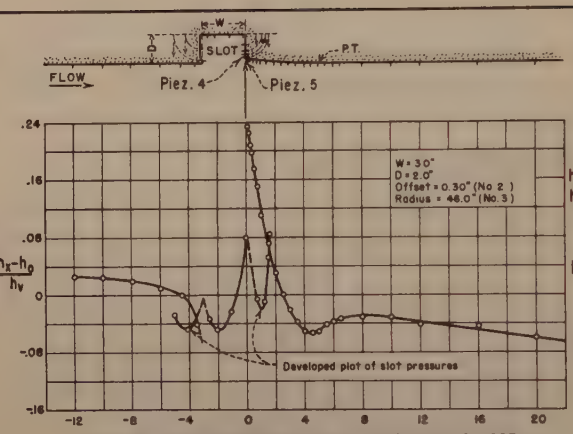

A. TYPICAL PRESSURE DISTRIBUTION CURVE

B. DIAGRAM OF SLOTS

W/D	0.5	1.0	1.5	2.0	2.5
OFFSET NO.1	0.15W	0.075W	0.05W	0.037W	0.03W
OFFSET NO.2	0.30W	0.15W	0.10W	0.075W	0.06W
OFFSET NO.3	0.45W	0.225	0.15W	0.112W	0.09W
RADIUS NO.1	12.6W	6.30W	4.20W	3.15W	2.52W
RADIUS NO.2	42.5W	21.25W	14.167W	10.625W	8.50W
RADIUS NO.3	46.0W	23.0W	15.33W	11.50W	9.20W
RADIUS NO.4	97.6W	48.80W	32.60W	24.45W	19.56W

C. OFFSETS AND RADII RELATIVE TO SLOT WIDTH

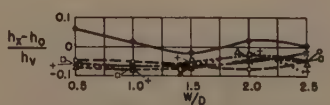

D. LOWEST PRESSURE IN SLOT

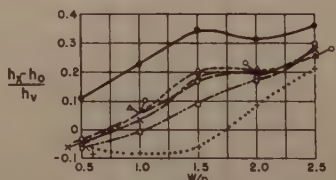

E. PRESSURE IN SLOT AT DOWNSTREAM CORNER (PIEZOMETER No. 4)

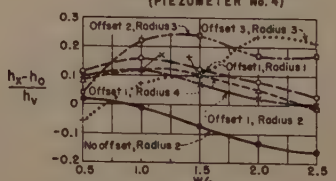

F. PRESSURE BELOW DOWNSTREAM CORNER OF SLOT (PIEZOMETER No. 5)

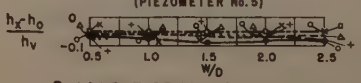

G. LOWEST PRESSURE ON CURVED CONVERGING WALL

FIGURE 15. PRESSURE CHARACTERISTICS-SLOTS WITH OFFSET DOWNSTREAM CORNERS AND CURVED CONVERGING WALLS

The pressures in the slot at the downstream corner were slightly below the reference pressure at small W/D ratios and increased rapidly as W/D increased. Higher pressures occurred when there was no offset of the downstream slot corner.

The pressures downstream from the slot corner were generally above the reference pressures for all arcs used in combination with the offset downstream corner. When no offset was provided the pressures were substantially lower and were much lower than the reference pressure at a W/D of 2.5.

The lowest pressures occurring on the curved converging wall sections were slightly below the reference pressures and were about the same for all arcs, offsets and W/D ratios tested.

Elliptical Convergence.—In some recent installations where regulation was required under no back pressure or under a great deal of back pressure, use was made of a slot with parallel, outwardly offset downstream walls and with a plate on each downstream corner that extended into the passage the amount of the wall offset. The plate was intended to induce separation at the wall to permit circulation of flow to relieve low pressures adjacent to the wall. This design was considered for only those cases with free flow or with high back pressures and no model studies were made at the time.

In a recent wheel gate installation it was necessary to regulate at various openings with moderate submergences. The slot design with the extended plate at the offset downstream corner was investigated.

Hydraulic model tests showed that the jet was unstable and shifted rapidly from side to side, indicating changes in pressure and flow pattern in the vicinity of the plates. Similar instability was shown in air model tests, and the pressures downstream from the plates were much below the reference pressure. It was reasoned that the instability, low pressures, and pressure fluctuations could be eliminated by better aeration and/or by filling the contraction areas just downstream from the plate with fillers of elliptical cross section (Fig. 16). It was found that venting the region just downstream from the plates had little influence on the unstable flow. However, the tests for this specific installation showed that the elliptical shape eliminated the unstableness and raised the pressures until they were only 2 to 8 feet below atmospheric.

Some reduction in capacity will result for elliptical shapes protruding into the stream. In the structure for which the tests were made, the discharge was limited by a long unlined tunnel, and the capacity reduction was not important. This reduction might be of prime importance where capacity counts.

One of the most important advantages of the elliptical shape protruding into the stream is that cavitation will not be induced at any gate opening, including very small openings. Particular conditions encountered at very small openings are discussed in detail in a subsequent part of this paper.

Rounded Upstream Corners

The effect of rounding the upstream corners of slots was investigated by testing two degrees of rounding at several W/D ratios. The tests showed that a small amount of rounding had little effect on the pressures in and near the slot, but that appreciable rounding produced a noticeable effect (Fig. 17). The larger radius caused a pressure build-up in the slot, increased the contraction, and lowered the pressures just below the downstream corner, as W/D increased. Thus, rounding of the upstream corner to any large degree would not seem desirable.

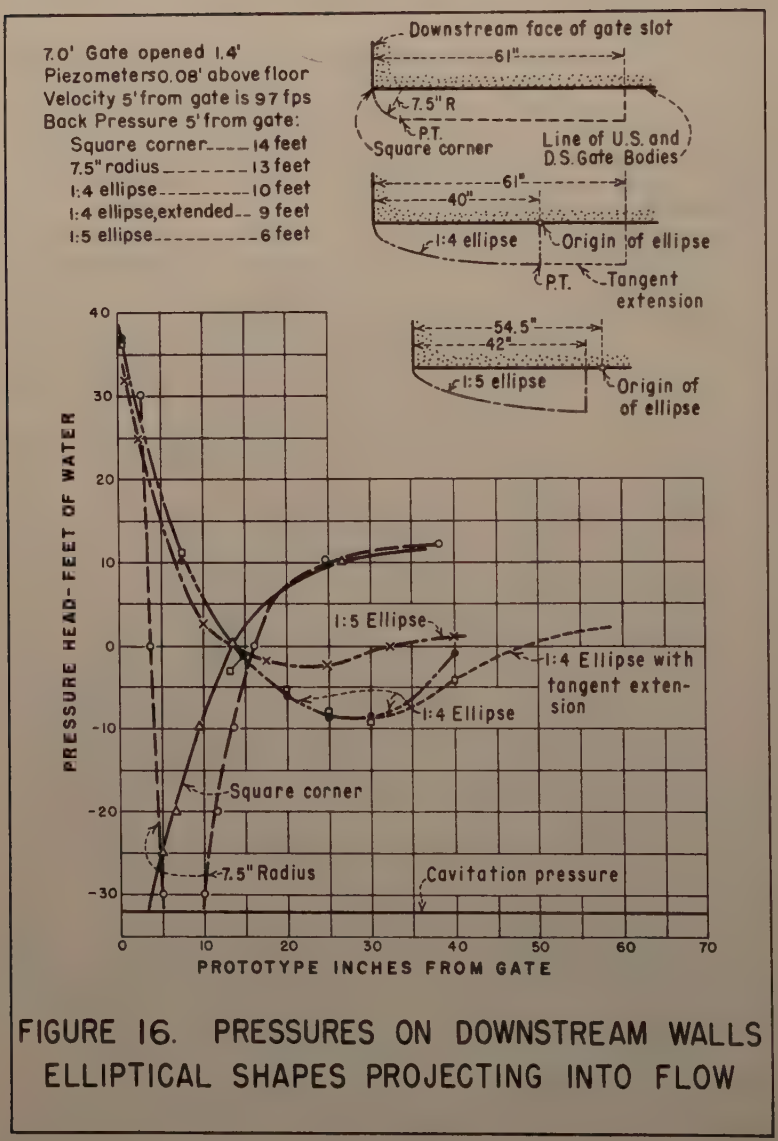

FIGURE 16. PRESSURES ON DOWNSTREAM WALLS ELLIPTICAL SHAPES PROJECTING INTO FLOW

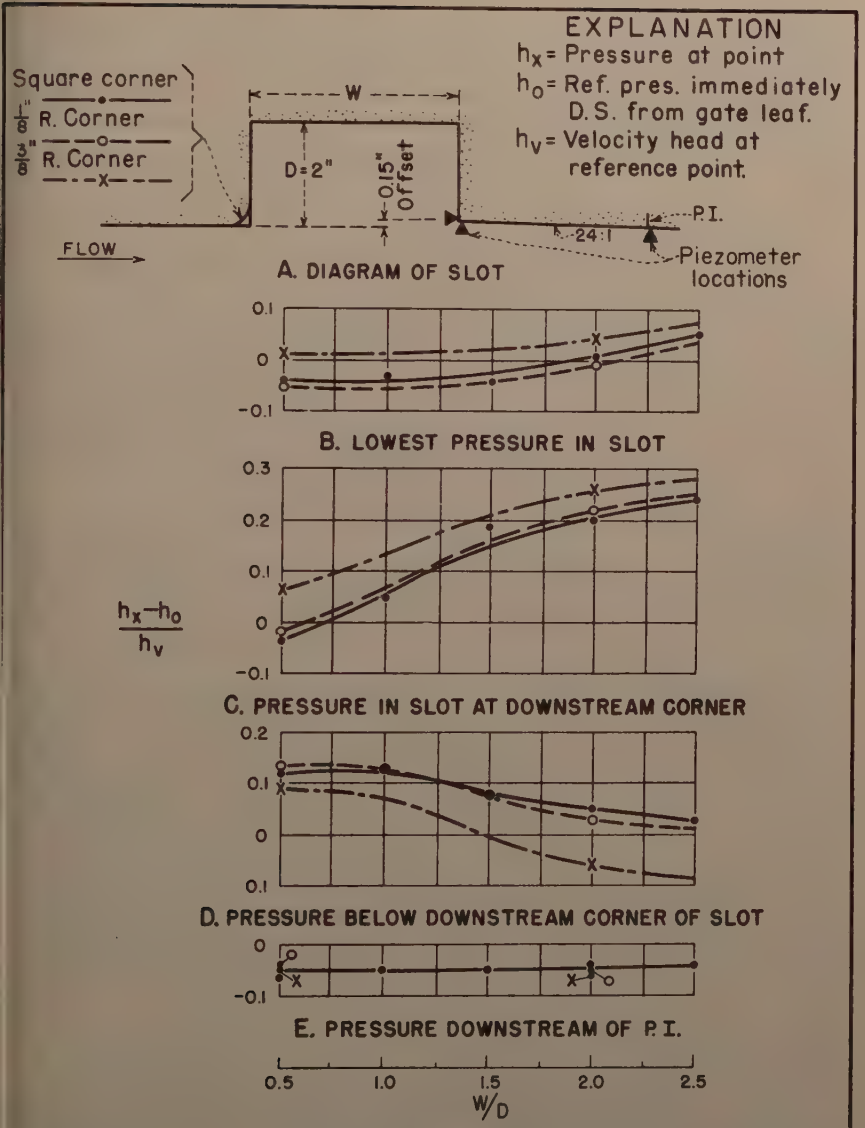

FIGURE 17. PRESSURE CHARACTERISTICS-SLOTS WITH ROUNDED UPSTREAM CORNERS AND OFFSET DOWNSTREAM CORNERS WITH 24:1 CONVERGING DOWNSTREAM WALLS

"Short-Tube" Action at Small Gate Openings

Because of the finite seal surface width needed on the bottom of a gate leaf, there will be times during operation at very small gate openings when "short-tube" action will take place between the leaf seal surface and the body. When such operation is at high heads, cavitation will occur and there will be noise, vibration, and damage. Use of the gate at openings where short-tube action occurs is not recommended. For free discharge conditions, the opening is not critical until it is less than about one-half the width of the seal surface.

Small Gate Openings with and Without Back Pressure

Extensive pressure measurements disclosed severe subatmospheric pressures near the floor just downstream from the slot for small submergences at gate openings equivalent to about 5 inches on a 9-foot high gate. Apparently, the area for water to enter the slot becomes large with respect to the area under the gate, and the downstream edge of the slot just beyond the leaf bottom acts as the edge of an orifice. A contraction forms at the corner, and if the velocities are high and no aeration can occur, the pressures are low and cavitation will occur. With no back pressure on the gate aeration will occur and the pressures will be near atmospheric.

A number of tests were made in an attempt to relieve the negative pressures which occur for back pressure conditions. One series of tests concerned reducing the slot width near the floor, and another concerned moving the slot upstream relative to the downstream leaf face (Fig. 18). No overall benefit was gained by narrowing the slot near the floor, and a local region of very severe negative pressure was created. The narrowed slot tests were therefore discontinued.

It was reasoned that the slot corner could not act as a control if the slot was moved upstream relative to the gate leaf. This design was tested, and proved entirely satisfactory hydraulically, but the arrangement was not ideal mechanically because of seal problems. A seal design which appeared satisfactory was suggested by the designers, but it has not been used to date. It should be noted that much less spray was created with the slot moved upstream than with the regular slots or the slots made narrow at the floor.

Another solution may be found in the design where elliptical shapes that project into the stream are placed downstream from the slot corner. Preliminary studies show that these shapes can be cavitation-free at all gate openings and downstream submergences. Additional studies are needed to establish the design factors.

Notch in Deflector Upstream from Slot

Tests on a deflector with a notch in the downstream corner (Fig. 9F) showed severe subatmospheric pressures in the notch when the gate leaf regulated the flow. These low pressures occurred in regions of the notch near the gate leaf bottom, and as the leaf moved up or down, the region of subatmospheric pressure moved accordingly. The removal of the notch eliminated the severe subatmospheric pressures. It was concluded that if a deflector is used it must continue without change in shape until it reaches the upstream edge of the slot.

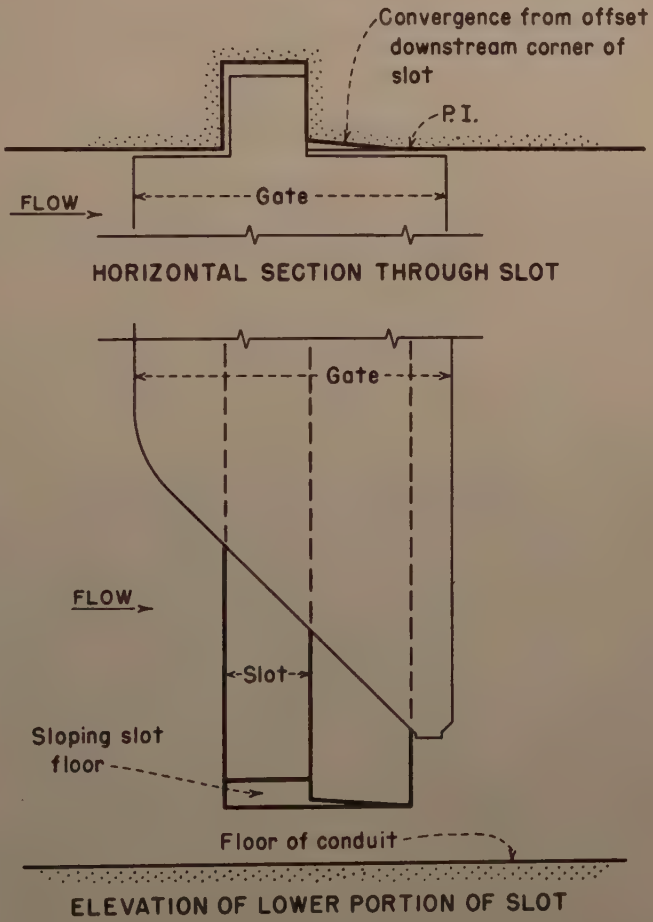

FIGURE 18. SLOT MOVED UPSTREAM RELATIVE TO GATE LEAF

Treatment of Downstream Corner of Slot

The downstream corner was kept sharp in most of the tests to simplify the design. Tests show this to be satisfactory at all openings for the free flow condition. Also, it permitted the use of a gate with a shorter span. However, in some cases, a rounding might prove beneficial. This is particularly true in cases where relatively wide slots are required and where submerged flow is present. An elliptical shape, such as shown in Fig. 16, is at present considered best for these conditions.

Field Experience

Gate Having Offset Slot Corners and Converging Walls

The slot with an offset corner and a constant rate converging wall was used in the Palisades Dam outlet works. The design was developed in the early tests made on the water model, and the convergence used was 60 to 1. The offset of the downstream corner was 1/2 inch.

The gate bodies were made up of welded plates. The floor and lower portion of the walls of the downstream gate frame were made from a single plate. A 2-inch radius was used where the plate was turned upward to form the walls. The transition from this rounded corner of the gate frame to the sharp corner in the concrete flow passage downstream was made by a concrete fillet about 10 inches long. This fillet produced surfaces that receded from the flow on about a 10.1 slope.

Since the slide gate used at Palisades outlets was a new design, and it was known that severe damage had been experienced on other designs, close tolerances were specified for constructing and installing the gates, and frequent and thorough inspections were recommended during the operating seasons. Before the first two gates were placed in operation, it was noted that the concrete walls projected inward from the metal surface of the gate body as much as 1/2 inch. Grinding of these abrupt into-the-flow offsets was required of the contractor. However, the grinding was done on a rather sharp bevel, in some cases as steep as 4:1.

An inspection of the downstream flow passages, after considerable operation, showed evidence of cavitation at several locations. The cavitation at these locations was determined to be of a local nature produced by surface irregularities in the concrete. Pitted areas were found on the walls immediately below the gate frames at points where small into-the-flow offsets in the concrete walls had not been ground. Other areas were found downstream of the rather steep bevels formed by grinding larger offsets. Cavitation was also noted in joints in the concrete surfaces and on the surfaces of the fillets placed in the bottom corners downstream from the gate frames.

After subsequent operation at small openings for about 30 days at a head of about 190 feet, another examination was made. The cavitation damage at all locations had increased somewhat, but the damage on the corner fillets had become serious. It was therefore necessary to repair the damaged areas, and to prevent future trouble by providing longer, better constructed bottom corner fillets.

A close examination of the flow passages disclosed other interesting factors. Cavitation had occurred just downstream from an abrupt, into-the-flow offset of about 1/8 inch (Fig. 19). This is in agreement with laboratory

tests made recently to determine the cavitation potential of abrupt offsets when subjected to high velocities and various pressures (Fig. 20).

Cavitation damage was also noted in the concrete downstream from voids commonly known as "bug holes." The damage was noticeable at the larger holes, and nonexistent at the small holes. The dividing point seemed to be about 1/2 inch.

There was no damage at the downstream end of the 60:1 converging wall, and there was no damage to any of the metal parts of the gate where installation had been made strictly in accordance with specifications.

From these observations, it is concluded that the cavitation downstream from the Palisades gates resulted from local surface irregularities and not from the gate slot design. The damage is being repaired and the known cavitation-producing irregularities removed. Periodical inspections will be continued to ascertain the effectiveness of the corrective measures and to detect any other characteristics which could be responsible for cavitation damage.

CONCLUSIONS

Low pressures just downstream from the downstream corner of slots with parallel inline upstream and downstream walls make this design susceptible

Figure 19

to cavitation. The pressures are much below the reference pressure at the downstream face of the leaf, and decrease as W/D increases. The design serves adequately for heads less than about 35 feet.

Deflectors at the upstream edges of slots produce an ejector action which lowers the pressures at the slot far below the reference pressure and will induce cavitation. There may be a small deflector design which would give satisfactory pressure conditions, but its size could be critical. A very large deflector which would cause a heavy contraction can be used successfully at a slot when aeration is provided.

Slots with offset corners and parallel downstream walls will have severe negative pressures within the slot and on the flow surfaces immediately downstream from the slots. The pressure within the slot will be lower for large offsets than for small ones, and the pressure downstream from the downstream corner will be lower for small offsets than for large ones. This design appears adequate for small offsets at moderate heads.

Slots with offset downstream corners and divergent walls have low pressures within the slot or immediately downstream from the downstream corner, depending on the amount of offset. The design is only satisfactory with large offsets at a limited range of slot widths, and small operating heads.

Slots with offset downstream corners and constant rate converging downstream walls have low pressures just downstream from the lines of intersection of the converging and parallel walls. The pressures decrease as the rate of convergence increases and the intersections may become cavitation potentials.

Slots with offset downstream corners and constant rate converging walls, with a rounded intersection will be free of cavitation at rather high heads. Further testing is required to determine the head limits. It is best to use

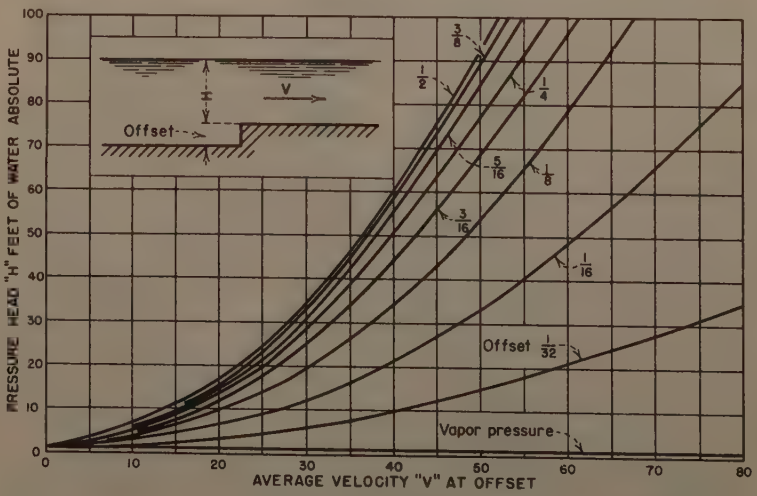

FIGURE 20. HEAD-VELOCITY RELATIONSHIP FOR INCIPIENT CAVITATION—ABRUPT, INTO-THE-FLOW OFFSETS

fairly rapid rates of convergence, insofar as the pressures within and just downstream from the slots are concerned, but the rate of convergence should not be rapid enough to cause difficulty in adequately rounding the line of intersection. A 24:1 rate of convergence with a 12-inch rounding is considered adequate for moderate heads, but a larger radius would be more desirable.

A slot design using offset corners and a variable rate of convergence is the most desirable from the hydraulic standpoint. Arcs used in this design should have radii in the range of about 100 to 250 times the offset of the downstream corner. Ellipses can also be used with excellent results.

The upstream corners of the gate slots should not be rounded or notched; both are detrimental to the pressure distribution.

The widening of slots permits more expansion of the jet into the slot, tending to increase the contraction at the downstream corner. However pressure conditions are acceptable for a wide range of W/D ratios in designs using offset corners with converging walls. This is particularly true for the 24:1 convergence and the long-radius curved convergence.

Sharp downstream corners of gate slots should always be offset away from the flow. The offset of the downstream corner of a gate slot should be small and related to the slot width. Within reasonable limits, this offset is not critical.

A cavitation-free slot for both free discharge and back pressure conditions, and small gate openings, has been developed. This design, which combines moving the slots upstream with a small offset at the downstream corner, is feasible. Some development work is needed to perfect a seal design, but this is considered practicable.

Sufficient field data have been obtained on a 7-1/2- by 9-foot free discharge gate to show that an offset of 1/2-inch followed by a 60:1 convergence is cavitation-free under a head of 200 feet.

Abrupt into-the-flow offsets and irregularities in flow surfaces are particularly troublesome. Offsets of less than 1/8-inch will cause damage. Also, cavitation may occur at offsets ground on steep bevels and at "bug holes." Thus, it is extremely important to provide smooth continuous surfaces downstream from gates operating under high heads.

Gate slot fillers have been used successfully to eliminate flow disturbances created by slots. However, the fillers are expensive and complicate the design of the gates. Furthermore, the wells needed to receive the followers may become plugged with debris and may present serious drainage problems. In cases where these limitations can be overcome, and where slot fillers produce truly flush, smooth flow surfaces, they can entirely eliminate the danger of cavitation at slots.

Cavitation will occur where the bottom corners of the frame of a gate are rounded, the corners of the flow channel downstream are square, and short fillets are used to blend the rounded corner into the square one. Long fillets will decrease the cavitation potential.

Where there is a finite seal width across the bottom of the gate leaf, there will be a gate opening below which cavitation will occur between the leaf seal and the floor. This opening will be about one-half the seal width for free discharge. In cases where the flow is submerged, the critical opening may be somewhat larger.

ACKNOWLEDGMENTS

Much credit is due W. P. Simmons, Jr. of the Bureau of Reclamation Hydraulic Laboratory staff for his part in conducting tests, analyzing data and preparing material used in this paper. Credit also goes to many foreign and rotation engineers in training with the Bureau who assisted in performing the numerous tests.

REFERENCES

1. Engineering News Record, August 23, 1945.
2. Hydraulic Laboratory Report 387, "Hydraulic Model Studies of the 7 foot 6 inch by 9 foot 0 inch Palisades Regulating Slide Gate"—Palisades Project—Idaho.
3. Symposium "Cavitation in Hydraulic Structures," Vol. 112, page 1, 1947, ASCE Transactions.

Journal of the
HYDRAULICS DIVISION
Proceedings of the American Society of Civil Engineers

AN ANALYSIS OF A SIMPLE SURGE TANK

Frank U. Druml[1]

ABSTRACT

This article presents a method for eliminating trials in the arithmetic-step analysis of accelerated flow in a conduit served by a surge tank. Equations are derived for analysis of a simple surge tank under maximum "load off" conditions, and solution of a problem is described.

INTRODUCTION

The writer's experience relative to accelerated flow in conduits served by a simple surge tank is limited to hydraulic design of pumping plants serving storm and sanitary sewer systems, and to filling and emptying systems for navigation locks. Another application is a water supply distribution tank, which acts as a simple surge tank with sudden imposition or rejection of a fire fighting load. In hydro-electric works the simple surge tank is seldom used today. However, it is believed that most designers make their first estimate on the basis of a simple surge tank. Further, it is used by students and young engineers to "cut their teeth" on.

The theory of surge tanks is described in sufficient detail in standard text books on the subject of hydroelectric design to preclude the necessity for repeating it in the present paper. Therefore, the author proposes to discuss the subject only to the extent necessary to describe the method of eliminating trials in the arithmetic solution of a simple surge tank problem. No attempt has been made to apply the method to the period of operation of turbines prior to complete closure of gates. Since each turbine has its own performance curves, it is doubtful whether the method applies to this period.

Note: Discussion open until March 1, 1960. To extend the closing date one month, a written request must be filed with the Executive Secretary, ASCE. Paper 2225 is part of the copyrighted Journal of the Hydraulics Division, Proceedings of the American Society of Civil Engineers, Vol. 85, No. HY 10, October, 1959.

1. Chief, Hydraulics Section, Louisville Dist. Corps of Engrs., Dept. of Army, Louisville, Ky.

Nomenclature

Nomenclature applicable to the analysis of a simple surge tank discussed herein is as follows:

- t = time of period (sec)
- Q = initial discharge in conduit or into tank (cfs)
- q_s = conduit discharge at beginning or end of period (cfs)
- q_z = rate of filling surge tank at beginning or end of period (cfs)
- q_a = change in conduit discharge during period (cfs)
- A = area of surge tank (sq ft)
- a = area of conduit (sq ft)
- L = length of conduit (ft)
- g = acceleration due to gravity (32.2 ft/sec^2)
- h_z = rise in surge tank during period (ft)
- h_a = retardation head at beginning or end of period (ft)
- h_f = hydraulic head losses in conduit at beginning or end of period (ft)
- C = coefficient of discharge

Subscripts of 1 or 2 represent values at beginning or end of period, respectively.

Simple Surge Tank

Now let us assume complete closure of gates of a turbine served by a conduit, which is controlled by a simple surge tank. The water level in the surge tank will immediately begin to rise and continue rising, until the flow in the conduit is zero. Thereafter, the level in the tank will fluctuate with successively smaller oscillations, until a steady level is attained. The change in surge tank levels (h_z) during a period of time (t) will depend on the area of the tank (A), and the average rate at which the tank is filled. It is expressed as follows:

$$h_z = \frac{q_{z_1} + q_{z_2}}{2} \frac{t}{A} \tag{1}$$

The change in discharge in the conduit is

$$q_a = q_{s_1} - q_{s_2} \tag{2}$$

For complete closure of turbine gates

$$q_{s_1} = q_{z_1} \quad \& \quad q_{s_2} = q_{z_2} \tag{3}$$

As the water level in the surge tank rises it builds up a certain amount of head, which retards the flow in the conduit. According to the laws of motion in pipes, the average head required to retard this flow during a period of time is

$$\frac{h_{a_1} + h_{a_2}}{2} = \frac{q_a L}{tga} \tag{4}$$

The total acceleration head necessary to reduce the conduit discharge during a period is

$$h_{a_2} - h_{a_1} \tag{5}$$

Retardation in conduit discharge will also result in a decrease in hydraulic head losses. The change in these losses during the period is expressed as

$$h_{f_1} - h_{f_2} \tag{6}$$

Under maximum "load off" conditions the head necessary to decelerate the flow in the conduit, plus the decrease in hydraulic head losses, should equal the change in levels in the surge tank during each period of the first quarter-cycle.

$$h_z = (h_{a_2} - h_{a_1}) + (h_{f_1} - h_{f_2}) \tag{7}$$

and

$$h_z - (h_{f_1} - h_{f_2}) = (h_{a_2} - h_{a_1}) \tag{8}$$

Table 1 shows the solution of a simple surge tank problem by the arithmetic-step method of integration, in which successive trials are made for each period until all factors are in balance. It is assumed that the tank will have a cross-sectional area (A) of 100 square feet, and controls a conduit with length (L) of 10,000 feet, and cross-sectional area (a) of 10 square feet. An initial discharge of 100 cubic feet per second is assumed. The total hydraulic head losses are assumed to be 36 feet. The procedure and sequence of analyses are shown in the footnotes of the table.

In the analysis, instead of assuming equal increments of time, equal increments of change in discharge are assumed. This method obviates computing a partial period at the end of the quarter-cycle. Also, if hydraulic head losses are considered, it fixes the amount of these losses for each period, thus precluding the necessity of computing these losses with each successive trial. Further, in considering complete closure of turbine gates, it has been found convenient to divide the flow into ten equal increments. Since the hydraulic head losses will vary as the square of the discharge, the losses at the end of the first to tenth periods will be .81, .64, .49, .36, .25, .16, .09, .04, .01 and .00 of the total. In like manner, the change in hydraulic losses during the ten periods will be .19, .17, .15, .13, .11, .09, .07, .05,.03 and .01, of the total loss, respectively.

Now consider the analysis in Table 1 from another aspect. It will be noted that the figures shown in column 4 of this Table are the average conduit discharges, and that they are also the average discharges into the tank. Therefore, for each period, "t" in Eq. (1) is the only unknown. Therefore Eq. (1) can be represented by a straight line, one for each period as shown in Fig. 1. In like manner Eq. (4) when re-solved into the form

$$h_{a_1} + h_{a_2} = \frac{2 q_a L}{tga} \tag{9}$$

COMPUTATION OF S
(INVOLVIN

Surge Ta
Conduit Length =
Initial Discharge = 100 cf
Pool Ele

Time		Conduit Discharge			Hydraulic Hea Losses		
Accumulated (sec)	Increment (sec)	Instantaneous (cfs)	Average (cfs)	Rise (ft)	Surge Tank W.S. Elevation (ft)	Instantaneous (ft)	In me
(1)	(2)	(3)	(4)	(5)	(6)	(7)	(
0.000		100			64.000	36.00	
	29.422		95	27.951			6.
29.422		90			91.951	29.16	
	13.140		85	11.169			6.
42.562		80			103.120	23.04	
	11.224		75	8.418			5.
53.786		70			111.538	17.64	
	10.290		65	6.689			4.
64.076		60			118.227	12.96	
	9.740		55	5.357			3.
73.816		50			123.584	9.00	
	9.389		45	4.225			3.
83.205		40			127.809	5.76	
	9.158		35	3.205			2.
92.363		30			131.014	3.24	
	9.007		25	2.252			1.
101.370		20			133.266	1.44	
	8.915		15	1.337			1.
110.285		10			134.603	.36	
	8.872		5	.444			.
119.157		0			135.047	.00	

(1) = Summation of (2)'s

(2) Determined by successive trials until (2) = $\frac{(9)\,L}{(10)\,ga}$ From eq. 4

(3) Assume conduit discharge is reduced in ten equal steps.

(4) = $\frac{(3)_1+(3)_2}{2}$

(5) = $\frac{(2)\times(4)}{A}$ From eq. 1 and 3

(6) = Water surface elevation at beginning of period plus (5)

(7) Losses for co in (3)

(8) = $(7)_1-(7)_2$ Fr

(9) = $(3)_1-(3)_2$ Fr

(10) = $\frac{(11)_1+(11)_2}{2}$ Fr

$(11)_2 = (11)_1+(12)$ Fr

(12) = (5) - (8) Fr

(13) = $(11)_1+(11)_2$

(14) = $2(11)_1-(8)$

1
ARITHMETICAL METHOD
SSIVE TRIALS)

= 100 sq ft
ft Area = 10 sq ft
draulic Head Losses = 36.00 ft
= 100.00 ft

Change in Discharge (cfs) (9)	Average (ft) (10)	Retardation Head: Instantaneous (ft) (11)	Retardation Head: Increment (ft) (12)	$h_{a_1} + h_{a_2}$ (ft) (13)	$2h_{a_1} - (h_{f_1} - h_{f_2})$ (ft) (14)
		0.000			
10	10.5555		21.111	21.111	-6.840
		21.111			
10	23.6355		5.049	47.271	+36.103
		26.160			
10	27.6690		3.018	55.338	+46.920
		29.178			
10	30.1825		2.009	60.365	+53.676
		31.187			
10	31.8855		1.397	63.771	+58.414
		32.584			
10	33.0765		.985	66.153	+61.928
		33.569			
10	33.9115		.685	67.823	+64.618
		34.254			
10	34.4800		.452	68.960	+66.708
		34.706			
10	34.8345		.257	69.669	+68.332
		34.963			
10	35.0050		.084	70.010	+69.566
		35.047			

nding discharges

6
2

4
5

8

Sequence: Complete (3), (4), (7), (8) and (9) for the entire quarter-cycle. Then determine (2), (5), (12), (11), (10), (1) and (6) successively for each period. (13) and (14) required only for purposes of this article.

can also be represented as a straight line logarithmically. Inasmuch as q_a is the same for each period, Eq. (9) is represented by a single straight line for all periods in Fig. 1. Since t is in the numerator of Eq. (1) and, in the denominator of Eq. (9), these lines will be at right angles to each other when plotted logarithmically.

By combining Eqs. (1) and (7) and substituting the equivalent of h_{a_2} of Eq. (9), the following is resolved:

$$\frac{q_{z_1} + q_{z_2}}{2} \frac{t}{A} = \frac{2q_a L}{tga} - 2h_{a_1} + (h_{f_1} - h_{f_2})$$

$$2\frac{q_a L}{tga} - \frac{q_{z_1} + q_{z_2}}{2} \frac{t}{A} = 2h_{a_1} - (h_{f_1} - h_{f_2}) \qquad (10)$$

or

$$h_{a_1} + h_{a_2} - h_z = 2h_{a_1} - (h_{f_1} - h_{f_2}) \qquad (11)$$

Eq. (11), as will be described later, is the basis for preparation of the Surge Functions table.

The portion of Eq. (10) to the right of the equals sign represents the difference in head between the two linear functions on the left hand side of Eq. (10). This difference in head is shown in Fig. 1 as a dashed line connecting the linear functions at the value of t for each period, as determined in Table 1.

It will be noted in Table 1 that this difference in head is known progressively for each period before any trials are made. Although not immediately apparent from the footnotes of Table 1, successive values of t are tried until the t is determined which results in a difference between h_z and $h_{a_1} + h_{a_2}$ equal to the value in column (14) of this table. The triangles thus formed represent all the factors included in Eqs. (10) and (11).

The Surge Functions Table

Now refer to Fig. 1, and note that the lines representing h_z and $h_{a_1} + h_{a_2}$ intersect at values of t and h other than those computed in Table 1. For purposes of this paper these intersections are designated as t_x, h_x. Their respective values are determined by setting Eqs. (1) and (9) equal to each other and resolving for t_x^2 as follows:

$$\frac{q_{z_1} + q_{z_2}}{2} \frac{t}{A} = \frac{2q_a L}{t_x ga}$$

$$t_x^2 = \frac{2q_a AL}{\frac{q_{z_1} + q_{z_2}}{2} ga} \qquad (12)$$

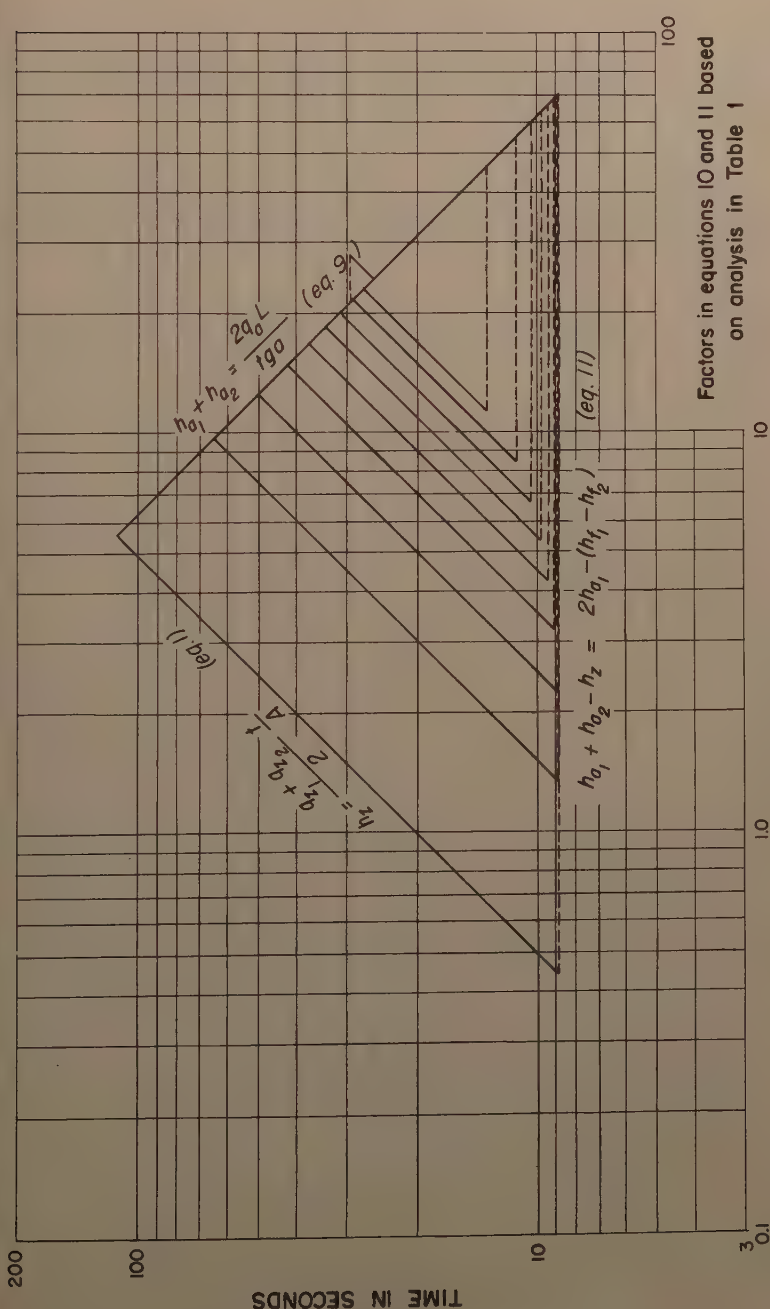

Factors in equations 10 and 11 based on analysis in Table 1

FIGURE 1

By substituting t_x in Eq. (1) determine h_x as follows:

$$h_x = \frac{q_{z_1} + q_{z_2}}{2} \frac{t_x}{A} \quad (13)$$

All factors in Eq. (12) are known as soon as the average flows into the tank, and the change in discharge for each period are established. As a resul t_x can be determined immediately for all periods, and by substituting these values in Eq. (13) the h_x values are also obtained.

Now refer to Fig. 2. The triangles for the first three periods shown on Fig. 1 are also shown in the upper right portion of Fig. 2. Only the first thre periods are shown to avoid the confusion of too many lines. It will be noted that the positions of the t_x and h_x are also shown. Now shift the triangles to the left parallel to the h-axis so that their apexes will be at h_x equals one foot.

In order to see what happens to the various values represented by these triangles when shifted in this manner refer to Fig. 3. Shown are several pair of linear functions which represent the left hand portion of Eq. (11) and have the same h_x. It will be noted that for t_x equals 10 seconds and the ratio of $\frac{t}{t_x}$ equals 0.40, the head represented by the right hand side of Eq. (11) is .210, 2.10 and 21.0 for h_x's of 0.1, 1, and 10 feet, respectively. Therefore, it is apparent that all values of h_z, $h_{a_1} + h_{a_2}$ and $(h_{a_1} + h_{a_2}) - h_z$ for h_x equals 1.00 are directly proportional to those of the computed h_x. In other words, dividing both sides of Eqs. (10) or (11) by the computed h_x does not change th relationship of the various factors in these equations.

Referring back to Fig. 3 and the two triangles with values of h_x equals 10.(feet, and $\frac{t}{t_x}$ equals 0.40. The difference between h_z and $h_{a_1} + h_{a_2}$ is 21.0 feet for t equals .4 and 4 seconds. In like manner, for any other identical h_x's and the same ratios of $\frac{t}{t_x}$, the difference between h_z and $h_{a_1} + h_{a_2}$ is the same re- gardless of the value of t_x. As a result, a basic table can be prepared for any t_x, h_x, and the values of $(h_{a_1} + h_{a_2})$ and $(h_{a_1} + h_{a_2}) - h_z$ in Eq. (11) can be de- termined for any assumed h_z. Then, knowing any other t_x, h_x and the head representing the right hand side of this equation, the remaining factors can b determined.

Table 3, entitled Surge Functions, was prepared using the lines shown in Fig. 2, which intersect at t_x equals one second, and h_x equals one foot. To identify values obtained from this table, capital letters are used. The first column of the table represents values of T and H_z, and since T_x and H_x equal unity, this column can also represent $\frac{T}{T_x}$, $\frac{H_z}{H_x}$, $\frac{t}{t_x}$ and $\frac{h_z}{h_x}$. These ratios, as will be explained later, are used in the solution shown in Table 2. The secon column represents values of $H_{a_1} + H_{a_2}$ for corresponding values of T in Eq. (9). The third column represents the right hand portion of Eq. (11) and is the difference between the first and second columns. In Eq. (1), h_z varies direct ly with t during any period. In like manner $h_{a_1} + h_{a_2}$ in Eq. (9) varies in- versely as t. Therefore, since the Surge Functions Table is based on a T_x and H_x of unity, T equals H_z, and $H_{a_1} + H_{a_2}$ is the recriprocal of T. It will be noted in the table, that for values of T greater than one, the values in the third column are negative. The table as presented herewith is computed for one-hundredth increments of T and H_z from .01 to 2.00. The writer actually

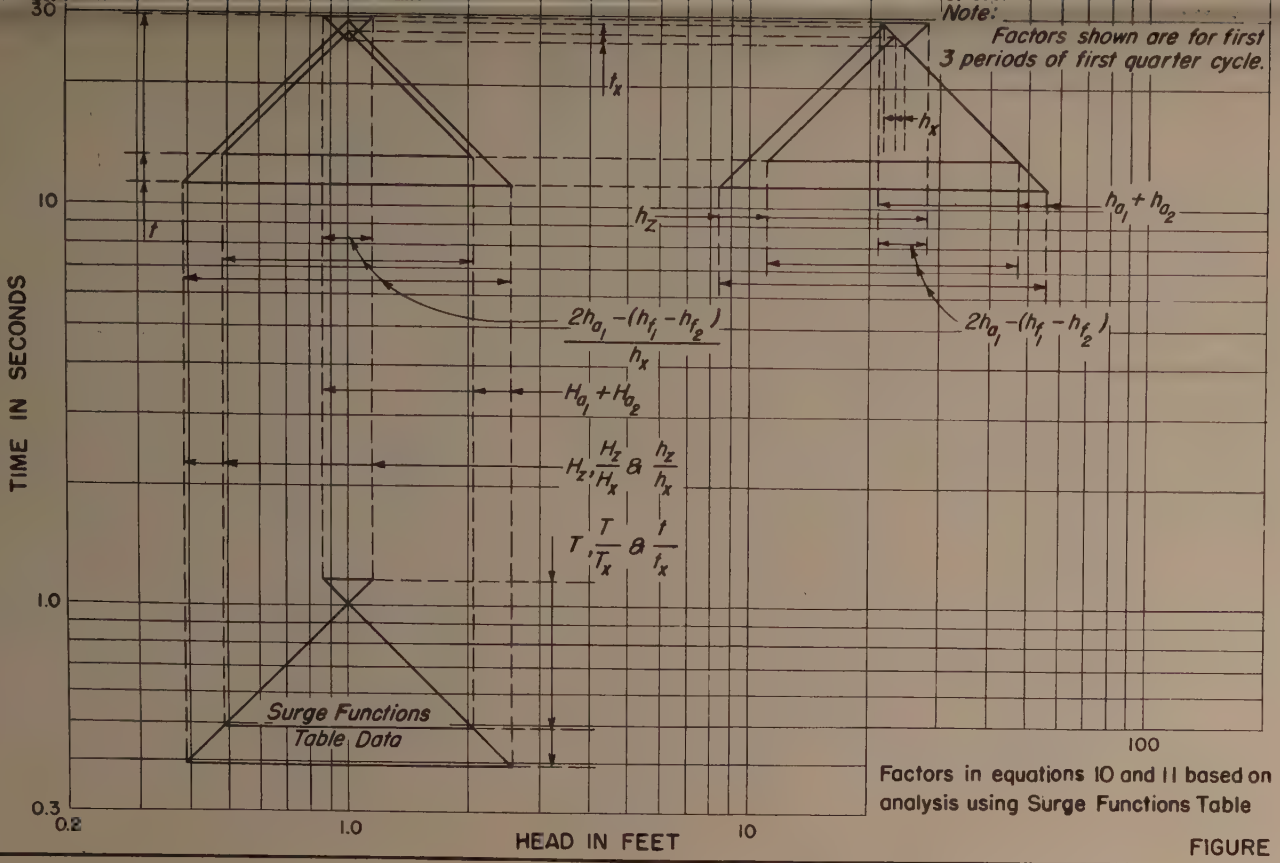

Factors in equations 10 and 11 based on analysis using Surge Functions Table

FIGURE 2

TABLE 2
COMPUTATION OF SURGE BY ARITHMETICAL METHOD
(USING SURGE FUNCTIONS TABLE)

Surge Tank Area = 100 sq ft
Conduit Length = 10,000 ft Area=10 sq ft
Initial Discharge=100 cfs Hydraulic Head Losses=36.00 ft
Pool Elevation=100.00 ft

Time		Conduit Discharge		Surge Tank	W.S. Elevation	Hydraulic Head Losses	
Accumulated	Increment	Instantaneous	Average	Rise		Instant.	Increment
(sec)	(sec)	(cfs)	(cfs)	(ft)	(ft)	(ft)	(ft)
(1)	(2)	(3)	(4)	(5)	(6)	(7)	(8)
0.000		100			64.000	36.00	
	29.423		95	27.952			6.84
29.423		90			91.952	29.16	
	13.140		85	11.169			6.12
42.563		80			103.121	23.04	
	11.223		75	8.418			5.40
53.786		70			111.539	17.64	
	10.291		65	6.689			4.68
64.077		60			118.228	12.96	
	9.739		55	5.356			3.96
73.816		50			123.584	9.00	
	9.388		45	4.225			3.24
83.204		40			127.809	5.76	
	9.158		35	3.205			2.52
92.362		30			131.014	3.24	
	9.007		25	2.252			1.80
101.369		20			133.266	1.44	
	8.919		15	1.338			1.08
110.288		10			134.604	.36	
	8.872		5	.444			.36
119.160		0			135.048	.00	

(1) = Summation of (2)'s
(2) = (11) x (15)
(3) Assume conduit discharge is reduced in ten equal steps.
(4) = $\frac{(3)_1 + (3)_2}{2}$
(5) = (12) x (15)
(6) = Water surface elevation at beginning of period plus (5)

(7) Losses for correspond
(8) = $(7)_1 - (7)_2$ Fr
(9) = $(3)_1 - (3)_2$ Fr
(10) = $\frac{2(9)\ LA}{(4)\ ga}$ Fr
(11) = $\sqrt{(10)}$
(12) = $\frac{(4) \times (11)}{A}$ Fr
(13) = $\frac{(8)}{(12)}$

t_x^2	t_x	h_x	Hf_{1-2}	$2Ha_1 - Hf_{1-2}$	$\frac{t}{t_x} \& \frac{h_z}{h_x}$	$Ha_1 + Ha_2$	Ha_1	Ha_2
$(sec)^2$	(sec)	(ft)	(ft)	(ft)	(ft)	(ft)	(ft)	(ft)
(10)	(11)	(12)	(13)	(14)	(15)	(16)	(17)	(18)
653.808	25.570	24.2915	.2816	- .2816	1.1507	.8691	.0000	.8691
730.727	27.032	22.9772	.2664	+1.5712	.4861	2.0573	.9188	1.1385
828.157	28.778	21.5835	.2502	+2.1738	.3900	2.5638	1.2120	1.3518
955.566	30.912	20.0928	.2329	+2.6713	.3329	3.0042	1.4521	1.5521
129.305	33.605	18.4828	.2143	+3.1603	.2898	3.4501	1.6873	1.7628
380.262	37.152	16.7184	.1938	+3.7038	.2527	3.9565	1.9488	2.0077
774.623	42.126	14.7441	.1709	+4.3821	.2174	4.5995	2.2765	2.3230
484.472	49.844	12.4610	.1445	+5.3527	.1807	5.5334	2.7486	2.7848
140.787	64.349	9.6524	.1119	+7.0783	.1386	7.2169	3.5951	3.6218
422.360	111.456	5.5728	.0646	+12.4818	.0796	12.5614	6.2732	6.2882

$\left[h_x \times \frac{t}{t_x}\right] = 119.160$ $\quad \frac{71.047}{64.000} = \sum\left[h_x \times \frac{h_z}{h_x}\right]$

$\overline{135.047}$

ges in (3)

(14)=2x (17)-(13)
From eq. 11

(15)&(16) Obtained from Surge Functions Table for a corresponding value of (14)

$$(17)_{2-3} = \frac{(18)_{1-2} \times (12)_{1-2}}{(12)_{2-3}}$$

(18) = (16) - (17)

Sequence: Complete (3), (4), (7), (8), (9), (10), (11), (12) and (13) for the entire quarter-cycle. Then determine (17), (14), (15), (16) and (18) successively for each period until quarter-cycle is completed. (2), (5), (1) and (6) can be computed for the entire quarter-cycle.

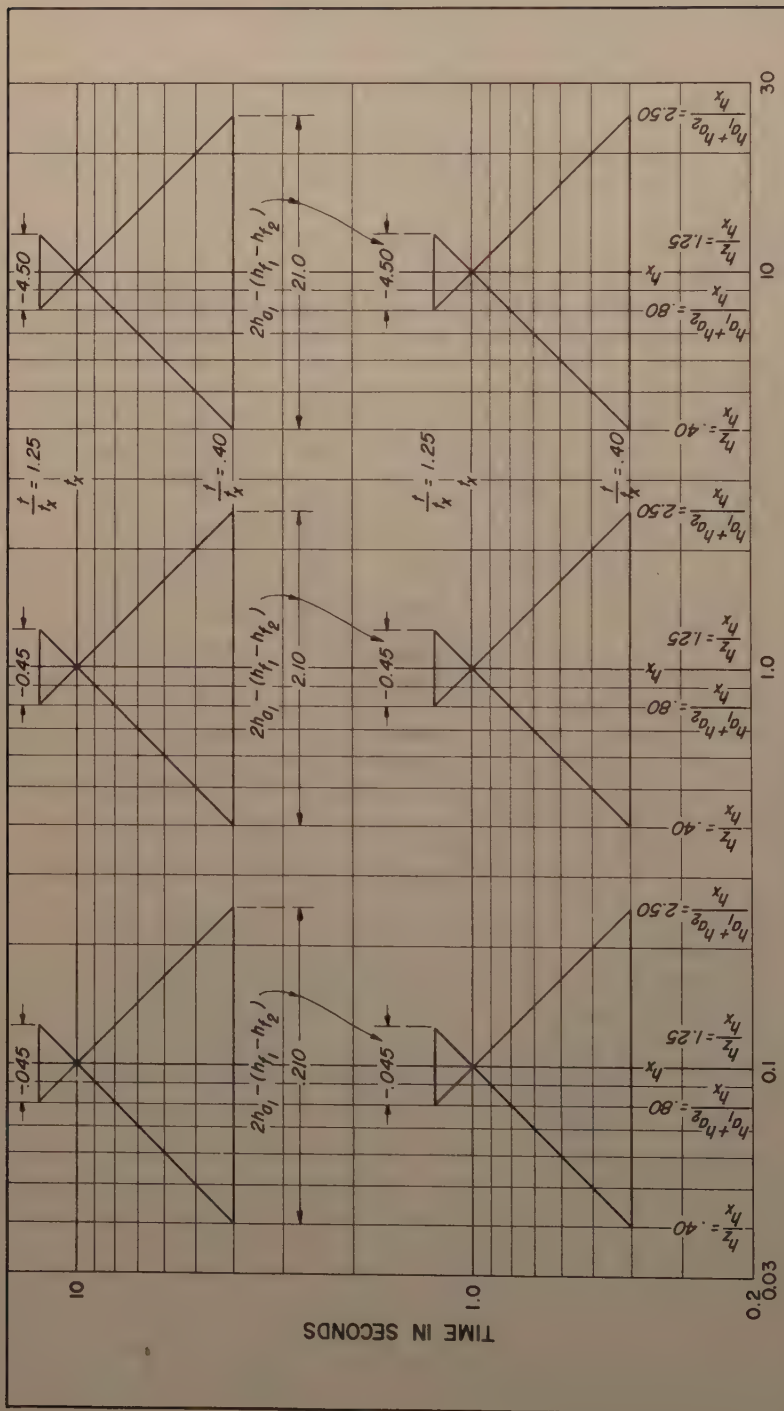

Relationship of factors in equations 10 and 11 for various values of t_x, h_x.

FIGURE 3

TABLE 3

SURGE FUNCTIONS

$\frac{t}{t_x}$ & $\frac{h_z}{h_x}$	$H_{a_1} + H_{a_2}$	$2H_{a_1} - (H_{f_1} - H_{f_2})$	$\frac{t}{t_x}$ & $\frac{h_z}{h_x}$	$H_{a_1} + H_{a_2}$	$2H_{a_1} - (H_{f_1} - H_{f_2})$
.00			.50	2.0000	1.5000
.01	100.0000	99.9900	.51	1.9608	1.4508
.02	50.0000	49.9800	.52	1.9231	1.4031
.03	33.3333	33.3033	.53	1.8868	1.3568
.04	25.0000	24.9600	.54	1.8519	1.3119
.05	20.0000	19.9500	.55	1.8182	1.2682
.06	16.6667	16.6067	.56	1.7857	1.2257
.07	14.2857	14.2157	.57	1.7544	1.1844
.08	12.5000	12.4200	.58	1.7241	1.1441
.09	11.1111	11.0211	.59	1.6949	1.1049
.10	10.0000	9.9000	.60	1.6667	1.0667
.11	9.0909	8.9809	.61	1.6393	1.0293
.12	8.3333	8.2133	.62	1.6129	.9929
.13	7.6923	7.5623	.63	1.5873	.9573
.14	7.1429	7.0029	.64	1.5625	.9225
.15	6.6667	6.5167	.65	1.5385	.8885
.16	6.2500	6.0900	.66	1.5152	.8552
.17	5.8824	5.7124	.67	1.4925	.8225
.18	5.5556	5.3756	.68	1.4706	.7906
.19	5.2632	5.0732	.69	1.4493	.7593
.20	5.0000	4.8000	.70	1.4286	.7286
.21	4.7619	4.5519	.71	1.4085	.6985
.22	4.5455	4.3255	.72	1.3889	.6689
.23	4.3478	4.1178	.73	1.3699	.6399
.24	4.1667	3.9267	.74	1.3514	.6114
.25	4.0000	3.7500	.75	1.3333	.5833
.26	3.8462	3.5862	.76	1.3158	.5558
.27	3.7037	3.4337	.77	1.2987	.5287
.28	3.5714	3.2914	.78	1.2821	.5021
.29	3.4483	3.1583	.79	1.2658	.4758
.30	3.3333	3.0333	.80	1.2500	.4500
.31	3.2258	2.9158	.81	1.2346	.4246
.32	3.1250	2.8050	.82	1.2195	.3995
.33	3.0303	2.7033	.83	1.2048	.3748
.34	2.9412	2.6012	.84	1.1905	.3505
.35	2.8571	2.5071	.85	1.1765	.3265
.36	2.7778	2.4178	.86	1.1628	.3028
.37	2.7027	2.3327	.87	1.1494	.2794
.38	2.6313	2.2516	.88	1.1364	.2564
.39	2.5641	2.1741	.89	1.1236	.2336
.40	2.5000	2.1000	.90	1.1111	.2111
.41	2.4390	2.0290	.91	1.0989	.1889
.42	2.3810	1.9610	.92	1.0870	.1670
.43	2.3256	1.8956	.93	1.0753	.1453
.44	2.2727	1.8327	.94	1.0638	.1238
.45	2.2222	1.7722	.95	1.0526	.1026
.46	2.1739	1.7139	.96	1.0417	.0817
.47	2.1325	1.6625	.97	1.0309	.0609
.48	2.0833	1.6033	.98	1.0204	.0404
.49	2.0408	1.5508	.99	1.0101	.0201
.50	2.0000	1.5000	1.00	1.0000	.0000

TABLE 3 (Cont'd)

SURGE FUNCTIONS

$\frac{t}{t_x}$ & $\frac{h_z}{h_x}$	$H_{a_1} + H_{a_2}$	$2H_{a_1} - (H_{f_1} - H_{f_2})$	$\frac{t}{t_x}$ & $\frac{h_z}{h_x}$	$H_{a_1} + H_{a_2}$	$2H_{a_1} - (H_{f_1} - H_{f_2})$
1.00	1.0000	.0000	1.50	.6667	-.8333
1.01	.9901	-.0199	1.51	.6623	-.8477
1.02	.9804	-.0361	1.52	.6579	-.8621
1.03	.9709	-.0591	1.53	.6536	-.8764
1.04	.9615	-.0746	1.54	.6494	-.8906
1.05	.9524	-.0976	1.55	.6452	-.9048
1.06	.9434	-.1166	1.56	.6410	-.9190
1.07	.9346	-.1354	1.57	.6369	-.9331
1.08	.9259	-.1541	1.58	.6329	-.9471
1.09	.9174	-.1726	1.59	.6289	-.9611
1.10	.9091	-.1909	1.60	.6250	-.9750
1.11	.9009	-.2091	1.61	.6211	-.9889
1.12	.8929	-.2271	1.62	.6173	-1.0027
1.13	.8850	-.2450	1.63	.6135	-1.0165
1.14	.8772	-.2628	1.64	.6098	-1.0302
1.15	.8696	-.2804	1.65	.6061	-1.0439
1.16	.8621	-.2979	1.66	.6024	-1.0576
1.17	.8547	-.3153	1.67	.5988	-1.0712
1.18	.8475	-.3325	1.68	.5952	-1.0848
1.19	.8403	-.3497	1.69	.5917	-1.0983
1.20	.8333	-.3667	1.70	.5882	-1.1118
1.21	.8264	-.3836	1.71	.5848	-1.1252
1.22	.8197	-.4003	1.72	.5814	-1.1386
1.23	.8130	-.4170	1.73	.5780	-1.1520
1.24	.8065	-.4335	1.74	.5747	-1.1653
1.25	.8000	-.4500	1.75	.5714	-1.1786
1.26	.7937	-.4663	1.76	.5682	-1.1918
1.27	.7874	-.4826	1.77	.5650	-1.2050
1.28	.7813	-.4987	1.78	.5618	-1.2182
1.29	.7752	-.5148	1.79	.5587	-1.2313
1.30	.7692	-.5308	1.80	.5556	-1.2444
1.31	.7634	-.5466	1.81	.5525	-1.2575
1.32	.7576	-.5624	1.82	.5495	-1.2705
1.33	.7519	-.5781	1.83	.5464	-1.2836
1.34	.7463	-.5937	1.84	.5435	-1.2965
1.35	.7407	-.6093	1.85	.5405	-1.3095
1.36	.7353	-.6247	1.86	.5376	-1.3224
1.37	.7299	-.6401	1.87	.5348	-1.3352
1.38	.7246	-.6554	1.88	.5319	-1.3481
1.39	.7194	-.6706	1.89	.5291	-1.3609
1.40	.7143	-.6857	1.90	.5263	-1.3737
1.41	.7092	-.7008	1.91	.5236	-1.3864
1.42	.7042	-.7158	1.92	.5208	-1.3992
1.43	.6993	-.7307	1.93	.5181	-1.4119
1.44	.6944	-.7456	1.94	.5155	-1.4245
1.45	.6897	-.7603	1.95	.5128	-1.4372
1.46	.6849	-.7751	1.96	.5102	-1.4498
1.47	.6803	-.7897	1.97	.5076	-1.4624
1.48	.6757	-.8043	1.98	.5051	-1.4749
1.49	.6711	-.8189	1.99	.5025	-1.4875
1.50	.6667	-.8333	2.00	.5000	-1.5000

used a table with one-thousandth increments of T and H_z and interpolated for values to four decimal places. It was considered impractical to include such an extensive table in this article.

Simple Surge Tank Analysis

Now proceed with solution of the problem analyzed in Table 1 by means of the Surge Functions table. These computations are shown in Table 2, and the procedure of analysis is presented in the footnotes of the table. Basically, the solution first resolves itself into determining the values of t_x and h_x for all periods. Then $H_{f_1} - H_{f_2}$ is obtained for each period by dividing the values of $h_{f_1} - h_{f_2}$ by their respective h_x's. Also, in Table 1, h_{a_1} for each period equals h_{a_2} of the previous period. Inasmuch as h_x does not have the same value for each period, H_{a_1} for each period as shown in Table 2 is not equal to H_{a_2} of the previous period. But H_{a_1} is computed from the ratio of h_x's for the period under consideration and the previous period, and H_{a_2} of the previous period. Then $2H_{a_1} - (H_{f_1} - H_{f_2})$ is computed and by entering the Surge Functions Table with this value $\frac{t}{t_x}, \frac{h_z}{h_x}$, and $H_{a_1} + H_{a_2}$ are obtained. This can be done progressively for each period of the quarter-cycle without determining actual values of t and h_z. If a stage hydrograph for the surge tank is required, values of t and h_z can be computed for each period, and the accumulated time and stage can be determined as in columns 1 and 6 of Table 2. If only the total time of the first quarter-cycle, and the maximum stage are required they may be computed as shown at the bottom of columns 11 and 12 of the same table, thus eliminating the necessity of columns 1, 2, 5 and 6. Factors in the analysis at the first three periods are shown graphically in Fig. 2.

The constants shown in Table 4 can be used to facilitate the computations and eliminate the necessity for columns 3, 4, 7, 8, 9 and 10 of Table 2. The coefficient "C" shown in the last column heading in Table 4 is based on the following relationship:

$$Q = Ca\sqrt{2gh_f} \qquad (14)$$

Concluding Remarks

It will be noted in Table 3 that the argument for entering this table is $2H_{a_1} - (H_{f_1} - H_{f_2})$, and that determination of the other values is by inverse interpolation. It would be more advantageous to make the above item the dependent variable and obtain the other quantities by direct interpolation. However, preparation of the table in this manner would require a great deal more work.

In the tabular computations the use of five to nine significant figures for values based on a three place value of g is actually unwarranted and misleading. However, this was done to provide a better mathematical balance between all of the related items.

TABLE 4

CONSTANTS FOR HYDRAULIC ANALYSIS

OF

SIMPLE SURGE TANK

PERIOD		$\frac{t_x}{\sqrt{\frac{2LA}{ga}}}$	$\frac{h_x}{Q\sqrt{\frac{2L}{gaA}}}$	$\frac{H_{f_{1-2}}}{\frac{1}{\sqrt{\frac{2L}{gaA}}}\left[\frac{Q}{2C^2ga^2}\right]}$
Maximum Load Off	Maximum Load On			
1st	10th	.3244428	.3082207	.6164414
2nd	9th	.3429970	.2915476	.5830952
3rd	8th	.3651484	.2738613	.5477225
4th	7th	.3922323	.2549510	.5099019
5th	6th	.4264014	.2345208	.4690416
6th	5th	.4714045	.2121321	.4242639
7th	4th	.5345225	.1870829	.3741657
8th	3rd	.6324556	.1581139	.3162277
9th	2nd	.8164966	.1224745	.2449489
10th	1st	1.4142136	.07071068	.1414214

Journal of the

HYDRAULICS DIVISION

Proceedings of the American Society of Civil Engineers

CONTENTS

DISCUSSION

SYNTHETIC FLOOD FREQUENCY[a]

Closure by Franklin F. Snyder

FRANKLIN F. SNYDER,[1] F. ASCE.—The author wishes to express his appreciation for the instructive discussions furnished by Messrs. Chow, Paulhus and Kohler.

All three writers commented on and were more or less skeptical of the use of an average rainfall-runoff relationship as a basis for obtaining the direct runoff volume of a particular frequency from the rainfall amount of the same frequency. There is little additional to say beyond what was in the paper. It was accepted that rains of the same duration and frequency occur with associated runoff producing conditions that vary from time to time depending on antecedent conditions. It was then reasoned that an average rainfall-runoff relationship for that group of rainfalls would produce an acceptable runoff volume for the particular frequency. The results of application to date do not contradict this reasoning. Questions as to the derivation of an appropriate rainfall-runoff relationship are discussed subsequently.

Professor Chow's conclusion as to the variability of the physiographic or antecedent factor seems reasonable. However, the author is unable to agree that rainfall and runoff conditions are sufficiently independent to permit the computation of the frequency of runoff volumes as a product of the frequencies of rainfall and physiographic condition.

In his discussion Mr. Paulhus expressed concern with the adequacy of the rainfall-frequency data used by the author. Before discussing in detail some of the points raised it is desired to make clear that the procedures of the paper are such as to permit the use of the best rainfall-duration-frequency data available to the user and such practice is highly recommended. The rainfall intensity-duration-frequency data presented in U. S. Weather Bureau Technical Paper No. 25[(3)] for Washington, D. C. were accepted by the author for use in that vicinity and the data in that report for 203 other long term Weather Bureau stations was proposed for general use. U. S. Weather Bureau reports (11) which furnish the means of interpolating between the long time stations are becoming available for various sections of the country for use as desired.

The flood-frequency data for Wills Creek near Cumberland, Md., as developed by Mr. Paulhus in his Table 1, using the author's procedures and rainfall data without adjustment for several surrounding first order Weather Bureau stations show considerable variation. If using Technical Paper No. 25, the author would develop synthetic flood frequency data for this basin about as follows. The basin lies on the eastern slope and near the ridge of the Allegheny Mountains with a mean elevation of 1850, a mean annual rainfall

---

a. Proc. Paper 1808, October, 1958, by Franklin F. Snyder.
1. Hydr. Engr., Office of the Ch. of Engrs., Washington, D. C.

of about 41 inches and a mean annual temperature of 50 degrees F. It is subject to interior storms from the southwest and to coastal storms from the south and east. Washington, D. C. with the same annual rainfall lies at sea level about 110 miles southeast of the basin. Elkins with a mean annual rainfall of 46.6 inches (59 years) lies about 88 miles to the southwest at an elevation of 2,000 feet on the western slope of the Alleghenies. An inspection of the rainfall intensity-duration-frequency data of TP No. 25 shows that there is significant difference in the two rainfall regimes. An average of the two should provide better results than using either by itself and this has been done with the results shown in Table 2C.

TABLE 2C. COMPUTATION OF SYNTHETIC FLOOD FREQUENCIES
WILLS CREEK NEAR CUMBERLAND, MD.

Dr. A. = 247 sq. mi.; L = 35 mi.; s = 0.8%; n = 0.05

$$T_c = 1.7 \left(\frac{10 \times 35 \times 0.05}{V\ 0.81}\right)^{0.6} = 10 \text{ hours}$$

Mean Temperature = 50° F; Mean Rainfall = 41" (Same as Washington);
Average Monthly Rainfall = 3.42"
Computed Mean Runoff = 41 - 0.6 (50-11) = 17.6"; % Runoff = 43
Adjustment to Elkins rainfall data = $\frac{41}{46.6} = 0.88$
Adjustment to Rainfall for drainage area = 0.97
Adjustment to Washington runoff curve $\cong \frac{43}{38} = 1.13$
$Q_p = 500\ AI_r = 123{,}500\ I_r$

Freq. (Recur. Int., Yrs.)	2	5	10	25	50	100
Elkins Precip /1, x 0.88, inches	1.99	2.52	2.89	3.48	4.00	4.36
Wash., D.C. Precip, /1, inches	3.05	3.79	4.29	5.10	5.70	6.20
0.97 x 0.5 (Elkins + Wash.) inches	2.44	3.06	3.43	4.16	4.70	5.12
Percent Runoff	35.5	40.0	43.5	48.0	51.5	54.0
Runoff, inches	0.866	1.22	1.51	2.0	2.42	2.76
I_r, inches per hr.	0.087	.122	.151	.200	.242	.276
Q_p, 1000 cfs /1	10.7	15.1	18.6	24.7	29.9	34.1
Obs. 28 Yr. Record /2	6.5	13.3	17.5	23.0	27.0	31.5
Obs. Adj. to Partial Duration	8.5	13.8	17.5	23.0	27.0	31.5
Obs. Adj. for Length of Record /3	9.2	15.5	20.3	26.8	31.6	36.2
Schwarz, 26 Yr. Record /4	6.0	11.0	15.0	20.5	25.0	29.5
Schwarz, Adj. to 59 Yrs. /4	6.0	10.0	13.5	17.5	22.0	26.0

/1 Partial duration
/2 U. S. Geological Survey records, after Gumbel, annual series
/3 By Mr. Paulhus
/4 Annual series, see Reference No. 12

Shown also in Table 2C for comparison are frequency data based on the observed record as computed by the author using the Gumbel approach, as computed by Mr. Paulhus, and two sets of annual series values based on studies by Mr. H. E. Schwarz.(12) The first set of values by Mr. Schwarz were obtained from the observed record using a logarithmic-normal function and the second set are the observed values adjusted on a basis of a regional study of 64 stations in the Potomac Basin.

Mr. Paulhus' value for the 100-year return period based on the observed record was 36,200 cfs. Consideration of these results indicates that with a moderate use of judgment in selection of the rainfall intensity-duration-frequency data, the synthetic flood frequency procedure gives acceptable results. The computed 100-year value is not quite as large as the writer apparently thinks interpretation of the observed record justifies but is larger than that obtained by Mr. Schwarz. It is of interest to note that the basin rainfall data used in Table 2C depart from the values obtainable from Technical Paper No. 29(11) by an average of less than 3 percent.

The monthly distribution of annual floods and annual rainfalls was discussed at some length by Mr. Paulhus. There is no disagreement with his contention that the monthly distributions of the two items are different and that the differences would be less for smaller drainage basins, although his demonstration of this for the smaller basin was based on a synthesized annual flood record using a procedure which in an example of the reference cited(13) produced only one synthetic flood out of the four highest that was for the same year as any of the four highest observed events. In concluding that the author's procedure should tend to yield flood-frequency values (this is assumed to refer to values of discharge for a given frequency) that are too high, particularly for larger basins, it is believed that Mr. Paulhus has failed to evaluate fully the use of the average rainfall-runoff relationship.

In order to clarify the point further, synthetic flood frequencies have been computed for the Potomac River above Point of Rocks, Md., with a drainage area of 9,650 square miles and for which a record of 69 years can be developed. The rainfall data for Washington, D. C. for the longer durations required in this test were obtained by extrapolation of 24-hour values through values for 120 hours prepared from data for the period 1920-1958. The relationship of these data for a given frequency was as follows:

$$P_T = P_1 \, T^{0.22} \qquad (14)$$

Where P_T is the rainfall for the desired duration, T, in days and P_1 is the 1 day rainfall. The annual peak discharges for the years 1890-94 were estimated by gage relation using stage data for the U. S. Weather Bureau gage at Harpers Ferry, W. Va. The results are shown in Table 2D. The synthetic flood frequencies assume a central position and compare quite favorably with various assumed distributions for the observed values.

In his comparison of observed and computed flood frequencies for the Rappahannock River, Goose Creek and Little Falls Branch, it appears that Mr. Paulhus has helped to affirm rather than disprove the author's expressed belief as to the adequacy of the procedure proposed in comparison to other possible approaches. In each example the synthetic flood frequencies compared quite favorably with the observed record and in the two cases where frequencies based on the procedures of Proc. Paper 1451(13) were presented, the synthetic flood frequencies were in the central position.

Mr. Paulhus' question as to the derivation of the Gumbel values presented by the author for the several gaging stations is readily answered. The Gumbel procedure was used to analyze observed records for comparative purposes, that is, a straight line was drawn through the average annual peak (2.33 year recurrence interval) and the computed 2,000 year event as proposed by Powell.(14) It is understood that Mr. Paulhus adjusts the values obtained by the basic Gumbel analysis for length of record. The procedure used for making that adjustment always results in an increase of the discharge values for given recurrence intervals. The author does not subscribe to use of such an adjustment, particularly for use with short records in most sections of the United States. For example many of the discharge records in the Potomac River Basin with about 25 years of record include three large floods. Using the 27-year record for the Potomac River near Washington, D. C., and adjusting the results to make them comparable with the data of Table 2D for Point of Rocks, the basic Gumbel analysis without adjustment for length of record gives a value of 480,000 cfs for a recurrence interval of 100 years. It is the author's belief that increasing this value still further for length of record would not improve the determination as an estimate of future possibilities.

Mr. Paulhus considered that the author's rainfall-runoff relationship is perhaps the weakest link in the procedure and that a duration or time of concentration parameter must be included. It is regretted that the author's

TABLE 2D. COMPUTATION OF SYNTHETIC FLOOD FREQUENCIES
POTOMAC RIVER AT POINT OF ROCKS, MD.

Dr. A. = 9650 sq. mi.; L = 212 mi.; s = 0.085; n = 0.05

$$T_c = 1.7 \left(\frac{10 \times 212 \times 0.05}{\sqrt{.085}}\right)^{0.6} = 52 \text{ hours}$$

Mean Temperature = 50° F; Mean Rainfall = 38"; Av. Monthly = 3.17"
Computed Mean Runoff = 38 - 0.6 (50-11) = 14.6"; Obs. Runoff = 13.9"
No adjustment to rainfall or runoff. Use data for Vicinity of Wash., D.C.
Adjustment to rainfall for drainage area = 0.92
$Q_p = 500\ AI_r = 4{,}830{,}000\ I_r$

Freq. (Recur. Int., Yrs.)	2	5	10	25	50	100
Point Rainfall, inches	4.02	5.05	5.75	6.76	7.52	8.30
Basin Rainfall, inches	3.70	4.64	5.29	6.22	6.92	7.63
Percent Runoff	39.8	46.1	50.2	55.8	59.2	62.8
Runoff, inches	1.47	2.14	2.65	3.47	4.09	4.79
I_r, inches per hr.	.0283	.0412	.0511	.0668	.0788	.0922
Q_p, 1000 cfs /1	137	199	247	322	380	445
Obs., 69 Yr. Record /2	143	200	243	308	356	403
Obs., log normal /3	127	180	220	285	335	390
Obs., log normal, skewed /3	121	194	260	377	482	606

/1 Partial duration
/2 U. S. Geological Survey and U. S. Weather Bureau records, after Gumbel, adjusted to partial duration
/3 Adjusted to partial duration

description of his derivation of this relationship for the vicinity of Washington, D. C. was not clear enough to have made unnecessary the study of monthly data presented by Mr. Paulhus. The relationship desired is, of course, that between rainfall and direct runoff and only the lower portion of the curve (below 3.5 inches of rainfall) was controlled by the location of the average monthly rainfall and runoff values (not individual monthly values). Because of the scatter of the points, the average of the twelve monthly averages was used as the control point, that is, one-twelfth of the average annual rainfall and runoff. An average annual runoff of 14 inches was used as typical of the Washington, D. C. area and it is not surprising that the montly data for Little Falls Branch, with an average annual runoff of 11.2", plot to one side of the author's curve on Mr. Paulhus' Fig. A.

Mr. Kohler and Mr. Paulhus feel that a single rainfall-runoff curve is inadequate for use with both small and large basins. If Mr. Paulhus will permit a reduction in his example of 5 inches of rainfall in one hour or 24 hours to one within the range experienced at Washington, D. C., say 3.4 inches in one hour or 24 hours, the author's Fig. 2, Appendix I, shows that this is a 100-year storm on the small area (one hour time of concentration) and about a 2-year storm on the large area (24 hour time of concentration). Thus there is no direct assumption that the antecedent conditions are identical. However, the author is on record[15] that moderate variations in duration have little effect on the amount of runoff from a given amount of rainfall under given conditions.

Pursuing the example further, the runoff factor is 38 percent for 3.4 inches of rainfall on the small area. For a comparable 100-year storm on the larger area, $T_c = 24$, the rainfall would be 7.45 inches and the runoff factor would be 62 percent. It is not known whether such an increase in runoff factor would satisfy Messrs. Kohler and Paulhus. However, it must eliminate Mr. Kohler's objection to the reduction factor for size of drainage basin as used by the author to the extent that his objection is based on the hypothesis that the rainfall-runoff relation is the same for small and large drainage basins.

In summarizing his comments and judging the reliability of the synthetic flood frequency procedure as compared to the procedures presented by Paulhus and Miller,[13] Mr. Paulhus is concerned among other things, with the subjectivity involved in selection of values of n, estimation of the percentage of the area that is impervious or drained by sewers, and the percentage of natural channels eliminated. It should be emphasized that these factors are used to incorporate synthetic unit hydrograph characteristics for areas with no stream flow records into the procedure whereas the approach as presented by Paulhus and Miller is applied only to drainage basins with streamflow records adequate for determination of unit hydrographs and verification of rainfall-runoff relationships. When stream flow or gage height records are available, observed values of T_c can be used in place of computed values, if desired. Although no concession as to comparative reliability is involved, it is pertinent to compare the two man-months[16] required for a study of the type preferred by the writer with the three man-hours involved in determining a synthetic flood frequency by the author's method.

The author suggested in the last paragraph of the paper that a rainfall-runoff relationship for use in a specific area could be developed from known flood frequency data for typical streams in the region by reversing the order of the computations. Mr. Kohler has done this using a number of streams in

Maryland, Virginia, and Pennsylvania. However, he used a considerably greater adjustment to point rainfall for size of drainage basin than used by the author and ended up with a relationship that shows the variation in rainfall intensity - runoff intensity relationship with the value of T_c or length of storm.

A quite similar family of curves can be obtained directly from Figs. 2 and 3, Appendix I, of the paper 1808 with or without an adjustment for size of area. If such an adjustment is incorporated a relationship between T_c and area must be assumed. The basic transformation is accomplished by tabulating and plotting values of rainfall and runoff intensity for several recurrence intervals corresponding to selected values of T_c. The parametric curves for the smaller values of T_c so obtained are positioned somewhat to the right of those obtained by Mr. Kohler.

The values of T_c used by Mr. Kohler are considerably smaller than those determined by the author for several of the basins. Because of the differences in values of T_c, the difference in amount of adjustment for size of drainage basin, and the use of synthesized frequency data by Mr. Kohler, it is difficult to assess the significance of the differences between the two sets of curves. Accordingly, Table 3 was prepared showing frequency data for several of the drainage basins used by Mr. Kohler, as computed by the author's procedure, as read from Mr. Kohler's chart, and as computed from observed records by several procedures. It is concluded from inspection of the table that the author's single rainfall-runoff curve gives quite acceptable results for the various drainage basins tested and that they are probably better determinations than those obtained from the relationships developed by Mr. Kohler.

The questions raised by Messrs. Chow, Paulhus and Kohler have been quite helpful in clarifying some of the procedures and objectives of the original paper. The discussions were primarily concerned with application to natural drainage basins where interest often centers on the more rare events such as the 50 and 100-year floods. In computing the frequency of rare floods the possible variation of the unit hydrograph peak with size of flood probably could cause more difficulty than any other one factor due to the lack of data. As it is, present practices and conditions seldom permit the direct measurement of peak discharges for the larger floods, particularly for the medium and smaller sized drainage basins. For the 16 drainage basins mentioned in the paper or discussions the maximum discharges of record were measured directly in one case and in the other 15 they vary from 160 to 930 percent of the maximum directly measured discharge with an average of 420 percent. For this reason and because of his conviction that weather and resulting floods are not random events, the author considers that application of refined statistical theories to frequency analyses of such data is primarily of benefit as a mental exercise so far as estimating the future occurrences of large floods is concerned.

The author's objective in developing the synthetic flood frequency procedures was not so much for use with the medium and larger size basins, particularly those with some discharge records, as for use on small ungaged areas such as are involved in the growing urban development of the country. Stated simply, he became tired of hearing the same qualification applied to the rational method as that given by his sanitary engineering professor about 30 years ago; namely, that, while the rational method was an improvement over most of the existing empirical formulas, the factor C in $Qp = CiA$ was

not rational, varied with frequency, and must be selected with considerable judgment since it included effects of storage as well as acting as a coefficient of runoff.

Corrections:

Appendix I - Procedure. For column number 15, step 6, replace the words, "Approximation is permissible" with ditto marks.

FURTHER REFERENCES

11. Rainfall Intensity - Frequency Regime. Part 1 - The Ohio Valley, 1957; Part 2 - Southeastern United States, 1958; Part 3 - The Middle Atlantic Region, 1958; Part 4 - Northeastern United States, 1959; U. S. Weather Bureau, Technical Paper No. 29, Washington, D. C.

TABLE 3. COMPARISON OF FLOOD FREQUENCY DATA

Data Source	Recurrence Interval, Years 2	5	10	25	50	100
N.W. Branch Anacostia River near Colesville, Md.; 21.3 Sq. Miles (100 cfs)						
Obs. 35 Yr. Record, Gumbel /1	17.0	25.0	30.7	39.1	45.2	51.2
Synthetic after Snyder /1	17.0	23.3	29.2	37.6	44.6	52.8
Synthetic with Kohler variation /1	11.7	-	18.6	-	-	38.3
Codorus Creek at Spring Grove, Pa.; 74.3 Sq. Miles (100 cfs)						
Obs. 22 Yr. Rec., ASCE Paper 1451 /2	25.3	48.5	63.8	83.2	97.5	112
Obs. 21 Yr. Rec., ASCE Paper 1451 /2	22.8	36.1	45.0	56.1	64.4	72.6
Synthesized Annual Floods, Paper 1451 /2	22.4	38.4	48.9	62.3	72.2	82.0
Synthetic after Snyder /2	23.2	37.2	48.3	60.8	71.8	87.2
Synthetic with Kohler variation /1	26.4	-	50.2	-	-	93.0
Goose Creek near Leesburg, Va.; 338 Sq. Miles (1000 cfs)						
Obs. 26 Yr. Record, Gumbel /1	12.5	21.0	27.3	36.0	42.5	49.0
Synthetic after Snyder /1	11.5	17.5	21.6	28.7	34.8	40.7
Synthetic with Kohler variation /1	11.2	-	21.9	-	-	34.6
Linganore Creek near Frederick, Md.; 82.3 Sq. Miles (100 cfs)						
Obs. 25 Yr. Record, Gumbel /1	26.6	32.6	36.7	43.0	47.6	52.0
Synthetic after Snyder /1	30.0	41.0	49.7	62.0	73.7	87.5
Synthetic with Kohler variation /1	29.8	-	51.5	-	-	89.0
Rappahannock River near Fredericksburg, Va.; 1599 Sq. Miles (1000 cfs)						
Obs. 51 Yr. Record, Gumbel /1	35.0	52.4	65.0	84.0	98.0	111
Obs. 51 Yr. Record, Log Normal /1	35.0	-	66.0	-	-	134
Synthetic after Snyder /1	37.5	55.7	71.8	95.0	115	133
Synthetic with Kohler variation /1	38.4	-	72.0	-	-	121

/1 Partial duration
/2 Annual series

12. "Determination of Flood Frequencies in a Major Drainage Basin", by H. E. Schwarz, Toronto General Assembly, IUGG, Gentbrugge, Belgium, 1958, Volume 3, pp 174-187.

13. "Flood Frequencies Derived from Rainfall Data", by J. L. H. Paulhus and J. F. Miller, Proc. Paper 1451, Jour. Hydr. Div., ASCE, Vol. 83, Dec. 1957.

14. "A Simple Method of Estimating Flood Frequency", by R. W. Powell, Civ. Eng., v. 13, pp 105-107, Feb. 1943.

15. "A Conception of Runoff - Phenomena" by Franklin F. Snyder, Trans. Am. Geophys. Union, 1939, Part IV, p. 727.

16. "Flood Frequencies Derived from Rainfall Data". Closure by J. L. H. Paulhus and J. F. Miller, Jour. Hydr. Div., ASCE, Vol. 84, Nov. 1958, p. 1856-22.

METEOROLOGICAL ASPECTS OF STORM SURGE GENERATION[a]

Closure by D. Lee Harris

D. LEE HARRIS,[1]—The writer agrees with most of the comments of Mr. Bowan, particularly those about the complexity of the problems involved in dealing with hurricane motions. A few of these problems were discussed briefly in the paper.

It would appear, at first consideration, that more dependable estimates of the size of the storm could be determined from data taken at a greater distance from the center of the storm. However, an examination of the data shows that this is not generally true. As mentioned in the paper, there is very little data over the ocean areas near most hurricanes and the storms change too rapidly after crossing the coastline to make land data very far from the center satisfactory for an objective determination of the size of the storm while still at sea. It is hoped that the improved radar data now being collected will permit an improvement in this, but there is not yet enough of the new data available for a statistical study.

The tidal response of Willets Point is similar to that of the Battery for those storms which pass to the west of New York City or to the east of Nantucket Island. The delayed peak of the type shown in my paper occurs only with the storms which enter land between these points. I believe that in these cases the peak surge at Willets Point is the result of a wave which travels westward through the Sound. The time history of the peak surge in the Sound supports this point of view. See Redfield and Miller (1957).(1)

REFERENCE

1. A. C. Redfield and A. R. Miller, "Water Levels Accompanying Atlantic Coast Hurricanes", Meteorological Monographs, Vol. 2, No. 10, June 1957.

a. Proc. Paper 1859, December, 1958, by D. Lee Harris.
1. Office of Meteorological Research, Storm Surge Research Unit, U. S. Weather Bureau, Washington, D. C.

HYDRAULIC ANALYSIS OF SURGE TANKS BY DIGITAL COMPUTER[a]

Discussions by P. Danel and G. Ransford, Rufus Oldenburger, Ignacy Swiecicki, R. A. Sutherland, Francis E. Swain, Evangelisti and B. Poggi

P. DANEL,[1] M. ASCE and G. RANSFORD,[2]—Three points may be mooted in connection with this particularly authoritative article.

A first comment concerns tee losses. It is worth while putting the additional test results obtained by A. Gardel(1) and J. McNown(2) on record. The Munich experiments described by Vogel have been reviewed in both these publications, which appeared independently of each other; the conclusion is that some revision of the early findings seems necessary. This, Mr. Barbarossa's program can of course take care of.

More generally speaking, none of the foregoing test results, being obtained under steady flow conditions, simulate unsteady flow effects occurring in real surge tanks. The generation of large breakaway vortices, and their damping out (a probable source of head-loss "hysteresis" in real surge structures) can be accounted for only on a dynamical scale model in which surges are actually produced. The appropriate equivalent head-loss coefficients should then be deduced from tests run at the same frequency as the anticipated surges. Systematic experiments in this connection seem to be urgently required. The degree of urgency is all the greater for schemes, such as underground power plants with downstream surge tanks, which have shorter period surges than usual. Small experimental effects, as measured to date on steady, one-way flow models only, already prove sufficient to reverse usual reasoning re stability in such cases.(3) This points to the likely fruitfulness of continuing some basic experimental research in conjunction with computer studies.

The second remark concerns machine error control. A surge-tank system can be assimiliated to a linear differential equation in a single dependent variable (the order depending on the number of risers, etc.) in respect of small oscillations about equilibrium. In the present case, this equation is of the fourth order. There would probably be some point in testing the error control method used by conducting at least one blank computer run on an artificially-constructed fourth order equation of which the solution is known. In the case of more complicated systems leading to still higher orders, a preliminary check on accuracy of this nature seems essential. Such a check should not prove too costly in machine time or programming.

The third point concerns possible future comprehensive studies including governor action. Such investigations may prove to be particularly useful in cases such as the short-period downstream surge systems already referred to, in which governor action may interfere markedly with the surging.

---

a. Proc. Paper 1996, April, 1959, by Nicholas L. Barbarossa.
1. Sogreath, Grenoble, France.
2. Sogreath, Grenoble, France.

However, there is every reason for simplifying the general problem by separate analysis of certain factors, as, for instance, the choice of optimum parameters in the case of the governors. Recent papers[4,5] furnish some indication as to what may be done in this respect; in particular, as explained in,[5] elastic water hammer can be satisfactorily approximated to in its effect on turbine governing alone by a high-order linear differential equation. Approximations such as the one just mentioned may be handled on the IBM 650 computer, though, in connection with linear governing problems at present under study by the present writers, some doubt subsists as to whether use of the Graeffe method to find the roots of the characteristic equation, and thence to explicit the solution of the differential equation itself, as done in paper,[5] may not compete successfully with the step-by-step method outlined here. The step-by-step method is of course the only one available for use when non-linear effects (here, large surges) are present, and this is unfortunately the rule in surge-tank problems. The problem of determining computational accuracy in Mr. Barbarossa's "Total Problem" then becomes paramount because no independent check such as the Graeffe-cum-partial-fraction approach, or in some cases the simpler Krasowsky theorem, as used in,[5] exists for the non-linear case.

REFERENCES

1. Gardel, A. "Chambres d'Equilibre—Analyse de quelques hypothèses usuelles. Méthodes de calcul rapide", F. Rouge & Cie, Lausanne, 1956.

2. McNown, J. S. "Mechanics of Manifold Flow", Paper n° 2714, Trans. ASCE, 1954, vol. 119, pp. 1103-1142.

3. Ransford, G. D. "The stability of a downstream surge tank—Extension of Mr. André Gardel's results for an upstream surge tank to one on the downstream side of a power station". La Houille Blanche, n° 2, 1957, pp. 213-219.

4. Ransford, G. D. and Arnaud P; "Optimization of the parameters of a hydraulic turbine governor taking account of the grid inherent stability factor and the turbine (efficiency/opening) droop—Case of medium specific speed Francis turbines". La Houille Blanche, n° 3, 1958, pp. 205-219.

5. Ransford, G. D. and Rottner J. "The optimization of hydraulic governor performance taking account of the grid inherent stability factor and elastic water hammer effects—Case of Pelton turbines". La Houille Blanche, n° 1, 1959, pp. 23-37.

RUFUS OLDENBURGER,[1]—The head losses are taken in this paper to be proportional to the signed square, that is "absquare", $|Q|Q$ of the discharge Q. An indirect proof of the validity of this assumption for dynamic hydraulic conditions in a hydroelectric installation was obtained by others and the write through the medium of frequency response runs at the Apalachia dam of the Tennessee Valley Authority. This installation involves an 8 mile penstock, a differential surge tank, and two 751-ft penstocks supplying water to two 53,500 hp. Francis turbines. These runs were made by oscillating the gates

1. Visiting Prof. of Eng. Univ. of Calif. at Los Angeles; Prof. of Mechanical Eng., Purdue Univ., Lafayette, Ind.

of one turbine sinusoidally over a frequency range of 1/2 cycle per hour to 2 cycles per second under all kinds of operating conditions, and recording system response. The writer (with H. Paynter) derived the partial differential equations of the hydraulic system. The differential of the absquare $|Q|Q$ of discharge Q is $2|Q|dQ$. For small values of $|Q|$, we can set $|Q| = 0$ in this differential. It is convenient in studies of dynamics to write the differential equations in terms of the changes in the variables from a steady state such as changes in head from equilibrium, rather than the variable themselves. The equations of a hydraulic system then involve the differentials of the losses, rather than the losses themselves. Taking these head losses proportional to the absquare of the discharge Q, and assuming that the flows are small, the differentials of the head losses are equal to zero for practical purposes, and these losses can be dropped from the differential equations. The predictions of frequency response based on this approach agreed very well with the actual experimental runs, indicating that the head losses were of the form $\pm cQ^n$ for constants c and n, where the exponent n is near 2, rather than near 1, and that the setting of $|Q| = 0$ in the differential $2|Q|dQ$ were justified.

The Tennessee Valley Authority frequency response runs also emphasized the validity of the lumped constant approach used in the paper. This considerably simplifies digital computer as well as manual computation of hydraulic surge, and other dynamic phenomena.

IGNACY SWIECICKI—The author merits the appreciation of the hydro power industry for this presentation of the practical application of machine computation to surge tank analysis. He should be commended especially for pointing out the short-comings of this particular program.

The following discussion is limited to the problem of stability after small power-demand changes. The digital computer results presented by the author failed to indicate how stability of a turbine governor can be achieved after a small power-demand increase. The author says that it may be entirely possible to develop a computer program which will yield a solution by utilizing methods other than those described in his paper. The writer's suggestion is that the most necessary change in the method is the introduction of speed droop. Without it, in the presence of any amount of water hammer, the turbine governor is known to be unsteady and this unsteadiness shows up no matter whether manual or computer calculation is utilized.

In presenting how speed droop can be introduced into this calculation, within the scope of this discussion, we would have to make several simplifying assumptions. With all the simplifications used we would try to approach the conditions of computer test No. 2 for Oahe turbine stability studies. During this test the surge tank water level elevation changed about 0.1 foot in 1.5 seconds, and the change of losses in the penstock was less than that. Therefore, for studying turbine transients in the first second or so after change of load from 75,000 Bhp to 78,000 Bhp we can consider a simplified pipe line consisting of: 24 foot diameter penstock 66 + 20 = 86 feet long (20 feet being added for distance from downstream surge tank to mid-point between two tanks) two 16 foot diameter 80 foot long risers and two 70 foot diameter surge tanks with water surface 32.85 feet above the risers. For this pipe line

$$\sum \frac{L}{gA} = \frac{1}{32.17}\left(\frac{86}{\frac{\pi}{4}24^2} + \frac{80}{2\frac{\pi}{4}16^2} + \frac{32.85}{2\frac{\pi}{4}70^2}\right) = 0.0125$$

If the variation of penstock friction losses is neglected, acceleration head is the difference between initial head H_o and turbine net head H

$$h_a = H_o - H = \sum \frac{L}{gA} \frac{dQ}{dt} \qquad (a\text{-}1)$$

For simplicity, let us consider a governor with the infinitely short characteristic time of promptness of response, so that the gate-time curve is a straight line without cushioning at the beginning and at the end of the curve. For small gate movements the unit discharge $q = \frac{Q}{\sqrt{H}}$ is proportional to the governor scale

and we can write

$$q = q_o \left(1 + \frac{t}{\tau}\right) \qquad (a\text{-}2)$$

where time in seconds t is a positive value measured from the moment the gates start to move and τ is a constant.

From table 9, test No. 2, we have $t_o = 0$; $Q_o = 5500$; $H_o = 130.080$ and $t = 1.5$; $Q = 6801$; $H = 115.471$. Therefore, we take $\tau = \frac{1.5}{\frac{6801}{5500}\sqrt{\frac{130.080}{115.471}} - 1} = 4.8$

for the opening of the turbine gates and $\tau = -4.8$ for closing.

As a further simplification we will ignore the governor dash pot. This is entirely justified for small load changes. From equation (a-2) we have

$$dt = \frac{\tau}{q_o} dq \qquad (a\text{-}3)$$

Using equation (a-3) we can write

$$\frac{dQ}{dt} = \frac{d(q\sqrt{H})}{dt} = \frac{q_o}{\tau} \frac{d(q\sqrt{H})}{dq} = \frac{q_o}{\tau}\left(q\frac{d\sqrt{H}}{dq} + \sqrt{H}\right) \qquad (a\text{-}4)$$

Substituting equation (a-4) in equation (a-1)

$$H_o - H = \frac{q_o}{\tau} \sum \frac{L}{gA}\left(q\frac{d\sqrt{H}}{dq} + \sqrt{H}\right)$$

or dividing by H_o

$$1 - \frac{H}{H_o} = \frac{1}{\tau} \frac{Q_o}{gH_o} \sum \frac{L}{A}\left(q\frac{d\sqrt{H/H_o}}{dq} + \sqrt{\frac{H}{H_o}}\right) \qquad (a\text{-}5)$$

The value $T_w = \frac{Q_o}{gH_o} \sum \frac{L}{A}$ is usually called hydraulic starting time.

Let us introduce a dimensionless number K which is the ratio of hydraulic starting time T_w to "governor time" τ, $K = \frac{T_w}{\tau}$. Using K, equation (a-5) transforms as follows:

$$1-\frac{H}{H_o} = K q \frac{d\sqrt{H/H_o}}{dq} + K\sqrt{\frac{H}{H_o}}$$

$$1-K\sqrt{\frac{H}{H_o}}-\frac{H}{H_o} = K q \frac{d\sqrt{H/H_o}}{dq}$$

$$\frac{1}{K}\int_{q_o}^{q}\frac{dq}{q} = \int_{1}^{\sqrt{H/H_o}}\frac{d\sqrt{H/H_o}}{1-K\sqrt{H/H_o}-H/H_o} \qquad (a-6)$$

$$-(\ln q-\ln q_o) = \frac{1}{2\sqrt{1+K_2^2}}\left[\ln\left|\frac{\sqrt{1+K_2^2}+\frac{K}{2}+\sqrt{H/H_o}}{\sqrt{1+K_2^2}-\frac{K}{2}-\sqrt{H/H_o}}\right| - \ln\left|\frac{\sqrt{1+K_2^2}+\frac{K}{2}+1}{\sqrt{1+K_2^2}-\frac{K}{2}-1}\right|\right]$$

$$\left(\frac{q}{q_o}\right)^{\frac{2}{K\sqrt{1+K_2^2}}} = \frac{\sqrt{1+K_2^2}-\frac{K}{2}-1}{\sqrt{1+K_2^2}+\frac{K}{2}+1}\;\frac{\sqrt{1+K_2^2}+\frac{K}{2}+\sqrt{H/H_o}}{\sqrt{1+K_2^2}-\frac{K}{2}-\sqrt{H/H_o}} \qquad (a-7)$$

Table (A-I) gives values pertinent to Oahe turbine. First, for several relative heads H/H_o relative unit discharge q/q_o is calculated by means of equation (a-7). Then, relative discharge Q/Q_o, times t in seconds and relative generated power $\frac{Bhp}{Bhp_o}$ is found assuming constant efficiency of turbine. Next, taking mechanical starting time $T_m = \frac{N_o^2\ WR_o^2}{1.62 \times 10^6\ Bhp_o} = 4$ seconds the calculation is continued to find relative speed change $\frac{N}{N_o}$ 100%. For time

TABLE A-I UNIFORM GATE MOTION, CONSTANT LOAD DEMAND, CONSTANT EFFICIENCY NO SPEED DROOP

H/H_o	1.11	1.10	1.08	1.06	1.04	1.02	1.00	0.98	0.96	0.94	0.92	0.90
q/q_o	0.869	0.902	0.939	0.961	0.977	0.989	1.000	1.011	1.027	1.048	1.087	1.270
Q/Q_o	0.916	0.947	0.976	0.989	0.996	0.999	1.000	1.001	1.006	1.016	1.043	1.205
$=\tau(q/q_o-1)$	0.630	0.468	0.293	0.189	0.112	0.052	0	0.055	0.129	0.229	0.419	1.296
Bhp/Bhp_o	1.016	1.041	1.054	1.048	1.036	1.018	1.000	0.981	0.966	0.955	0.959	1.084
$\text{er.}\left(\frac{Bhp}{Bhp_o}-1\right)$	+0.029	+0.048	+0.051	+0.042	+0.027	+0.009	-0.009	-0.026	-0.040	-0.043	+0.022	
Δt	0.162	0.175	0.104	0.077	0.060	0.052	0.055	0.073	0.101	0.189	0.878	
$\frac{\Delta N}{N_o}$ x 100%	+0.116	+0.208	+0.127	+0.081	+0.041	+0.012	-0.013	-0.049	-0.100	-0.203	+0.481	
$\frac{\Delta N}{N_o}$ x 100%	+0.585	+0.469	+0.261	+0.134	+0.053	+0.012	0	-0.013	-0.062	-0.161	-0.364	+0.117

nitial Conditions: Net Head H_o = 130.08 ft.; Turbine Discharge Q_o = 5500 C.F.S.; R.P.M. = N_o
Power Bhp_o = 75000; Unit Discharge $q_o = Q_o/\sqrt{H_o}$; Time t_o = 0 Sec.

ydraulic Starting Time $T_w = \frac{Q_o}{gH_o}\sum\frac{L}{A} = 0.528$ Sec; "Governor Time" $\tau = q_o\frac{dt}{dq} = \pm 4.8$ Sec.

echanical Starting Time $T_m = \frac{N_o^2\ WR^2}{1.62 \times 10^6\ Bhp_o} = 4$ Sec.; $K = \frac{T_w}{\tau} = 0.11$

interval t relative speed increment is

$$\frac{\Delta N}{N_o} = \frac{\Delta t}{T_m} \times \text{AVERAGE}\left(\frac{Bhp - \Delta Bhp}{Bhp_o} - 1\right) \qquad (a\text{-}8)$$

where ΔBhp is instantaneous load demand increment. Values in table (a-I) were calculated for infinitesimally small load change just sufficient to promote initial deflection of the governor. It is clearly seen that any very small movement of gates in opening direction results in an instantaneous drop of generated power; and vice versa, closing of the gates instantaneously increases power.

The same data are plotted on Fig. (A-1), curve K=o.11 and on Fig. (A-2) indicating instability of the governor without speed droop.

Let us now consider a governor with speed droop δ defined by equation

$$\delta = \frac{d\, q/q_o}{d\, N/N_o} \qquad (a\text{-}9)$$

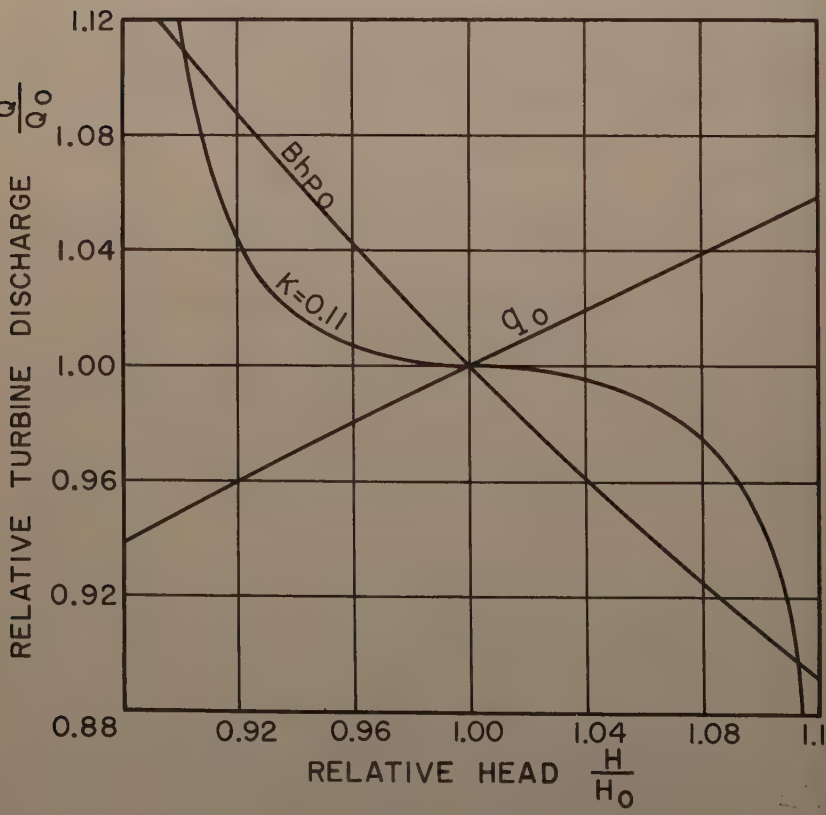

Figure (A-1)

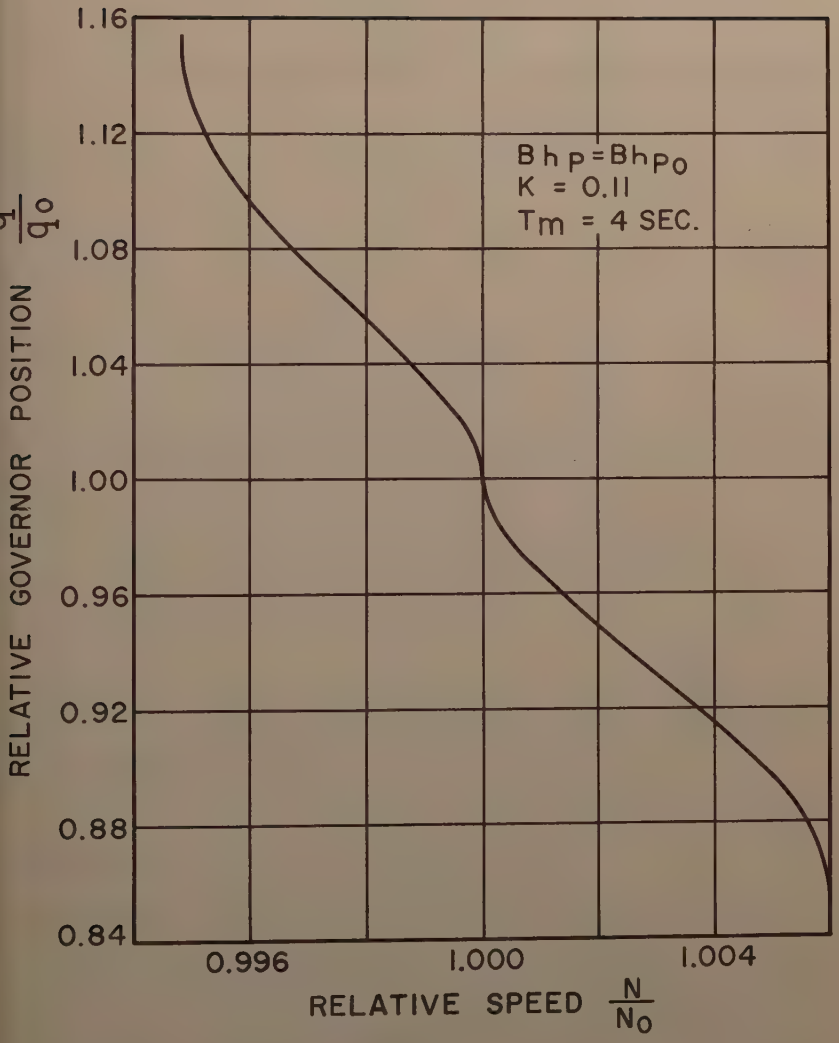
1.16
1.12
1.08
1.04
1.00
0.96
0.92
0.88
0.84
RELATIVE GOVERNOR POSITION q/q0
Bhp=Bhp0
K = 0.11
Tm = 4 SEC.
0.996
1.000
1.004
RELATIVE SPEED N/N0

Figure (A-2)

From equations (a-8) and (a-9) we have

$$dt = \frac{\delta\, T_m}{\frac{Bhp - \Delta Bhp}{Bhp_o} - 1}\, d\frac{q}{q_o}$$

combining this with equation (a-3), momentary "governor time"

$$\tau = \frac{\delta\, T_m}{\frac{Bhp - \Delta Bhp}{Bhp_o} - 1} \qquad \text{(a-10)}$$

Therefore

$$K = \frac{T_w}{\tau} = \frac{T_w}{\delta\, T_m}\left(\frac{Bhp - \Delta Bhp}{Bhp_o} - 1\right) \qquad \text{(a-11)}$$

K being variable, equation (a-6) cannot be integrated over any large interval. Integration has to be done in small intervals from H_{n-1} to H_n and from q_{n-1} to q_n. Therefore instead of equation (a-7) we write:

$$\left(\frac{q_n}{q_{n-1}}\right)^{\frac{2}{K}\sqrt{1+\frac{K^2}{2}}} = \frac{\sqrt{1+\frac{K^2}{2}} - \frac{K}{2} - \sqrt{\frac{H_{n-1}}{H_o}}}{\sqrt{1+\frac{K^2}{2}} + \frac{K}{2} + \sqrt{\frac{H_{n-1}}{H_o}}} \cdot \frac{\sqrt{1+\frac{K^2}{2}} + \frac{K}{2} + \sqrt{\frac{H_n}{H_o}}}{\sqrt{1+\frac{K^2}{2}} - \frac{K}{2} - \sqrt{\frac{H_n}{H_o}}} \qquad \text{(a-12)}$$

It is permissable to take K at the beginning of each interval and regard it as a constant value in equation (a-11) throughout small intervals.
Henry M. Paynter* arrived at the conclusion that the best speed droop value is $\delta = 2\,\frac{T_w}{T_m}$. In our case it is $\delta = 2\,\frac{0.528}{4} = 0.264$. Using this value of speed droop and considering instantaneous load demand change from Bhp_o = 75,000 to 78,000, $\frac{\Delta Bhp}{Bhp_o} = 0.04$, the values of pertinent transients are shown in table (A-II) and on Fig. (A-3), curve $\delta = 0.264$. The calculation was carried on, approximately to the moment when opening of the turbine gates end. In the next intervals generated power exceeds power demand; K changes its sign and equation (a-12) indicates that the gate begins to close towards the final steayd state condition at $q/q_o = 1.04$.

We see that in case of a small load change the governor with speed droop operates much slower than the governor without speed droop. It adjusts the rate of gate motion so that the prescribed speed droop is maintained during its motion. As a result the stability is achieved without any difficulty.

*Methods and Results from M.I.T. Studies in Unsteady Flow, Journal of the Boston Society of Civil Engineers, April, 1952.

TABLE A-II INSTANTANEOUS LOAD DEMAND INCREASE $\frac{\Delta Bhp}{Bhp_o} = 0.04$

SPEED DROOP $\delta = 0.264$

CONSTANT EFFICIENCY

n	0	1	2	3	4	5	6
τ	26.4	22.0	22.4	29.0	42.2	46.3	352
K	0.0200	0.0240	0.0236	0.0182	0.0125	0.0114	0.0015
H/H_o	1	0.990	0.980	0.978	0.981	0.986	0.990
q_n/q_{n-1}		1.007	1.016	1.012	1.007	1.010	1.002
q/q_o	1	1.007	1.023	1.038	1.045	1.050	1.052
Q/Q_o	1	1.002	1.013	1.026	1.035	1.043	1.047
Bhp/Bhp_o	1	0.992	0.993	1.004	1.015	1.029	1.037
$\frac{Bhp-\Delta Bhp}{Bhp_o} - 1$	-0.040	-0.048	-0.047	-0.036	-0.025	-0.011	-0.003
Aver. $\left(\frac{Bhp-\Delta Bhp}{Bhp_o} - 1\right)$		-0.044	-0.047	-0.043	-0.030	-0.018	-0.007
Δt		0.185	0.352	0.336	0.203	0.211	0.093
$\frac{\Delta N}{N_m} \times 100\%$		-0.203	-0.414	-0.361	-0.152	-0.095	-0.016
	0	0.185	0.537	0.873	1.006	1.217	1.310
$\Sigma \frac{\Delta N}{N_o} \times 100\%$	0	-0.203	-0.617	-0.975	-1.127	-1.222	-1.238

Initial Conditions: Net Head $H_o = 130.08$ ft.; Turbine Discharge $Q_o = 5500$ CFS; RPM = N_o
Power $Bhp_o = 75000$; Unit Discharge $q_o = Q_o/\sqrt{H_o}$; Time $t_o = 0$ Sec.
Hydraulic Starting Time $T_w = 0.528$ Sec.; Mechanical Starting Time $T_m = 4$ Sec.

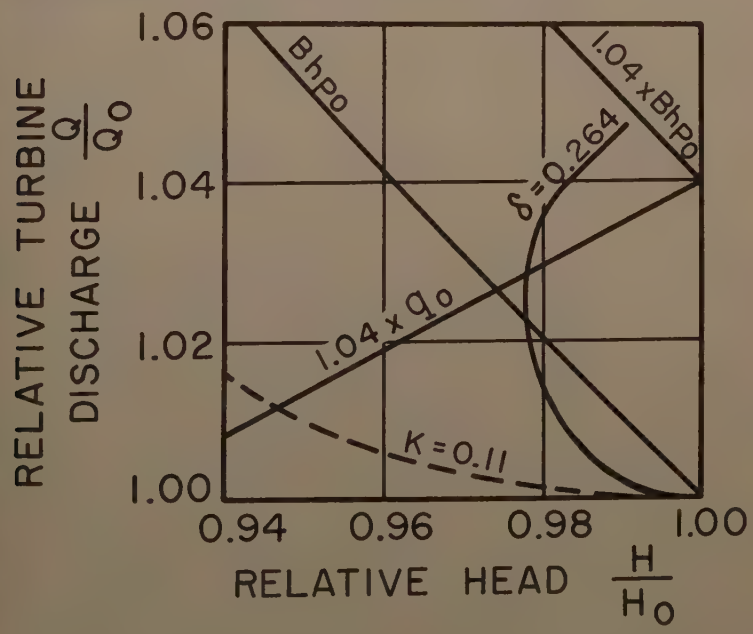

$Bhp = 1.04\ Bhp_o$; $T_w = 0.528$ SEC.

$T_m = 4$ SEC.

FIGURE (A-3)

R. A. SUTHERLAND,[1] F. ASCE—Mr. Barbarossa is to be congratulated on presenting his very interesting paper on procedure used with the IBM 650 for the solution of certain surge tank problems. It is noted with interest that he proposes to prepare complete details including flow charts and machine codes. Inasmuch as there are many 650 machines available and their use is very reasonable in cost, this further contribution will be of immense benefit to the profession. Anyone who has gone through the laborious "manual" computations involved in surge tank problems with multiple tanks will appreciate the tremendous potential saving in time and effort which will be available when it is possible to obtain a quick answer for the effect of changes in such variables as tank or orifice sizes, for example. The writer agrees that the saving in time, and the ability to study a wider range of variables than can ordinarily be done, will result in important savings in design cost and time and in many cases in construction cost.

The Author mentions the possibility of solutions of the "total transient problem" by the use of larger and faster machines. The input data will no doubt include estimated turbine performance between certain load conditions, and unless the turbine has been already in service and tested, such information must be obtained from "expected performance" curves. Some margin of error exists in the use of expected performance data, and such error may or may not have an important effect on the accuracy of the solutions obtained. Engineers familiar with turbine applications will recall instances where a turbine either exceeded or failed to meet its expected performance. Therefore the use of an expensive computer such as the 704 or 709 should be recommended only if it can be shown that results will not be substantially affected by discrepancies between expected and actual performance of turbines and other components. Computers have been programmed to take account of certain tolerances of input data, but the amount of work becomes greatly increased.

Mr. Barbarossa's work points the way to a wider knowledge of the interaction of the components in the surge problem through an increased ability to solve hypothetical cases.

FRANCIS E. SWAIN,[2] M. ASCE—Many important factors regarding the intelligent use of electronic computers are brought out clearly by the author. with hydraulics studies, as with all problems for which electronic calculating equipment may be used, it is essential that the problems be completely and accurately defined before any attempt is made to utilize such machines. Onc the definition is completed and it is determined that an electronic computer should properly be used for the solution, it is necessary that an accurate program be written for the problem. As the author states, "* * * the computer does the job with slavish adherence to instructions, and, as a consequence, the analyst cannot afford to slight or overlook any pertinent detail in the preparation of the machine program." The computer is equally as conte to process utter nonsense as it is to produce complete and meaningful result It is unfortunate that largely through writings in the popular press during the early history of electronic computers, they were given the titles of "magic brains" and "machines that think." Since, on the contrary, they more closel

1. Prin. Engr., Ebasco Services Inc., New York, N. Y.
2. Head, Electronic Data Processing Section, Office of Assistant Commr. and Chf. Engr., U. S. Bureau of Reclamation, Dener, Colo.

proach being "rapid moronic slaves," the engineer must not only know his roblem, but must also be completely familiar with the capabilities and limitions of the machines. Complete unification of the "what" of the problem d the "how" of the machine is requisite to the efficient and effective apication of electronic computers to any problem. A proper decision to use gh-speed computing equipment can result in optimum solutions being obined rapidly and economically. An improper decision may result in costly aos.

The inherent capabilities of the electronic digital computer make it posble, in certain instances, to eliminate many of the simplifying assumptions quired by manual solutions, as noted by the author. Controlling criteria n be varied over a wide range of values when an electronic computer is ed, thus making it possible to determine the effects of such variations and obtain what is more likely to be an optimum solution, rather than merely satisfactory one. More data are thereby available to the engineer permitng him to make more intelligent decisions than those possible with a naller volume of manual results. Having the computer do the vast amount numerical operations frees the engineer from the drudgery of routine anual calculations, and permits him to use his time for more professional ork. The obvious reasons for using high-speed computers—the reduction time and cost for accomplishing a set of calculations—also obtain for oper applications

The author tacitly indicates how the electronic computer can handle inrmation required for the solution of problems not only in hydraulics, but the field of hydrology as well; namely, the evaluation of single-valued nctions and the use of values of tabular data. The effects of the variations turbine wicket-gate openings during the initial interval of governor action e determined by evaluating the mathematical relationship representing the te-time curve each time a value is required. The same procedure is emoyed in computer solutions which require the evaluation of many other ngle-valued functions, such as trigonometric quantities, logarithms, exnentials, etc.

It is not possible, in many instances, to represent data required in the lution of a problem by a single-valued mathematical relationship. When is condition obtains, it is often possible to use "table look-up" commands routines with an electronic computer. Given a value of the argument for ich the corresponding value of the function is required, the computer arches the memory for the corresponding argument or the next higher lue if an exact correspondence does not exist. Interpolation routines can so be used with table look-up if desired. More efficient use of the memory pacity of a machine usually results if a mathematical relationship can be ed to evaluate a desired quantity. This may not be possible in certain stances, in which event the table look-up procedure must be used.

In his conclusions, the author notes that a better understanding of problem enomena associated with a particular installation is possible by the examation of the results from a number of different machine solutions in which e or more major factors have been changed from run to run. This is cerinly one of the more important benefits to be realized from the use of ectronic computers. The conclusion also serves to point out, however, that ile the computer offers many benefits and advantages, it is not in any sense substitute for sound engineering analysis, judgment, or experience. It is a ol which provides a means whereby the engineer can increase his informaon readily, and thus be more capable of making engineering decisions more elligently.

G. EVANGELISTI,[1] AND B. POGGI,[2]—Starting from a numerical analysis performed for the hydro-electric station of Oahe in South Dakota by means of an IBM 650 computer, the author develops a general investigation on the use and performances of electronic computers in the problems of unsteady flow in pressure conduit with surge tanks. The writers, who have also been dealing with the same hydraulic problem, using the same computing means, for a rather long time, are in a substantial agreement with the basic theme developed by the author, i. e. that the use of the automatic computing technique widely deepens the theoretical knowledge of the surge tank problems and strongly broadens the connected power of design. In fact, the conventional mathematical schemes ignore many effects, and it is important to check their field of validity and limits of accuracy in all the many operating conditions which have to be taken into account. This is primarily ture for the big stations, where the design of the tank structure is submitted to severe requirements of cost and operating features, and the designer has to choose among a great variety of solutions. The author gives the computing program for a conduit with two surge tanks in series, both for load rejection and load acceptance operations. In such a mathematical treatment many effects are taken into account, which are usually neglected. They are mainly: the inertia in the shaft and riser for the chamber and differential tanks; the departure of the friction losses from the quadratic law; the tank entrance losses (included the trottling orifices, whose value can be made different according to the sense of the flow). The elastic effects in the conduit are neglected, but the author proposes to put them into account in a further and more extended research.

When repeating their agreement with the leading idea of the author, i. e. that such a powerful means as an electronic computer is to be taken profit of to inspect a number of effects which are usually neglected, the writers would point out that sometimes a preliminary inspection of the particular problem can decide whether such effects are to be considered or can be neglected (making resort, in the second case, to a simpler program and shorter machine time). The writers like to mention, in a short review, their own experience on the subject.

Having put the friction loss of head in the Darcy-Weisbach formula (with the same simbols of author's paper)

$$h_f = f \frac{L}{D} \frac{Q|Q|}{2 g A^2} \qquad (1)$$

it is easy to detect in advance whether the variations of the coefficient f with the velocity are worth putting into account. In the big plants the departure from a pure hydraulic law of resistance is often quite slight. For instance, in an actual case studied by the writers, when the conduit had a diameter of 7.00 m ($A = 38{,}48\ m^2$), the Colebrook formula gives the following results in the two extreme values of the absolute roughness assumed in the calculations

1. Prof. of Hydr. Constrs. in the Univ. of Bologna, Bologna, Italy.
2. Prof. of Hydr. Special Plants in the Univ. of Bologna, Bologna, Italy.

V m sec^{-1}	f	
	e = 10^{-4} m	e = $3 \cdot 10^{-3}$ m
0.5	0.010316	0.01633
1.0	0.009632	0.01623
1.5	0.009337	0.01620
2.0	0.009169	0.01619
2.5	0.009060	0.01618
3.0	0.008983	0.01617
3.5	0.008926	0.01616
N_R = 6.116.000 V (t = 15 °C)		

It is seen that in the above instance the deviation from the quadratic law becomes substantial only at very low velocities, when the friction term is much smaller than the other terms in the varied flow equation.

Concerning the problem of taking into account the propagation effects in the conduit, it can be noted that such a problem, which gives rise to partial differential equations, allows a strict solution only in very particular cases (for instance, for a sudden load rejection or acceptance in an uniform frictionless conduit with a cilindrical surge tank*). On the contrary, the problem can be easily handled on an automatic computer by means a process of lumping.

The writers think that the wave effects in a normal conduit - tank system is never so strong to introduce substantial changes in the basic features of the phenomenon, so that the simplest and most obvious process of lumping—i. e. the representation of the elasticity of the water and the conduit walls by a piezometer—is quite adequate. The area of such a piezometer is readily calculated. If the total length L of the conduit is lumped in n equal cells, each of the n piezometers must have the area:

$$A_p = \frac{g\, A\, L}{n\, c^2} \qquad (2)$$

where c represents the wave celerity.

In such a theoretical case, the water level oscillations Z are given by the equation

$$Z = 2V_o \sum_{n=1}^{\infty} \frac{\sin \frac{C}{L} x_n t}{\frac{A_f}{A} \frac{C}{L} x_n + \frac{g}{C} \frac{X_n}{\sin^2 X_n}}$$

In this equation X_n are the roots of the trascendental equation

$$X_n \operatorname{tg} x = \frac{A}{A_f} \frac{gL}{C^2}$$

where A and A_f are the conduit and tank area, and c is the celerity of the elastic waves in the conduit.

In such a way the conduit is represented by a system of 2n ordinary differential equations of the first order, which is easily handled by an electronic computer. The writers used systematically such a procedure to inspect some water hammer phenomena on a Bendix D 12 differential analyzer.

Last (but not least) field where the use of the electronic computers can prove precious is that of the tanks of a particular structure. A problem of this kind was met by the writers in a big surge tank (the conduit, with a diameter of 7.00 m, was 15,400 m long, with a maximum discharge of 120 m^3 sec^{-1}), whose lower chamber was to face severe conditions of load acceptance with a rather restricted room at its disposal. A special type of chamber was tried, whose scheme is reproduced in Fig. 1. The idea of such a layout is to create a strong accelerating head on the water column in the conduit as rapidly as possible.

For the scheme of Fig. 1 the equation of continuity is:

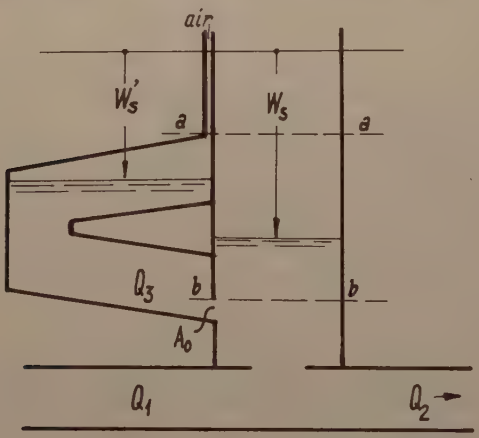

Fig.1

$$Q_1 - Q_2 + Q_3 = A_f \frac{dW_s}{dt} \qquad (3)$$

if the water level W_s is included between the level a-a and b-b . The discharge Q_3 is:

$$Q_3 = \pm m A_o \sqrt{2 g | W_s - W_s' |} \qquad (4)$$

and must be taken positive or negative according to whether W_s is greater or smaller then W_s' . In turn, the value of W_s' is a function of the total volume which has been exchanged by the chamber at the given instant t, starting from the time t_o when the two water levels begin to be different (level a-a during emptying, level b-b during filling). Thus, the value of W_s' is given by

$$W_s'(t) = F \left(\int_{t_o}^{t} Q_3 \, dt \right) \qquad (5)$$

where the function F depends upon the geometry of the chamber.

Thus, the lower chamber is represented by the system of equations (3), (4) and (5), which is obviously quite hard to handle without the help of an automatic computer.

PRESSURE CHANGES AT OPEN JUNCTIONS IN CONDUITS[a]

Discussion by John C. Geyer

JOHN C. GEYER,[1] F. ASCE—The experiments reported should improve he design and reduce the criticism of unchannelized junction boxes used in urface water and ground water drains. Manholes and junctions in sanitary ewerage systems will still require channels in order to prevent the deposi- ion of nuisance causing solids.

Channelizing of junctions has merits other than the improved hydraulic erformance which formerly was thought to be an important benefit, but hich, on the basis of work reported, seems not to be of much consequence. f the outflow pipe is cast into the walls of a junction after the bottom of the unction box is poured, the pipe invert will be above the floor of the box by at east the thickness of the pipe wall. This permits water to stand in the box fter flow has ceased and provides an ideal place for mosquitoes to breed. nder certain conditions debris will be deposited in rectangular junction oxes. If this debris contains much organic matter, some nuisance might esult. It appears, therefore, that some filling and shaping of the bottom, or t least a final pouring of concrete in the bottom, is desirable to prevent onding and reduce deposition.

The principal advantage of a plain or unchannelized juntion is reduced ost due to simplicity of construction. A knowledge of relative costs of ifferent types of bottom construction would assist the engineer in deciding he type of construction to use for a given situation.

The authors are certainly to be complimented for providing an adequate asis for the hydraulic design of open junction boxes.

. Proc. Paper 2057, June, 1959, by Sangster, Wood, Smerdon, and Bossy.
. Prof. San. Eng., Johns Hopkins Univ., Cockeysville, Md.

The technical papers published in the past year are identified by number below. Technical-division ownership is indicated by an abbreviation at the end of each Paper Number, the symbols referring to: Air Transport (AT), City Planning (CP), Construction (CO), Engineering Mechanics (EM), Highway (HW), Hydraulics (HY), Irrigation and Drainage (IR), Pipeline (PL), Power (PO), Sanitary Engineering (SA), Soil Mechanics and Foundations (SM), Structural (ST), Surveying and Mapping (SU), and Waterways and Harbors (WW) divisions. Papers sponsored by the Department of Conditions of Practice are identified by the symbols (PP). For titles and order coupons, refer to the appropriate issue of "Civil Engineering." Beginning with Volume 82 (January 1956) papers were published in Journals of the various Technical Divisions. To locate papers in the Journals, the symbols after the paper number are followed by a numeral designating the issue of a particular Journal in which the paper appeared. For example, Paper 1859 is identified as 1859 (HY7) which indicates that the paper is contained in the seventh issue of the Journal of the Hydraulics Division during 1958.

VOLUME 84 (1958)

OCTOBER: 1790(EM4), 1791(EM4), 1792(EM4), 1793(EM4), 1794(EM4), 1795(HW3), 1796(HW3), 1797(HW3), 1798(HW3), 1799(HW3), 1800(HW3), 1801(HW3), 1802(HW3), 1803(HW3), 1804(HW3), 1805(HW3), 1806(HY5), 1807(HY5), 1808(HY5), 1809(HY5), 1810(HY5), 1811(HY5), 1812(SM4), 1813(SM4), 1814(ST6), 1815(ST6), 1816(ST6), 1817(ST6), 1818(ST6), 1819(ST6), 1820(ST6), 1821(ST6), 1822(EM4), 1823(PO5), 1824(SM4), 1825(SM4), 1826(SM4), 1827(ST6)[c], 1828(SM4)[c], 1829(HW3)[c], 1830(PO5)[c], 1831(EM4)[c], 1832(HY5)[c].

NOVEMBER: 1833(HY6), 1834(HY6), 1835(SA6), 1836(ST7), 1837(ST7), 1838(ST7), 1839(ST7), 1840(ST7), 1841(ST7), 1842(SU3), 1843(SU3), 1844(SU3), 1845(SU3), 1846(SU3), 1847(SA6), 1848(SA6), 1849(SA6), 1850 (SA6), 1851(SA6), 1852(SA6), 1853(SA6), 1854(ST7), 1855(SA6)[c], 1856(HY6)[c], 1857(ST7)[c], 1858(SU3)[c].

DECEMBER: 1859(HY7), 1860(IR4), 1861(IR4), 1862(IR4), 1863(SM5), 1864(SM5), 1865(ST8), 1866(ST8), 1867 (ST8), 1868(PP1), 1869(PP1), 1870(PP1), 1871(PP1), 1872(PP1), 1873(WW5), 1874(WW5), 1875(WW5), 1876 (WW5), 1877(CP2), 1878(ST8), 1879(ST8), 1880(HY7)[c], 1881(SM5)[c], 1882(ST8)[c], 1883(PP1)[c], 1884(WW5)[c], 1885(CP2)[c], 1886(PO6), 1887(PO6), 1888(PO6), 1889(PO6), 1890(HY7), 1891(PP1).

VOLUME 85 (1959)

JANUARY: 1892(AT1), 1893(AT1), 1894(EM1), 1895(EM1), 1896(EM1), 1897(EM1), 1898(EM1), 1899(HW1), 1900(HW1), 1901(HY1), 1902(HY1), 1903(HY1), 1904(HY1), 1905(PL1), 1906(PL1), 1907(PL1), 1908(PL1), 1909(ST1), 1910(ST1), 1911(ST1), 1912(ST1), 1913(ST1), 1914(ST1), 1915(ST1), 1916(AT1)[c], 1917(EM1)[c], 1918(HW1)[c], 1919(HY1)[c], 1920(PL1)[c], 1921(SA1)[c], 1922(ST1)[c], 1923(EM1), 1924(HW1), 1925(HW1), 1926 (PL1), 1927(HW), 1928(HW1), 1929(SA1), 1930(SA1), 1931(SA1), 1932(SA1).

FEBRUARY: 1933(HY2), 1934(HY2), 1935(HY2), 1936(SM1), 1937(SM1), 1938(ST2), 1939(ST2), 1940(ST2), 1941(ST2), 1942(ST2), 1943(ST2), 1944(ST2), 1945(HY2), 1946(PO1), 1947(PO1), 1948(PO1), 1949(PO1), 1950(HY2)[c], 1951(SM1)[c], 1952(ST2)[c], 1953(PO1)[c], 1954(CO1), 1955(CO1),1956(CO1),1957(CO1), 1958(CO1), 1959(CO1).

MARCH: 1960(HY3), 1961(HY3), 1962(HY3), 1963(IR1), 1964(IR1), 1965(IR1), 1966(IR1), 1967(SA2), 1968(SA2), 1969(ST3), 1970(ST3), 1971(ST3), 1972(ST3), 1973(ST3), 1974(ST3), 1975(ST3), 1976(WW1), 1977(WW1), 1978(WW1), 1979(WW1), 1980(WW1), 1981(WW1), 1982(WW1), 1983(WW1), 1984(SA2), 1985(SA2)[c], 1986 (IR1)[c], 1987(WW1)[c], 1988(ST3)[c], 1989(HY3)[c].

APRIL: 1990(EM2), 1991(EM2), 1992(EM2), 1993(HW2), 1994(HY4), 1995(HY4), 1996(HY4), 1997(HY4), 1998 (SM2), 1999(SM2), 2000(SM2), 2001(SM2), 2002(ST4), 2003(ST4), 2004(ST4), 2005(ST4), 2006(PO2), 2007 (HW2)[c], 2008(EM2)[c], 2009(ST4)[c], 2010(SM2)[c], 2011(SM2)[c], 2012(HY4)[c], 2013(PO2)[c].

MAY: 2014(AT2), 2015(AT2), 2016(AT2), 2017(HY5), 2018(HY5), 2019(HY5), 2020(HY5), 2021(HY5), 2022(HY5), 2023(PL2), 2024(PL2), 2025(PL2), 2026(PP1), 2027(PP1), 2028(PP1), 2029(PP1), 2030(SA3), 2031(SA3), 2032(SA3), 2033(SA3), 2034(ST5), 2035(ST5), 2036(ST5), 2037(ST5), 2038(PL2), 2039(PL2), 2040(AT2)[c], 2041(PL2)[c], 2042(PP1)[c], 2043(ST5)[c], 2044(SA3)[c], 2045(HY5)[c], 2046(PP1), 2047(PP1).

JUNE: 2048(CP1), 2049(CP1), 2050(CP1), 2051(CP1), 2052(CP1), 2053(CP1), 2054(CP1), 2055(CP1), 2056 (HY6), 2057(HY6), 2058(HY6), 2059(IR2), 2060(IR2), 2061(PO3), 2062(SM3), 2063(SM3), 2064(SM3), 2065 (ST6), 2066(WW2), 2067(WW2), 2068(WW2), 2069(WW2), 2070(WW2), 2071(WW2), 2072(CP1)[c], 2073(IR2)[c], 2074(PO3)[c], 2075(ST6)[c], 2076(HY6)[c], 2077(SM3)[c], 2078(WW2)[c].

JULY: 2079(HY7), 2080(HY7), 2081(HY7), 2082(HY7), 2083(HY7), 2084(HY7), 2085(HY7), 2086(SA4), 2087 (SA4), 2088(SA4), 2089(SA4), 2090(SA4), 2091(EM3), 2092(EM3), 2093(EM3), 2094(EM3), 2095(EM3), 2096 (EM3), 2097(HY7)[c], 2098(SA4)[c], 2099(EM3)[c], 2100(AT3), 2101(AT3), 2102(AT3), 2103(AT3),2104(AT3), 2105(AT3), 2106(AT3), 2107(AT3), 2108(AT3), 2109(AT3), 2110(AT3), 2111(AT3), 2112(AT3),2113(AT3), 2114(AT3), 2115(AT3), 2116(AT3), 2117(AT3), 2118(AT3), 2119(AT3), 2120(AT3), 2121(AT3),2122(AT3), 2123(AT3), 2124(AT3), 2125(AT3).

AUGUST: 2126(HY8), 2127(HY8), 2128(HY8), 2129(HY8), 2130(PO4), 2131(PO4), 2132(PO4), 2133(PO4),2134 (SM4), 2135(SM4), 2136(SM4), 2137(SM4), 2138(HY8)[c], 2139(PO4)[c] 2140(SM4)[c].

SEPTEMBER: 2141(CO2), 2142(CO2),2143(CO2), 2144(HW3), 2145(HW3), 2146(HW3), 2147(HY9), 2148(HY9), 2149(HY9), 2150(HY9), 2151(IR3), 2152(ST7)[c], 2153(IR3), 2154(IR3), 2155(IR3), 2156(IR3), 2157(IR3), 2158 (IR3), 2159(IR3), 2160(IR3), 2161(SA5), 2162(SA5), 2163(ST7), 2164(ST7), 2165(SU1), 2166(SU1), 2167(WW3), 2168(WW3), 2169(WW3), 2170(WW3), 2171(WW3), 2172(WW3), 2173(WW3), 2174(WW3), 2175(WW3), 2176 (WW3), 2177(WW3), 2178(CO2)[c], 2179(IR3)[c], 2180(HW3)[c], 2181(SA5)[c], 2182(HY9)[c], 2183(SU1)[c], 2184 (WW3)[c], 2185(PP2)[c], 2186(ST7)[c], 2187(PP2), 2188(PP2).

OCTOBER: 2189(AT4), 2190(AT4), 2191(AT4), 2192(AT4), 2193(AT4), 2194(EM4), 2195(EM4), 2196(EM4), 2197(EM4), 2198(EM4), 2199(EM4), 2200(HY10), 2201(HY10), 2202(HY10), 2203(PL3), 2204(PL3), 2205 (PL3), 2206(PO5), 2207(PO5), 2208(PO5), 2209(PO5), 2210(SM5), 2211(SM5), 2212(SM5), 2213(SM5), 2214 (SM5), 2215(SM5), 2216(SM5), 2217(SM5), 2218(ST8), 2219(ST8), 2220(EM4), 2221(ST8), 2222(ST8), 2223 (ST8), 2224(HY10), 2225(HY10), 2226(PO5), 2227(PO5), 2228(PO5), 2229(ST8), 2230(EM4), 2231(EM4), 2232(AT4)[c], 2233(PL3)[c], 2234(EM4)[c], 2235(HY10)[c], 2236(SM5)[c], 2237(ST8)[c], 2238(PO5)[c], 2239(ST8), 2240 (PL3).

[c] Discussion of several papers, grouped by divisions.

AMERICAN SOCIETY OF CIVIL ENGINEERS

OFFICERS FOR 1959

PRESIDENT

FRANCIS S. FRIEL

VICE-PRESIDENTS

Term expires October, 1959:
WALDO G. BOWMAN
SAMUEL B. MORRIS

Term expires October, 1960:
PAUL L. HOLLAND
LLOYD D. KNAPP

DIRECTORS

Term expires October, 1959:
CLINTON D. HANOVER, Jr.
E. LELAND DURKEE
HOWARD F. PECKWORTH
FINLEY B. LAVERTY
WILLIAM J. HEDLEY
RANDLE B. ALEXANDER

Term expires October, 1960:
PHILIP C. RUTLEDGE
WESTON S. EVANS
TILTON E. SHELBURNE
CRAIG P. HAZELET
DONALD H. MATTERN
JOHN E. RINNE

Term expires October, 1961:
THOMAS J. FRATAR
EARL F. O'BRIEN
DANIEL B. VENTRES
CHARLES W. BRITZIUS
WAYNE G. O'HARRA
FRED H. RHODES, JR.
N. T. VEATCH

PAST PRESIDENTS

Members of the Board

MASON G. LOCKWOOD

LOUIS R. HOWSO

EXECUTIVE SECRETARY

WILLIAM H. WISELY

ASSISTANT SECRETARY

E. LAWRENCE CHANDLER

ASSISTANT TREASURER

ENOCH R. NEEDLES

PROCEEDINGS OF THE SOCIETY

HAROLD T. LARSEN
Manager of Technical Publications

PAUL A. PARISI
Editor of Technical Publications

MARVIN SCHECHTER
Assistant Editor of Technical Publications

COMMITTEE ON PUBLICATIONS

HOWARD F. PECKWORTH, *Chairman*

PHILIP C. RUTLEDGE, *Vice-Chairman*

E. LELAND DURKEE
CHARLES W. BRITZIUS
TILTON E. SHELBURNE
FRED H. RHODES, JR.